INTERNATIONAL JOURNAL OF
IJCOE
COASTAL, OFFSHORE & ENVIRONMENTAL ENGINEERING

Volume 8 | Issue 1 | Feb 2023

www.ijcoe.org info@ijcoe.org

International Journal of Coastal, Offshore and Environmental Engineering (IJCOE)
Vol. 8 / Issue. 1 / Feb 2023
30

ISSN: 2980-8731 (online)

International Journal of Coastal, Offshore & Environmental Engineering

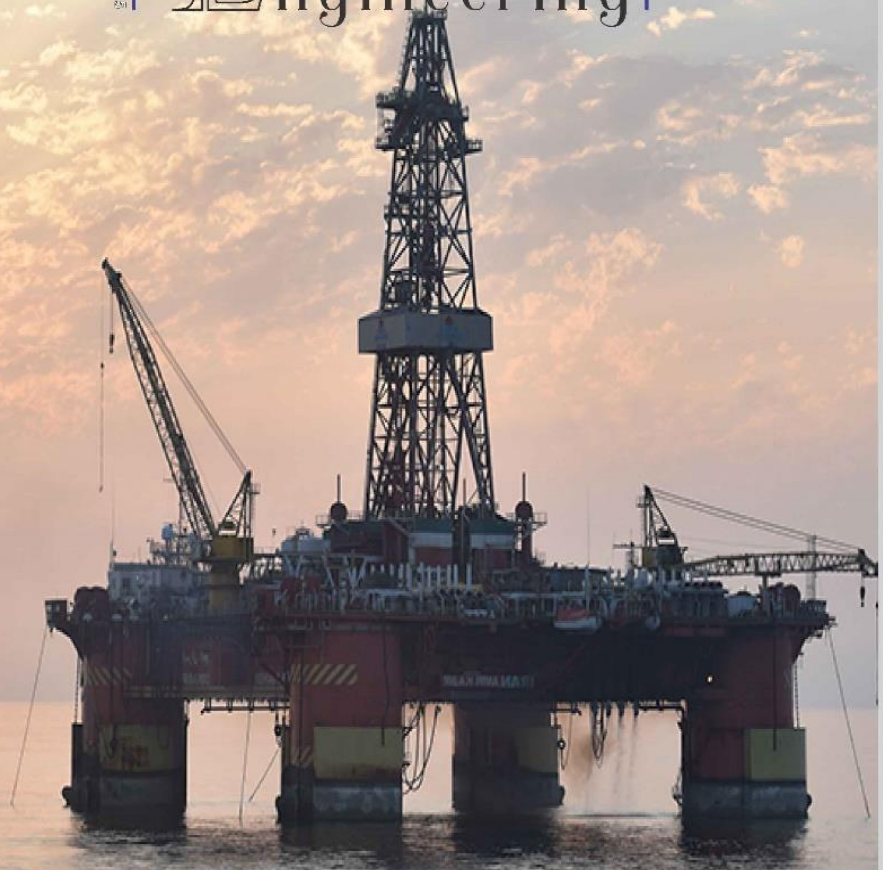

Volume 8 | Issue 1 | Feb 2023

IJCOE

International Journal of Coastal, Offshore & Environmental Engineering
Since 2015
ISSN: 2980-8721 (online)

In The Name of God

Message from the Editor-in-Chief

The IJCOE journal office was established in 2015,and its first issue was published in 2016. TheIJCOE covers a wide range of research in thefields of oceanography & ocean technology, aswell as marine industries & marine engineering.The editorial board of IJCOE consists of nearly130 of the greatest scientists and researchersfrom over 30 countries worldwide, and thejournal's review board comprises 1,000 membersfrom all five continents. The membership andapplication process for joining the editorial andreview boards of this journal is ongoing. IJCOE isa research-academic quarterly journal that haspublication and distribution permissions fromthe Press Organization and permission topublish scientific-research articles from theMinistry of Science, Research, and Technology(MSRT) with an "A" rating. It also holds a "Q1"rating from the ISC institute with an impactfactor (IF) of approximately 0.43 and isconsidered a "core journal" (prestigious andoutstanding journal). IJCOE is an open-accessjournal and allows the download and receipt ofaccepted articles in full text for free. It respectsand adheres to copyright and COPE regulations.The journal's office operates 24/7, providingservices to researchers. In addition to publishinga regular quarterly journal, IJCOE has 16 specialissues on specific topics in preparation. It alsoprovides conditions for publishing specializedbooks, references, and handbooks. Moreover, itis ready to cooperate with the secretariats ofreputable international conferences to publishtheir selected and outstanding articles. IJCOEevaluates, appraises, and publishes books,articles, and the scientific achievements andfindings of esteemed researchers and scientistsworldwide who are innovating and conductingin-depth research in the "important and strategicfield of the maritime technology & Oceanengineering." It welcomes any form of jointcooperation with universities, research institutes,and related research centers at the national,regional, and international levels, and extends ahand for collaboration.

Classification of Editorial Board in IJCOE

- Editor-in-Chief
- Director-in-Chief
- Deputy Editor
- Executive Managers
- English Text Editor
- Technical Editor
- International Editorial Board
- National Editorial Board
- Editorial Board Associate
- Editorial Board Assistant
- Guest Editorial Board
- Advisory Board
- Administrative Coordinator
- Honorary Board Member
- Methodology Advisor

Author Benefits

- Open Access
- Rapid Publication
- Thorough Peer-Review
- No Copyright Constraints
- Coverage by Leading Indexing Services
- Discounts On Article Processing Charges (APC)
- No Space Constraints, No restriction on the maximum length of the papers, number of figures or colors

INTERNATIONAL JOURNAL OF IJCOE COASTAL, OFFSHORE & ENVIRONMENTAL ENGINEERING

Aims of IJCOE

Hydrodynamics

Marine equipment

Structural mechanics

Ocean environmental predictions

Stochastic calculations Experimental

Automatic Control of Marine Systems

Scope of IJCOE

Marine Hazards

Ocean Acoustics

Naval Architecture

Ocean Engineering

Coastal Engineering

Marine Meteorology

Marine Earth Sciences

Underwater Technology

Marine Renewable Energy

Polar & Arctic Engineering

Marine Renewable Energy

Marine Geography & Geodesy

Marine Environmental Engineering

Automatic Control of Marine Systems

Hydro Physics & Physical Oceanography

Type of papers

- Case Studies
- Book Reviews
- Review Article
- Letters to the Editor
- Methodology Papers
- Editorials and Commentaries
- Response or Rejoinder Papers
- Perspective or Opinion Papers
- Conceptual or Theoretical Papers
- Meta-Analysis and Systematic Reviews
- Short Communications or Brief Reports
- Research Articles (Original Research Papers)

Scientific Research Journal

Ministry of Science, Research And Technology (MSRT)

Jurnal Ranking 2023: A

Ministry Of Science, Research And Technology (ISC)

Citation Impact 2022: 0.429

Quartile 2022 : Q1

Core Collection

IJCOE is a Member of

Cantact Us

Office 1 | Research Institute of Meteorology and Atmospheric Science

Address | Tehran, Shahid Kharrazi Highway, Pajoohesh Blvd, Research Institute of Meteorology and Atmospheric Science, Sand and Dust Storm International Research Center (SDS-IRC), No. 13, 1st floor.

Phone | +982144787652

Postal code | 13611-14977

website | www.rimac.ac.ir

Office 2 | Iranian National Institute for Oceanography and Atmospheric Science

Address | Tehran, Dr. Fatemi Gharbi St., Shahid Etemadzade St., No. 3, third floor.

Phone | +982166944873

Postal code | 13389 – 14118

website | www.inio.ac.ir

Email | Info@ijcoe.org

Website | www.ijcoe.org

Follow Us

www.ijcoe.org

INTERNATIONAL JOURNAL OF IJCOE COASTAL, OFFSHORE & ENVIRONMENTAL ENGINEERING

Volume & Issue:

Volume 8, Issue 1, February 2023

Number of Articles: 6

Content

INTERNATIONAL JOURNAL OF
COASTAL, OFFSHORE & ENVIRONMENTAL ENGINEERING IJCOE Vol.8/No. 1/winter 2023 (1-9)

Available online at: www. Ijcoe.org

Investigating the downwelling of Persian Gulf Water in the Gulf of Oman

Hossein Ramak[1], Maryam Soyuf Jahromi[2*], Akbari, Parastoo[3]

[1] *PhD of physical oceanography, Department of Nonliving Resources of Atmosphere and Ocean, Faculty of Marine Science and Technology, University of Hormozgan, Bandar Abbas, Iran; Department of physics, Education office of Hormozgan Province, Education Ministry, Parsiyan, Iran, hoseynramak@gmail.com*
[2] *Assistant Professor of physical oceanography, Department of Nonliving Resources of Atmosphere and Ocean, Faculty of Marine Science and Technology, University of Hormozgan, Bandar Abbas, Iran, soyufjahromi@yahoo.com.au*
[3] *Department of physics, Education office of Khoozestan Province, Education Ministry, Ahwaz, Iran, pakbari91@yahoo.com*

ARTICLE INFO

Article History:
Received: 26 Dec. 2022
Accepted: 02 Feb. 2023

Keywords:
Water Mass
Seasonal change
Downwelled Water
Vertical Velocity
FVCOM

ABSTRACT

In Gulf of Oman, the sinking of Persian Gulf Water mass has been reported. In the current study, the FVCOM ocean model has been used in 20 layers to investigate the phenomenon of downwelled Persian Gulf Water in the Gulf of Oman. The bathymetry of the simulated area (47˚-59.45˚E, 22˚-32˚N) was achieved from GEBCO-2019 by the resolution of 30 seconds. Triangular grid was generated in SMS. The open boundary fluctuations were also extracted from TMD. The temperature and salinity were obtained from the output of HYCOM (standard depths). Satellite data were used for the verification. The results showed the downward vertical velocity of Persain Gulf Water is higher in the area of the sudden depth change than the other parts in all seasons. This fact indicated the downwelled water was in a form of a spot. The rate of downwards penetration of water was different (winter: -2cm/s, spring: -1cm/s, summer: -1.2cm/s, autumn: -1.7cm/s). In summer, the salinity contours were very close to each other in the east of the Strait of Hormuz, or intense stratification. Therefore, the slope of the salt wedge was less. In winter, the calculated slope of the salt wedge (1.5×10^{-1} degrees) was greater than summer (3.8×10^{-2} degrees). The larger angle or slope of the salt wedge means the greater horizontal component of the weight of water ($mg\sin\theta$). It causes the displacement of saline water, and faster movement of Persian Gulf Water. Therefore, the water of the Persian Gulf moves faster to lower depths in Gulf of Oman in winter than summer.

1. Introduction

Downwelling is the opposite process of upwelling, in which surface water flows downward and replaces deep water. This happens in parts of the ocean where the surface winds are converging. A cyclonic wind causes a decrease in sea level, an increase in the thermocline, the divergence and upwelling, while an anticyclonic wind leads to an increase in the sea level, a lower thermocline, and convergence and downwelling. One of the places where upwelling or downwelling occurs is in the center of the gyres, cycles and eddies even if there is no prevailing wind [1].

Upwelling and Downwelling are two prominent features that appear in an annual cycle on the west coast of India [2-6]. Heat transfer [7] and mass transfer [8] (such as carbon dioxide) from the ocean to the atmosphere and vice versa are key processes that accompany downwelling currents [7]. Even the primary biological production in the eastern Arabian Sea is not only done by the upwelling phenomenon, but can also occur under the influence of the proper downwelling phenomenon caused by Kelvin waves that lower the thermocline [9-12] in the northeast of the Arabian Sea during the northeast monsoon (November-February) [13-14]. Therefore, understanding and studying the phenomenon of downwelling and upwelling is of great scientific importance in designing fisheries management strategies to provide maximum sustainable yield.

It was seen in the northeast of the Arabian Sea that the vertical downwelling of the water causes the heating of the mixing layer waters during winter. Because the vertical velocity of water in these areas is negative, which indicates the phenomenon of downwelling. The simulation showed that the atmospheric currents tend to cool the mixing layer of the Arabian Sea, but this

cooling of the mixing layer is countered by the warming caused by horizontal advection. Downwelling is the tendency to heat the lower layer and reduce or neutralize the rate of cooling of the mixing layer, and it can continue, and even as the mixing layer becomes shallower. This causes the formation of a weak barrier layer under the mixing layer in the south-northeast of the Arabian Sea, which prevents the cooling of this layer [13].

The role of vertical subsidence, which tends to heat the mixing layer and is due to the downwelling phenomenon, has been largely ignored in studies, and more attention has been paid to the upwelling phenomenon. This study aims to investigate the downwelling of Persian Gulf water in the Oman Sea by using numerical simulation, and evaluates the changes of the Persian Gulf water fall in the Gulf of Oman during the seasons.

2. Materials and Methods

2.1. The study area

The Gulf of Oman is a water basin that is located in the northwest of the Arabian Sea, the Indian Ocean, and the east of the Strait of Hormuz and the Persian Gulf, and it is spread in latitude of 22˚N to 26˚N and longitude 56˚E to 60˚E. Iran is located in the north of this gulf and Oman is in the south. The continental slope is sharp in the east of 56˚E and along the coast of Oman. So that the depth of more than 3000 meters is found in the south of 24.30˚N and in the east of 58.30˚E in this gulf [15] (with a maximum depth of 3398 meters [16]). This gulf is located in the warm region of the earth, where the maximum sea surface temperature of 33˚C in August, and the minimum of 19.8˚C in January. It is different from part to parts. The maximum of sea surface temperature anomaly occurs in Auguest [17] in most parts. The tide of the Gulf of Oman is also the same as the tide of the Arabian Sea [16] and is different from Persain Gulf [18] which which affects the region's renewable energies at different points and times [19]. The circulation pattern in this basin includes an outflow from the Strait of Hormuz to a depth of approximately 200 meters, which extends throughout the basin, and the other one is the rotation of clockwise in the west and anti-clockwise in the east [16]. The dominant wind in this region is the south wind in summer and the northwest wind in winter [16]. The direction of wind movement in the Gulf of Oman is associated with seasonal reversal, corresponding to the monsoon system of the Indian Ocean, so that during the winter monsoon (October-May), the northwest wind prevails and during the summer monsoon (June-September), the southeast wind prevails [20].

In order to investigate the water mass of the Persian Gulf in the Gulf of Oman, an area was chosen that includes the Persian Gulf. Hence the study area of this research was located between 22˚N to 32˚N and 47˚E to 59.45˚E, on the north of Arabian Sea.

2.2. The numerical simulation

The FVCOM 3D numerical ocean model of Finite-Volume Coastal Ocean Model version 3.2.1, hereafter FVCOM, is a finite volume model that can provide suitable simulations for ocean projects by discretizing the equations [21] in an unstructured horizontal triangular computational grid [22]. The model has the ability to use sigma coordinates (with uniform or variable resolution from the surface to the bed) in the vertical direction [23]. Hence, the ability to accurately solve the equations by encoding in a Cartesian or spherical coordinate system, while maintaining the scale and topological flexibility provided by the unstructured meshing and the simplicity of the coding structure, has made this model suitable for many coastal and interdisciplinary scientific applications with complicated conditions [23].

2.2.1. Inputs

The initial input files of FVCOM included entering the horizontal computational grid, depth, sigma layer (20 layers), boundary points, sponge layer information and Coriolis meter, water level and initial conditions of temperature and salinity.

First, the data related to the coastline of the studied area was extracted from the GEBCO-2019 database in Shapefile format [24]. The specialized software of Surface-water Modeling System version 10.0 [25-26], hereafter SMS, was used to create an unstructured triangular mesh from the prepared bathymetry data for FVCOM. All three modules Mesh Module, Map Module and Scatter Module of SMS were used to generate the computing grid. After changing the structure in the SMS software environment and creating the ability to smooth the coastline, the necessary corrections were applied to the file, and then an unstructured two-dimensional computing mesh with appropriate resolution was created in different areas of the study area. This mesh of 11136 cells and 5879 nodes with a horizontal resolution between 950 m and 4700 m was used in 20 sigma layers in the vertical direction. The bathymetry data were extracted from GEBCO-2019 data, relative to the mean sea level in meters, with a resolution of 30 seconds [27] and interpolated on the computational grid, so that a depth was assigned to each node of the grid. In different areas of the model, the depths were not the same and there were depths less than 2 meters (1.02 m) and greater than 3000 meters (3256 m) in the Gulf of Oman. In order to investigate the downwelling of the Persian Gulf water in the Gulf of Oman from the Strait of Hormuz towards the Gulf of Oman, a finer grid was used. Figure 1 illustrates the part of the computational fine mesh of Gulf of Oman used in FVCOM.

The information of the sponge layer and the Coriolis parameter were entered into the model as separate ASCII files.

The open boundary was located at 59.45˚E, and the number of points on the open boundary was considered to be 35 nodes. They were also entered into the model as separate ASCII files. The water level, as the main settings of the model, at the open boundry nodes with NetCDF format was extracted from Tidal Model Driver, hereafter TMD, as constant values of the domain in the coordinates corresponding to the location of the nodes of the open boundry of the computing grid with a time step of one hour.

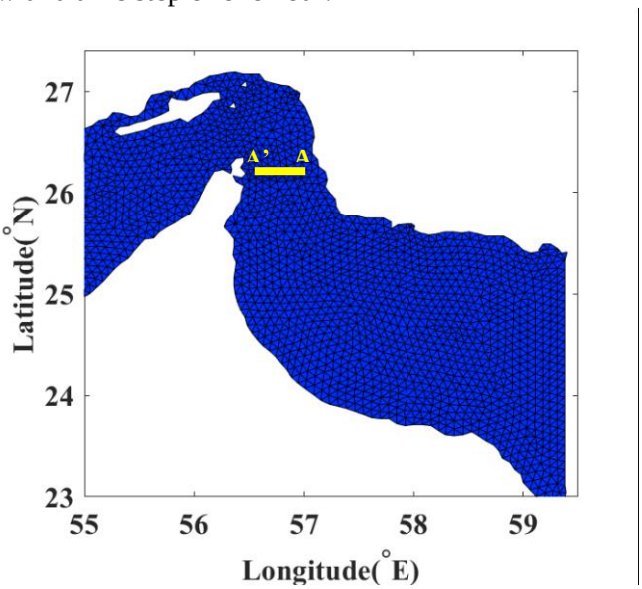

Figure 1: The computational mesh generated by SMS in Gulf of Oman and used for FVCOM simulation. The AA' (yellow line) is a cross section regarding Figures 4 and 6.

The initial conditions of temperature and salinity used in the model were considered non-uniform, and these initial conditions were entered into the model as a NetCDF field of temperature and salinity. Temperature and salinity data fields by a horizontal resolution of 0.08 degrees were used from the HYbrid Coordinate Ocean Model, hereafter HYCOM [28], at standard depths (ten levels of depth).

2.2.2. Outputs

The initial conditions of temperature and salinity used in the model were considered non-uniform, and these initial conditions were entered into the model as a NetCDF field of temperature and salinity. Temperature and salinity data fields by a horizontal resolution of 0.08 degrees were used from the HYbrid Coordinate Ocean Model, hereafter HYCOM [28], at standard depths (ten levels of depth).

The output files included hourly water level and daily salinity, temperature and current, which were prepared in NetCDF format. MATLAB 2016 software [29] with appropriate coding was used to illustrate the outputs of the simulation.

2.2.3. Validation

The simulation had been run for 6 years (from 2014 to 2020) so that the properties of the water mass of Persian Gulf reach a stable cycle.

To validate the results of the simulation, it was used satellite data from the Group for High Resolution Sea Surface Temperature, GHRSST, with the resulation of 0.05˚ and an accuracy of 0.01˚C known as OSTIA [30]. The maximum difference between OSTIA and the simulation was about 1.9˚C (warm season) and 0.7˚C (cold season). In warm season, in most of the Gulf of Oman and its east, the difference was around +0.4˚C, and in the cold season, it was around -0.2˚C to +0.2˚C.

3. Results and Discussion

The results of the numerical FVCOM simulation show the pattern of vertical water velocity during seasons in the Gulf of Oman. Figure 2 shows that in most of the studied range in the deep layers, the velocity is close to zero (green areas), but in some areas, the vertical velocity of water from neutral buoyancy is positive (red dots) and negative (blue spots) which represents rising (upwelled) and sinking (downwelled) water, respectively.

In winter (the first row of figure 2), in the 18th and 19th sigma layers in the southern regions of the Gulf of Oman, the downward vertical velocity of water is higher than in other regions. In the 18th layer, there is a spot with a velocity of -1.2 cm/s and in the 19th layer, the vertical velocity of water in the same areas is -1.8 cm/s. It finally reaches -2 cm/s In addition, in the southern regions of the Gulf of Oman, near the coast of Oman, there is a narrow strip of water with a vertical velocity of -1 cm/s. Therefore, in winter, with the depth increase from the 18th sigma layer to the 20th sigma layer, the downward vertical velocity of water is increasing, so that it has the highest value in the 20th sigma layer.

In spring (the second row of figure 2), the vertical velocity of water in most areas of the Strait of Hormuz and the Gulf of Oman in the 20th sigma layer is in the range of -0.1 cm/s to 0.1 cm/s, and in the central areas of the Gulf of Oman, the vertical water speed is also -0.03 cm/s to -0.5 cm/s. In the east of the Strait of Hormuz, at the longitude of 57.12˚E, the maximum downward vertical velocity can be seen, and its value is about -1 cm/s. In the southern regions of the Gulf of Oman, near the coast of Oman, there is also a strip parallel to the coast, the vertical speed of the water is -1.2 cm/s, and in the eastern regions of the Gulf of Oman, the vertical speed of the water is around -0.3 cm/s to -1.1 cm/s (figure 3, the second row). In the spring, the vertical downward velocity in the 18th and 19th layers of the eastern regions of the study area is higher than in other regions. In the southeastern regions of the Gulf of Oman, the vertical downward velocity reaches -1 cm/s. In the 18th and 19th layers in the Strait of Hormuz and east of it, there is no significant vertical downward velocity, but in the 20th layer and in the east of the Strait of Hormuz, the velocity has increased compared to the above layers.

In summer (the third row of figure 2), the vertical velocity of water in most areas of the Strait of Hormuz and the Gulf of Oman in the 20th sigma layer is in the range of -0.1 cm/s to -0.1 cm/s. In this season, like other seasons in the east of the Strait of Hormoz, the maximum vertical velocity of water is downward and about -2.1 cm/s in the longitude of 57.12 ˚E to 57.26˚E. In the east of the Gulf of Oman and in the range of longitude 59˚E, the downward vertical velocity is higher than in other areas (-1cm/s). In the southern regions of the Gulf of Oman, water with a vertical velocity of -1.8 cm/s covers those regions in a narrow manner (the third row of figure 2). In summer, the downward vertical velocity in the 18th and 19th layers are in the range of -0.8 cm/s to -1 cm/s. In the eastern areas of the Strait of Hormuz, the downward velocity has increased in this season compared to spring. In the east of the Gulf of Oman, the downward vertical velocity increases and its value reaches -1 cm/s. In the south, the speed of -1.5 cm/s can be seen in some areas. From the 18th to the 20th sigma layer, with the increase in depth in this season, the downward vertical velocity has also increased, so that in the 20th sigma layer, the vertical downward velocity is more than other layers.

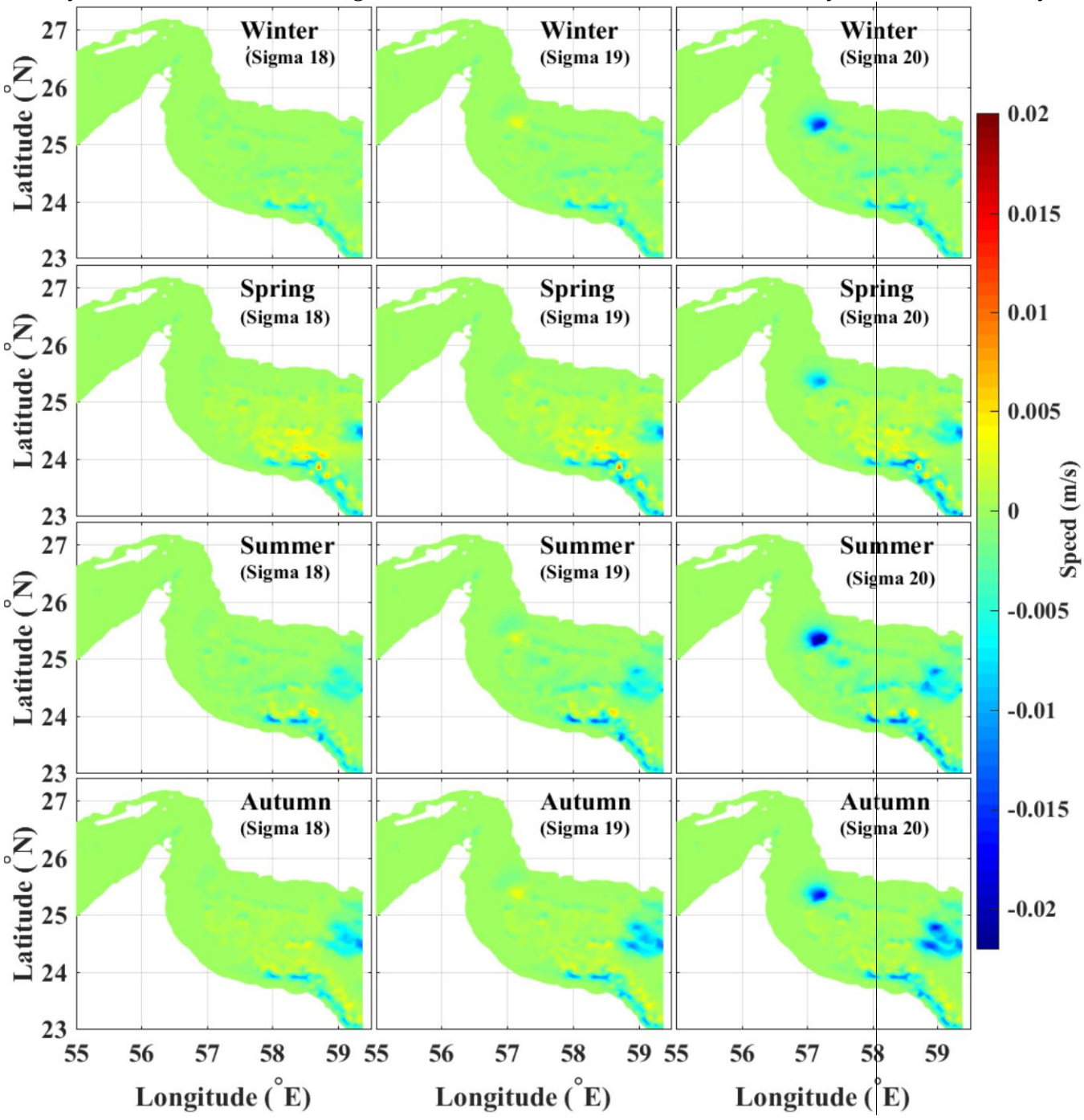

Figure 2. The water simulated vertical velocity in Gulf of Oman in winter, spring, summer and autumn, in last three layers near the bed (the first column: 18th, the second column: 19th, and the third column: 20th sigma layers, respectively). Positive values are upward and negative values are downward.

In autumn (the last row of figure 2) the vertical velocity of water in the 20th sigma layer is -0.2 cm/s to -0.1 cm/s in the Gulf of Oman and more than other areas in the longitude of 57.12˚E by the maximum value of -1.7

cm/s. In the eastern regions of the Gulf of Oman, in the longitude of 58.8˚E to 59.4˚E, the vertical velocity of water is about -0.8 cm/s to -1.7 cm/s, which is higher than other areas of this region. In the southern regions of the Gulf of Oman, there is a water strip that runs parallel to the coast and its velocity is -1.1 cm/s. In autumn, the downward vertical velocity is higher in the eastern regions of the study area than the other regions. In the 19th layer, the value of this speed in the east of the Gulf of Oman has reached 1.5 cm/s, which has increased compared to the summer and spring.

Overall, the east area of the Strait of Hormuz and the Gulf of Oman, the vertical velocity has more changes from latitude of 25.19˚N to 25.48˚N and longitude of 57.12˚E to 57.26˚E. The values of this velocity are -2cm/s in winter, -1 cm/s in spring, -1/2 cm/s in summer, and -1/7 cm/s in autumn. In the places where there is a sudden change in depth or the slope of the continental plateau, a downward velocity change, and the size of this speed is almost close to each other in all seasons. This sudden negative velocity change indicates downwelling in this area. This sinking of water is not caused by the surface wind tension, but it is the result of the change of the slope of the continental plateau. In all four seasons, as the depth increases from the 18th sigma layer to the 20th layer, the downward vertical velocity also increases. Therefore, the velocity shows that the outflow water of the Persian Gulf has entered the Gulf of Oman from near Jask Cape in the deep layer (yellow spots of sigma 19 in Figure 2).

Figure 3 shows the horizontal velocity of the 20th layer. In the areas where there was a downward vertical velocity value (56.9˚E to 57.25˚E), the horizontal velocity was also higher (red colors). It is -44 cm/s in winter, -32cm/s in spring, 70cm/s in summer and 60cm/s in autumn. In this area, there is a continental shelf break and a change in depth. In the surrounded areas, the flow velocity is lower (about 20 cm/s). In spring and autumn, in the eastern regions of the study basin (59 to 60˚E longitudes), the horizontal velocity is higher and its value reaches 30 cm/s. In a study that presented the general circulation of salinity in the Strait of Hormuz, the horizontal velocity of the dense water flow from the Persian Gulf to the Gulf of Oman was found to be 41 cm/s [31]. Another study [32] found the maximum velocity value for PGW flow in these areas to be 40 cm/s in summer and 55 cm/s in winter. Also, the speed of PGW in August and March was 35 cm/s and 69 cm/s, respectively [33]. The results of this study are in good agreement with the mentioned studies.

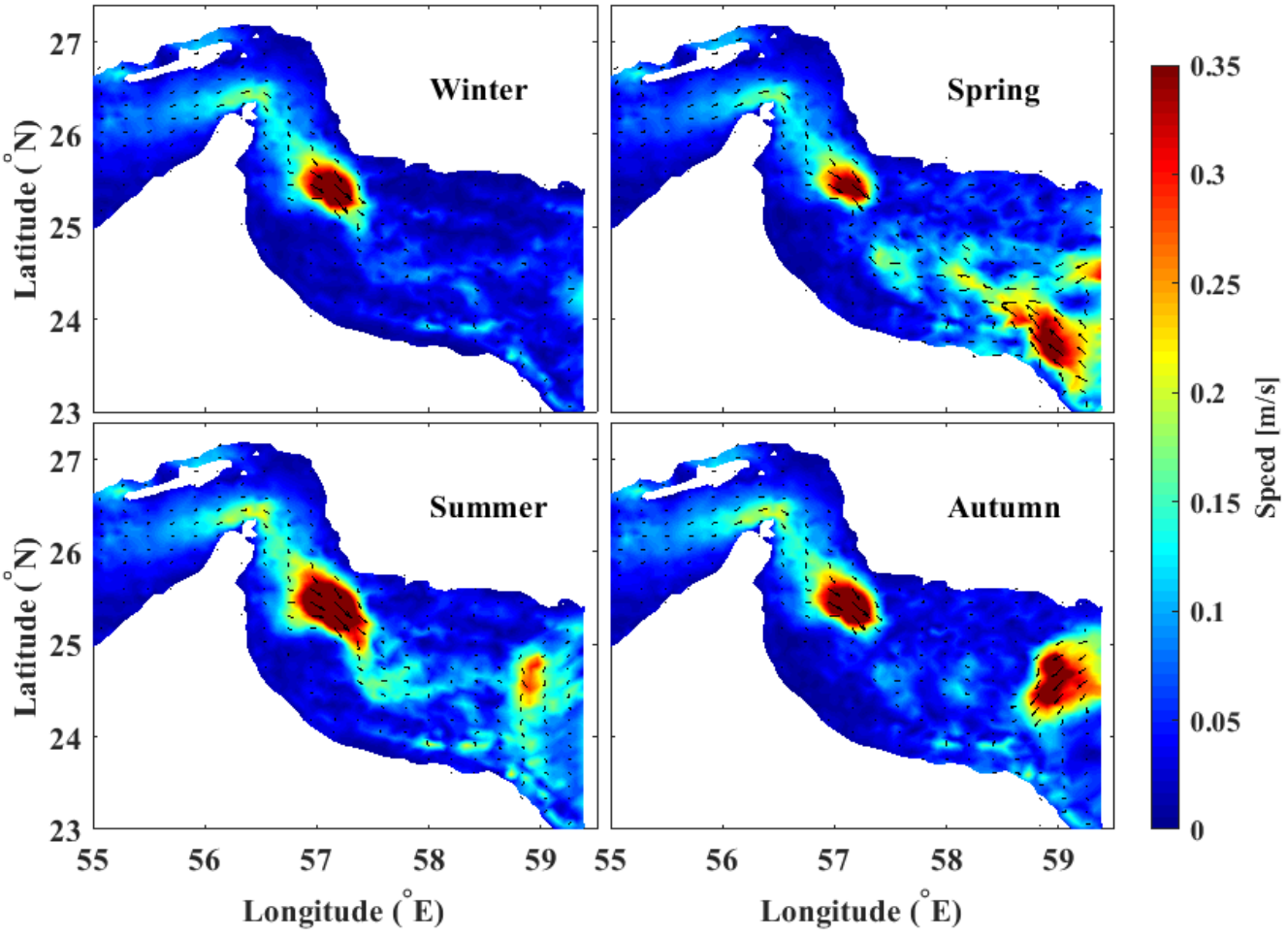

Figure 3. The simulation of the horizontal speed in the lowest layer (sigma=20) for winter, spring, summer and autumn.

It can be seen from Figure 4 that in winter, the eastern areas, which contain Gulf of Oman water entering to the Persian Gulf, have lower salinity (about 36.6 psu to 36.9 psu), and although in the western part, the surface

water has a salinity of 36.6 psu but in these areas, with increasing depth, the water salinity is increasing, and at depths more than 60 meters to 110 meters, the water salinity reaches between 37 psu and 37.8 psu (Figure 4, winter). The water salinity in the surface layer in spring is around 37.5 psu to 37.2 psu. The salinity more than 37.5 psu covers most of the deep water area in this season, which shows that the water with higher density has settled in the lower layers. (Figure 4, spring). In summer, the water in the eastern part is less saline, but in compared with winter, its salinity has increased. In the surface layers, the water salinity ranges from 36.5 psu to 37.2 psu, and in the western part, in the deep layers, the salinity is from 38 psu to 38.2 psu, which is the water outflow of the Persian Gulf (Figure 4, summer). In autumn, a saline water spot can be seen in the deep parts of the area, which indicates that water with more salinity has penetrated to the deep parts the same as winter (Figure 4, autumn).

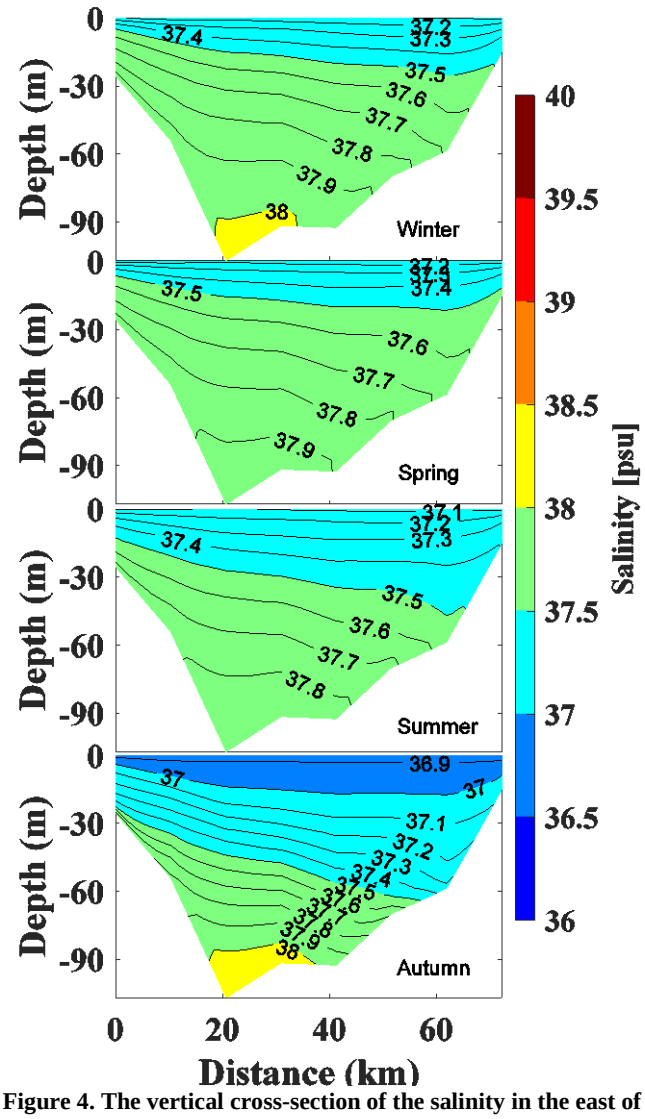

Figure 4. The vertical cross-section of the salinity in the east of the Strait of Hormuz in winter, spring, summer and autumn in section AA' (Figure 1).

The comparison of summer and winter from Figure 4 clearly shows the infiltration of salt water in winter season compared to summer. Figure 4 also shows the slope of the salt wedge exiting the Persian Gulf. The slope in Figure 4 is the boundary between cyan and light green color. It can be seen that these borders have different slopes in different seasons. In the summer, it can be seen that the color change occurs at a distance of about 60 kilometers (in the longitudinal direction) from a depth of 20 meters to a depth of 60 meters (40-meters differences in the vertical direction), that is, the calculated angle for this boundary is equal to 3.8×10^{-2} degrees. In the winter, at a horizontal distance of 40 kilometers from a depth of 20 meters to 80 meters (60-meters differences in the vertical direction), the color change is observed, that is, the angle calculated for winter slope is equal to 5.1×10^{-1} degrees. Although these angles are very small values, they are different for two seasons, summer (3.8×10^{-2} degrees) and winter (5.1×10^{-1} degrees). This fact indicates a stronger stratification of salinity in the summer season than in the winter season. Figure 4 also shows that in summer, the salinity contour lines are very close to each other, as a result, there is a stronger stratification in summer. In winter, the calculated slope is larger than summer, and the larger angle or the steeper slope (tangent of angle) of the boundry layer, the greater horizontal component of the water weight force ($mg\sin\theta$) that causes the water to move downward (Figure 5), and the water moves faster (Figure 5). According to this reasoning, the water in the Persian Gulf drains earlier and moves to lower depths sooner.

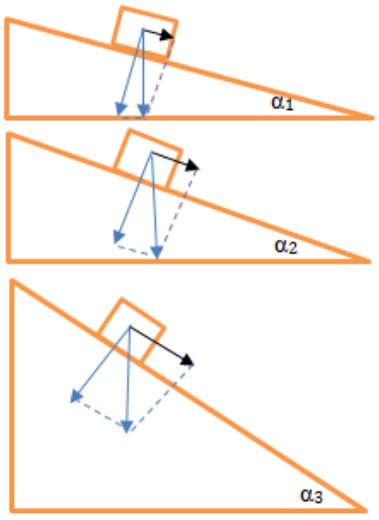

Figure 5. The comparison of the horizontal component of three water parcels placed on three different inclined surfaces with slopes α_1, α_2 and α_3 ($\alpha_1 < \alpha_2 < \alpha_3$).

The vertical section of temperature for the Strait of Hormuz for the seasons of the year is drawn in Figure 6. In winter, the water temperature of the surface layer is about 28°C, it is higher in the middle region, and lower in the western regions. The temperature of the lower layers decreases as the depth increases. In the lower layers, there is a larger volume of water in winter, with a lower temperature than summer, which shows that the outgoing mass, which has a higher salinity (Figure 4), has penetrated to deeper parts and indicates

the existence of the phenomenon of submergence in these areas (Figure 6). In spring, the water temperature in the western regions of the region is lower than other seasons (27.2°C) and a larger volume of water with a temperature of about 26.3°C is located in the middle layers. In summer, the surface water temperature is 30°C to 31°C, which decreases from east to west. In central areas, the water temperature is 30.4°C, and in the western part, from the surface to the depth, the water temperature decreases, and in the lower depths, the water temperature has reached 24.5°C (Figure 6, summer). In autumn, there is water with a temperature of 28°C in the surface layer, and water with a higher temperature (28.5°C) is also seen in middle areas, and with the depth increase, the temperatures of the lower layer decrease. The bed temperature reaches 26.7°C in autumn. A week stratification of temperature is also observed in autumn.

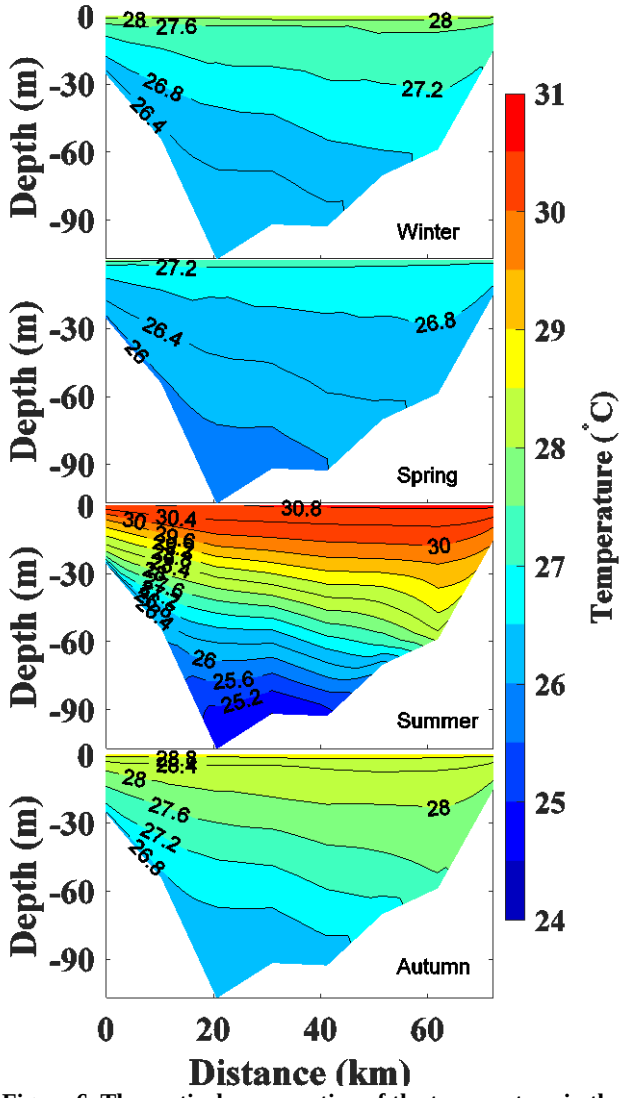

Figure 6. The vertical cross-section of the temperature in the east of the Strait of Hormuz in winter, spring, summer and autumn in section AA' (Figure 1).

This sinking of the saline water mass in winter mentioned in Figure 4 may be due to the lower temperature (Figure 6) and as a result, its higher density. It is expected that the movement of this warm and saline water mass will continue towards greater longitudes and greater depths, which is in good agreement with Khalilabadi (2015) [34]. Although many studies have shown the presence of Persian Gulf water in the Gulf of Oman [15-17, 20, 31-33, 35-38], the seasonal changes of its penetration in Gulf of Oman can be seen in [39-41]. Ramak et al., (2023) [41] showed that the Persian Gulf water mass with salinity (38.00 psu) flows out through the south of the Strait of Hormuz in the form of a subsurface flow in summer, and this water mass penetrates to greater depths and moves further away from the Strait of Hormuz in winter.

5. Conclusions

Investigating the seasonal changes of speed in this study clearly showed that an increase in speed can be seen in the lower layers. This increase of the speed for the deep layer (20th layer) and and a layer before the last layer (19th layer) is in opposite directions near Jask Cape. This fact indicates a two-way movement in the deep layers. The examination of temperature and salinity changes also showed that water infiltration in 25.19-25.48°N and 57.12-57.26°E is more in winter than all other seasons which indicates that more water sinks in these areas. This feature is in good agreement with other studies.

List of Symbols

E	Longitude [in ˚]
FVCOM	Finite-Volume Coastal Ocean Model
GHRSST	Group for High Resolution Sea Surface Temperature [in ˚C]
HYCOM	HYbrid Coordinate Ocean Model
N	Latitude [in ˚]
OSTIA	The Operational Sea Surface Temperature and Sea Ice Analysis
SMS	Surface-water Modeling System
TMD	Tidal Model Driver

8. References

[1] Brown E., Colling A., Park D., Phillips J., Rothery D., and Wright J. (2004), *Ocean Circulation*. 2nd ed. Boston Johannesburg: Jointly published by the Open University.

[2] Johannessen O.M., Subharaju G. and Blindhelm J. (1981), *Seasonal variation of the oceanographic conditions off the southwest coast of India during 1972-75*. Fiskeridirektoratets Skrifter Serie Havunders kelser, Vol.18, p.247-261.

[3] Mathew B. (1983), *Studies on upwelling and sinking in the seas around India*. University of Cochin, Cochin. PhD Thesis. p. 159

[4] Shetye S.R., Gouveia A.D., Shenoi S.S.C., Sundar D., Michael G.S., Almeida A.M., and Santanam K., (1990), *Hydrography and circulation off the west coast of India during the south-west monsoon 1987*. Journal of Marine Research, Vol.48(2), p.359-78.

[5] Hareesh Kumar P.V. and Basil M. (1997), *Salinity distribution in the Arabian sea.* Indian Journal of Marine Science, Vol.26(1), p.272-77.

[6] Mathew B., Sanilkumar K.V., Hareesh Kumar P.V., Madhusoodanan P. and James V.V. (1992), *Thermohaline and current structure off Cochin during December 1986*. Indian Journal of Marine Science, Vol.20, p.244-48.

[7] Zhou S., and Flynn P.C. (2005), *Geoengineering Downwelling Ocean Currents: A Cost Assessment*. Climatic Change. Vol.71, p.203–220. doi.org/10.1007/s10584-005-5933-0

[8] Sadrinasab M. (2009), *Three-dimensional numerical modeling study of the coastal upwelling in the Persian Gulf.* Research Journal of Environmental Science. Vol.3(5), p.560-566.

[9] McCreary J.P., Kundu P.K., and Molinari R.L. (1993), *A numerical investigation of dynamics, thermodynamics and mixed-layer processes in the Indian Ocean*, Progress in Oceanography, Vol.31(3), p.181–244, doi.org/10.1016/0079-6611(93)90002-U.

[10] Shetye S.R., Suresh I., Shankar D., Sundar D., Jayakumar S., Mehra P., Prabhudesai R.G., and Pednekar P.S. (2008), *Observational evidence for remote forcing of the West India Coastal Current*, Journal of Geophysical Research, Vol.113, p.C11001, doi.org/10.1029/2008JC004874.

[11] Shankar D. (1998), *Low-frequency variability of sea level along the coast of India*. PhD thesis, Goa University, Goa, India

[12] Shankar D., Vinayachandran P. and Unnikrishnan A.S. (2002), *The monsoon currents in the north Indian Ocean*. Progress in Oceanography, Vol.52, p.63–120.

[13] Shankar D., Remya R., Vinayachandran P.N., Chaterjee A., and Behera A. (2016), *Ihibition of mix-layer deepining during winter in the north-estern Arabian Sea by the west India Coastal Current.* Climate Dynamics, 47, 1049-1072. doi: 10.1007/s00382-015-2888-3.

[14] Vijith V., Vinayachandran P.N., Thushara V., Amol, P., Shankar D., and Anil A.C. (2016), *Consequences of inhibition of mixed-layer deepening bythe West India Coastal Current for winter phytoplankton bloom in the northeastern Arabian Sea*, Journal of Geophysical Research: Oceans, Vol. 121, p.6583–6603, doi:10.1002/2016JC012004.

[15] Pous S., Carton X., and Lazure P. (2004), *Hydrology and circulation in the Strait of Hormuz and the Gulf of Oman—Results from the GOGP99 Experiment: 1.Strait of Hormuz.* Journal of Geophysical Research Oceans. 109(C12). doi:10.1016/0016/2003JC002145 .

[16] Reynolds R.M. (1993), *Physical oceanography of the Gulf, Strait of Hormuz, and the Gulf of Oman—Results from the Mt Mitchell expedition*. Marine Pollution Bulletin. 27, 35-59.

[17] Soyufjahromi M. (2023). *The spatial and temporal monitoring of the sea surface temperature anomaly of the Strait of Hormuz*. International Journal Of Coastal and Offshore, And Environmental Engineering, accepted manuscripted. Available on line: 2023-01-16.

[18] Akbari P. Sadrinasab M. Chegini V. and Siadatmousavi M. (2016). *Tidal constituents in the Persian Gulf, Gulf of Oman and Arabian Sea: a numerical study*. Indian Journal of Geo-Marine Sciences. 45(8), 1010-1016.

[19] Soyuf Jahromi M. and Emami M. (2021). *The role of different positions of tidal turbines for energy extraction in Qeshm channel*. International Journal Of Coastal, Offshore And Environmental Engineering, 6(5), 1-9.

[20] Yao F. and Johns W.E. (2010), *A HYCOM modeling study of the Persian Gulf: 2. Formation and export of Persian Gulf Water*. Journal of Geophysical Research Oceans. 115(C11). doi:10.1029/2009JC005788.

[21] Chen C., Beardsley R., Cowles G., Qi J., Lai Z., Gao J., Stuebe D., Xu Q., Xue P., Ge J., Hu S., Ji R., Tian R., Huang H., Wu L., Lin H., Sun Y. and Zhao L. (2013), *An Unstructured Grid, Finite-Volume Community Ocean Model FVCOM User Manual*. FVCOM user manual, 416p.

[22] Chen C., Beardsley R.C. and Cowles G. (2006), *An unstructured grid, finite-volume coastal ocean model: FVCOM User Manual*. SMAST/UMASSD Technical Report-06-0602, University of Massachusetts-Dartmouth, New Bedford.

[23] Li B., Tanaka K.R., Chen Y., Brady D.C. and Thomas, A.C. (2017), *Assessing the quality of bottom water temperatures from the Finite-Volume Community Ocean Model (FVCOM) in the Northwest Atlantic Shelf region*. Journal of Marine Systems, 173, 21-30.

[24] IOC, IHO and BODC, (2003), *Centenary Edition of the GEBCO Digital Atlas, PUblished on CD-ROM on behalf of the Intergovernmental Oceanographic Commissioner and the International Hydrographic Organisation as part of the General Bathymetric Chart of the Ocean*. British Oceanographic data center, Liverpool.

[25] Brigham Young university, (2011), *SMS-Surface Water Modeling System Reference Manual Version 10*. Brigham young university-Enviromental Modeling Reference Laboratory, Provo, UT

[26] http://www.aquaveo.com

[27] http://www.gebco.net

[28] https://hycom.org

[29] The MathWorks Inc., (2016), *MATLAB and Statistics Toolbox 64-bit*, Version 2016a, Release 2016a, Natick, Massachusetts, USA.

[30] MetOffice, (2018), *The Operational Sea Surface Temperature and Sea Ice Analysis (OSTIA) system* https://www.ecmwf.int/sites/default/files/elibrary/2018/17975-operational-sea-surface-temperature-and-ice-analysis-ostia-system.pdf

[31] Thoppil P.G., and Hogan P.J., (2009), *On the mechanisms of episodic salinity outflow events in the Strait of Hormuz*. Journal of Physical Oceanography 39(6), 1340–1360.

[32] Bower A.S., Hunt H.D. and Price J.F. (2000), *Character and dynamics of the Red Sea and Persian Gulf outflows.* Journal of Geophysical Research: Oceans, 105(C3), 6387-6414.

[33] Ezam M., Bidokhti A.A. and Javid, A.H., (2010), *Numerical simulations of spreading of the Persian Gulf outflow into the Oman Sea*. Ocean Science., 6, 887–900, 2010.

[34] Khalilabadi M., (2015), *Three-dimensional simulation of water circulation in Oman Sea using MITgcm model*, Hydrophysics, Vol.2 (1), p.61-68.

[35] Johns, W. E., Yao, F., Olson, D. B., Josey, S. A., Grist, J. P., and Smeed, D. A. (2003). *Observations of seasonal*

exchange through the Straits of Hormuz and the inferred heat and freshwater budgets of the Persian Gulf. Journal of Geophysical Research: Oceans, Vol.108(C12).

[36] Azizpour J., Siyadat Mousavi Seyed Mostafa Siadat Mousavi S.M., and Chegini V. (2015). *Study of Physical Oceanographic Parameters in the Strait of Hormuz*, Hydrophysics, Vol.1(1), p.15-24.

[37] Ramak, H., Soyufjahromi, M., and Akbari, P. (2022). *Using surface temperature data of the Oman Sea to identify subsurface water of the Persian Gulf*. Hydrophysics, Vol.7(2), accepted manuscripted. Available on line: 2022-11-19.

[38] Ramak H, Soyufjahromi M, Akbari P. (2022). *Persian Gulf Water mass tracking by surface temperature and salinity properties*. Journal of Oceanography, Vol.12 (48), p.13-28.

[39] Ramak H, Soyufjahromi M, Akbari P. (2023). *Investigation of salinity and temperature of Persian Gulf water by FVCOM Model*. Journal of Oceanography, accepted manuscripted, 2022-11-19.

[40] L'Hégaret, P., Carton, X., Louazel, S., & Boutin, G. (2016). *Mesoscale eddies and submesoscale structures of Persian Gulf Water off the Omani coast in spring 2011*. Ocean Science, Vol.12(3), p.687-701.

[41] Ramek H, Soyufjahormi M, Akbari. P, (2023). *Investigation of physical properties of Persian Gulf water exchange using FVCOM Model*. Journal of oceanography, accepted manuscript 2022.

INTERNATIONAL JOURNAL OF
COASTAL, OFFSHORE & ENVIRONMENTAL ENGINEERING IJCOE Vol.8/No. 1/winter 2023 (10-15)

Available online at: www. Ijcoe.org

Underwater Ship-radiated Acoustic Noise Recognition Based on Mel-Spectrogram and Convolutional Neural Network

Mohammad Reza Khalilabadi

Faculty of Naval Aviation, Malek Ashtar University of Technology, Iran; khalilabadi@mut.ac.ir

ARTICLE INFO

Article History:
Received: 16 Jan. 2023
Accepted: 14 Feb. 2023

Keywords:
Underwater Acoustic
Deep Learning
Recognition
Noise
CNN

ABSTRACT

The abstract should include the One of the most exciting topics for researchers over the past few years is detecting underwater acoustic noises. Meanwhile, the complicated nature of the ocean makes this task very challenging. Also, making signals formatted data compatible with machine learning approaches needs much knowledge in signal processing for feature detection. This paper proposed a method to overcome these challenges, which extracts features with Convolutional Neural Network (CNN) and Mel-spectrogram (converting signal data to images). This method needless knowledge in signal processing and more knowledge in machine learning; because using CNNs find the hidden pattern and knowledge of the data automatically. The proposed approach detected the presence of the ships and categorized them into different kinds of them with 99% accuracy that is a noticeable improvement considering state of the art. The performed CNN models consist of 2 CNN layers for feature extraction and a Dense layer for classification the underwater ship noises.

1. Introduction

Underwater acoustic noise is one of the most attractive and widely used topics in acoustic oceanography. Several researches have been done by the author in the field of oceanography (e.g. [1]–[12]), and especially acoustic oceanography([13]-[14]). Recently, this path of development has progressed towards the use of artificial intelligence in predicting the environmental characteristics of the ocean[15].

Detecting underwater noises played an essential role in many oceanographic applications like navigation systems and defense systems.

The source of the underwater noises can be categorized as human maids like ships, drilling rigs, and aircraft; the other category is natural noises like raining noise, marine mammal's noise, and wind. There are many different radiated noise signals in the oceans, making the detection task quite tricky.

The most challenging part of this challenge is extracting efficient features that maid ship radiated noise feature extraction an active area in many years. In all of the research, three different feature extraction strategies alongside a classification model were used for this task.

The hand-designed features that need prior knowledge of data set and expertness in signal processing engineering are the first to extract features. For example, using spectral and cepstral, which used by Das et al. [16] and Santos-Domínguez et al.[17], Jain et al., used line spectrum density for feature extraction and support vector machine for classification. Wei et al. [18] used features based on wavelet packets. Yang et al. [19] dissimilarity-based evaluation-based features for classification. Zhang et al. [20] used Mel-Spectrum coefficient features for ship radiated recognition. Wei et al., used $1_{1/2}$D spectrum-based spectrum features for ship radiated noise classification. First-order alongside second-order differential MFFC were used by Zhang et al.[20] for underwater signal recognitions. However, these approaches suffer from low detection rates in noisy, shallow seas and unavailability to find time-series and complicated hidden patterns of data and need domain skill in signal engineering.

The second strategy for extracting the features from underwater noise signals is using automatically generated features like Shen et al., that used one dimensional CNN for extracting features directly from spectrums[21]. Cao et al. used a stack auto-encoder that extracted hidden and complicated information and patterns from data[22]. Yang et al. used Deep Belief Network

(DBN) for feature extraction[19]. Finally, yuan et al. used a multimodal Deep Learning approach for ship radiate noise recognition[23].

The 3rd strategy is the combination of the two first strategies, which means using the hand-designed features alongside the automatically generated features or feeding the hand-designed features to a machine learning feature extractor model. For example, Ke et al., used Restricted Boltzmann Machine (RBM) to generate automatic features and used these features alongside wavelet, spectral, etc.[24]. Finally, they feed these two kinds of features to two-dimensional feature fusion.

In this paper, we proposed a model for underwater ship radiated noise recognition based on 3rd strategy, which means we are not using the original spectrum as input of CNN like Shen et al., but using a pre-processing approach for transforming the spectrums into images named Mel-Spectrogram and then using Deep Neural Network with two, two dimensional CNN layers and one dense layer to find the hidden pattern of data and then detect the label[21]. Our proposed approach performed better or at least competitive to under introduced approaches. Also, using Mel-Spectrogram makes the model converge very fast (30 epochs).

2. Materials and Methods

In this section, an explanation of the proposed methodology for ship radiated noise has been provided.

In this research, we used Mel-Spectrogram as a preprocessing stage to make the spectrums compatible as the input of the 2-dimensional CNN. A Mel-spectrogram is a spectrogram where the frequencies are converted to the Mel scale.

In this method, the signal is first converted from time domain to frequency domain by using of FFT (Fast Fourier Transform). Then, the frequency converts to the mel scale.

After that, we applied power-to-DB scaling to convert a power spectrogram (amplitude squared) to decibel (dB) units. This algorithm is calculated by equation 1.

$$db_{units} = 10\log(\text{spectrogram}) \qquad (1)$$

This algorithm makes the spectrum more visible. the effect of power-to-DB scaling before and after applying this algorithm can be followed in the research of Lavanya et al. [25]. After that, a deep CNN model will be applied to the model for prediction. CNN is a class of deep neural networks, most commonly applied to analyze visual images[26]. Typical of a simple neural network, a CNN consists of three input, output, and hidden layers. Any neural network layers between input and output are named hidden because their inputs and outputs are transformed by the activation function, feature mapping, and convolution.

In a CNN, the hidden layers include layers that performed a transformation named convolutions. That is a layer that performs a feature mapping using the dot product of the convolution kernel with the layer's input.

As the kernel slides along the input matrix for the layer, a feature map will be generated using convolutional operation, which is devoted to the input of the next layer. The convolutional layers are the layers with the input shape of the number of inputs, input height, input width, and input channels. After input data passed through a convolutional layer, it is transformed to an abstracted feature map that is also named an activation map with a shape with axis similar to input but different dimensions.

A convolutional layer contains different hyper parameters which are:

1. Convolutional kernels: extract features from input data that is moved across the image and multiplied with the image.
2. The number of input and output channels.
3. Padding: defined the padding strategy to apply in the input like Valid Padding and Same Padding.
4. Stride: filters that modify the amount of movement over the image

Convolutional layers convolve the input and pass its result to the next layer. This is similar to the response of a neuron in the visual cortex to a specific stimulus[27].

The advantage of convolution is reducing the number of free parameters and allowing the network to be deeper[28].

The designed model includes four convolutional, two max-pooling, one Flatten, one Dropout, and one dense layer. Figure 1, shows the structure of the proposed model.

2.1. Experimental Dataset

All data of ship-radiated noise used in this paper come from a database called Ships-Ear[17].

During 2012 and 2013, sounds of many different ships were recorded on the Spanish Atlantic coast and included in the Ships-Ear database(available at http://atlanttic.uvigo.es/underwaternoise/).

The recordings were made with autonomous acoustic digitally SR-1 recorders manufactured by Mar Sensing LDA (Faro, Portugal). According to Santos-Domínguez et al. [17], 11 vessel types are merged into four practical classes (based on vessel size) and one background noise class, as shown in Table 1. Some ship pictures and ship-radiated noise of each class are demonstrated in figure 2.

Table 1. Ships Grouping

Class	Type
Class A	fishing boats, trawlers, mussel boats, tugboats, dredgers
Class B	motorboats, pilot boats, sailboats
Class C	passenger ferries
Class D	ocean liners and ro-ro vessels
Class E	background noise recordings

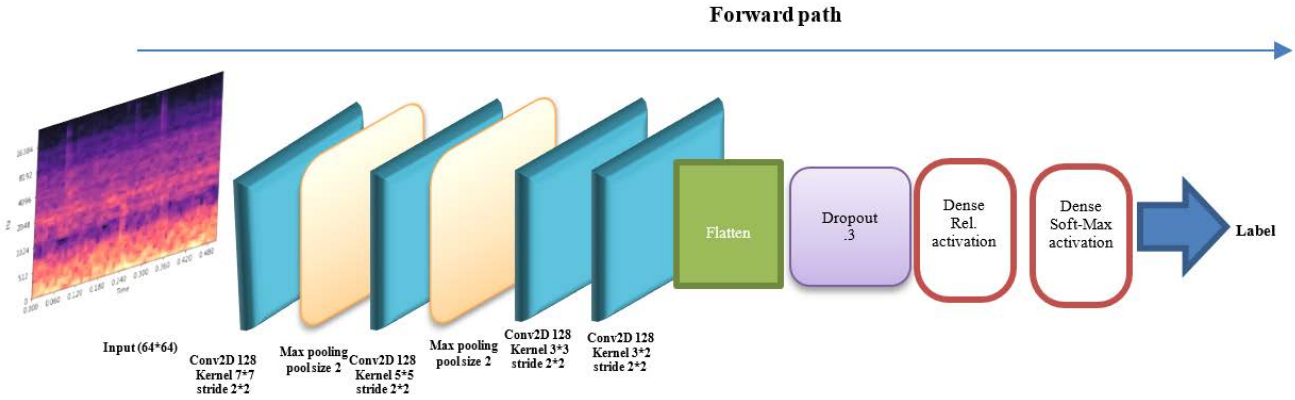

Figure 1. Proposed CNN Structure

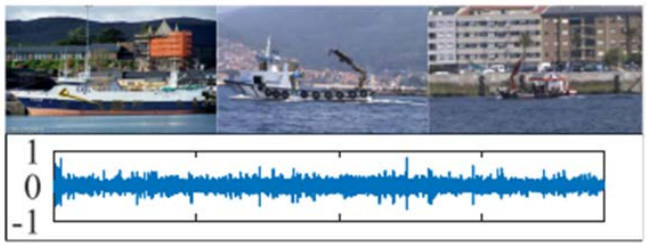

(a)

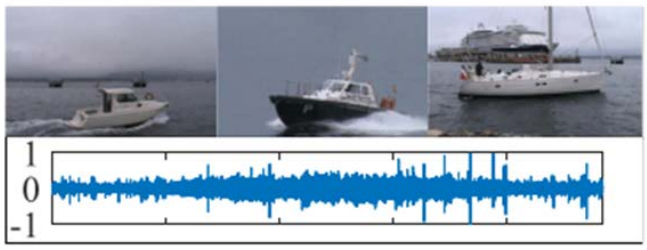

(b)

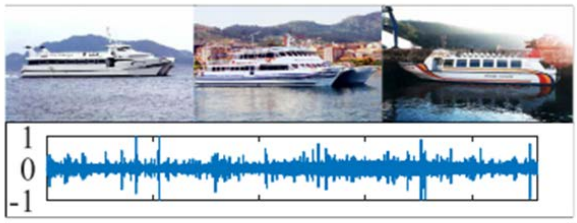

(c)

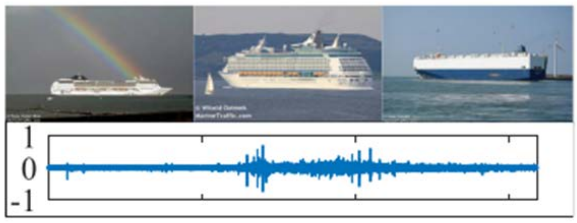

(d)

Figure 2. Ship pictures and ship-radiated noise of each class. (a) class A. (b) class B. (c) class C. (d) class D

2.2. Experimental Setup

All the codes are performed using google collaborator with python language and GPU enable Tensor Flow.
The hyper parameter of the framing and spectrogram generation have been provided in table 2.
All of these hyper-parameters have been calculated using cross-validation strategy. Also, we randomly select .8 of data as training set and .2 data as the testing set.

Table 2. Hyper-Parameters of the Pre-Processing Stages

Stage	Hyper parameters	
Loading data	Sampling rate	52,734
Framing	frame length	26,367
	hop length	5,273 (.8 overlapping)
Mel spectrogram	Sampling rate	52734
	n_mels	64
	hop length	415
	n_fft	1280

2.3 Evaluation Metrics

Our approach's performance was evaluated using the following metrics:

1. Accuracy rate (AC): Percentage of correctly classified records overall records Formula.

$$AC = \frac{TP + TN}{TP + TN + FP + FN} \times 100\% \quad (2)$$

2. Precision rate (P): Percentage of correctly classified anomaly records over a total of classified anomalies[29].

$$P = \frac{TP}{TP + FP} \times 100\% \quad (3)$$

3. Recall (R): Percentage of correctly classified anomalies divided by the number of attack entries[29].

$$R = \frac{TP}{TP + FN} \times 100\% \quad (4)$$

4. F-Measure (F1-Score): Harmonic mean of precision and recall, which is considered.

$$F = \frac{2 \times P \times R}{P + R} \times 100\% \quad (5)$$

4. Results and Discussion

In this section, the evaluation results considering the mentioned evaluation metrics have been provided.
As a result, we achieved a noticeable accuracy in ship-radiated noise recognition (99.20%), which is quite an outstanding achievement.
Table 3 shows the classification report of the proposed approach on different class labels, which shows 99% precision, 99.25% recall, and 99.12% f1-score.

Also, Table 4 shows the confusion matrix of the proposed approach that shows how many instances of each class have been predicted correctly and, in the case of incorrect classification, what class it was detected.

Table 3. Classification report of proposed approaches in different classes

Class label	Precision%	recall%	f1-score%	Accuracy%
A	98.91	98.72	98.81	-
B	97.31	99.09	98.19	-
C	99.67	98.98	99.33	-
D	99.69	99.73	99.71	-
E	99.42	99.73	99.57	-
macro Average	99.00	99.25	99.12	99.20

Also, for showing that our model training convergence process and the effect of the process on training and testing data figure 3 shows the accuracy improvement during testing. Figure 4 shows the loss changing during training.

Table 4. Confusion matrix of the proposed model

Predicted label / True Label	A	B	C	D	E
A	3460	34	10	1	0
B	5	3033	14	0	9
C	22	48	8469	11	6
D	11	0	2	4885	0
E	0	2	2	3	2564

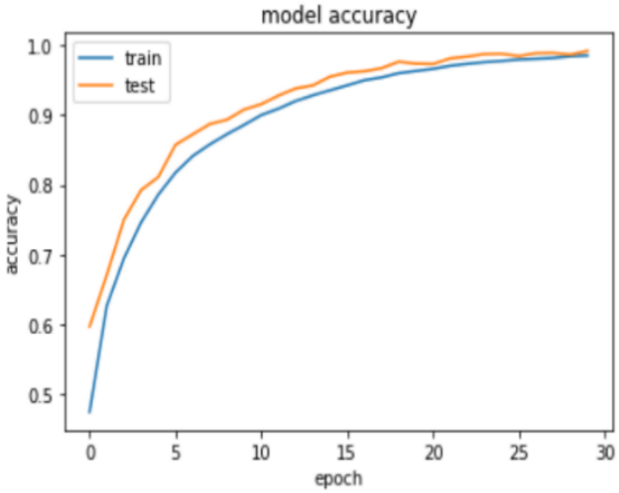

Figure 3. Changing of accuracy in training set and testing set during training

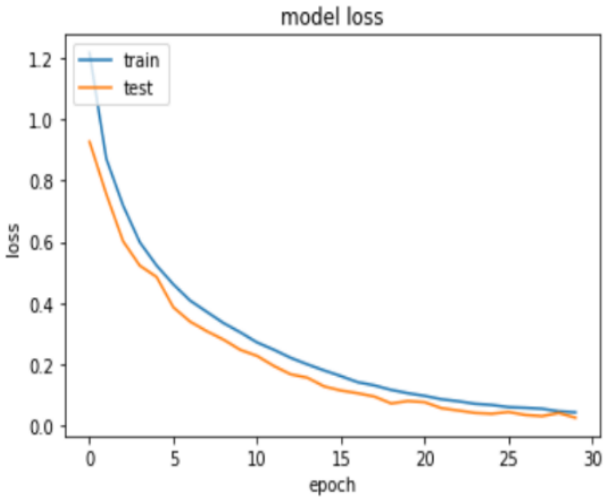

Figure 4. Changing of loss in the training set and testing set during training

3. CONCLUSION

In this research, we proposed a ship radiated noise recognition model based on Mel-Spectrogram and Convolutional Neural network. As an essential stage of studies in the same field is to provide features for the machine learning model, we used the Mel-Spectrogram for this process and fed the 64*64 generated images to the CNN. The result shows our proposed approach achieved a significant result considering accuracy, precision, recall, and f1-score.

References

[1] M. R. Khalilabadi, "Underwater Terrain and Gravity aided inertial navigation based on Kalman filter," *Int. J. Coast. Offshore Eng.*, vol. 5, no. 3, pp. 15–21, 2022.

[2] M. R. Khalilabadi, "The effect of meteorological events on sea surface height variations along the

northwestern Persian Gulf.," *Curr. Sci. 00113891*, vol. 110, no. 11, 2016.

[3] M. R. Khalilabadi, " 3D modeling of Circulation in the Oman Sea Using the MITgcm Model," *Hydrophysics*, vol. 2, no. 1, pp. 61–68, 2016.

[4] M. R. Khalilabadi, "Tide–surge interaction in the Persian Gulf, Strait of Hormuz and the Gulf of Oman," *Weather*, vol. 71, no. 10, pp. 256–261, 2016.

[5] M. R. Khalilabadi and M. Akbari Nasab, "Study of static stability and double diffusion in the Oman Sea," *Iran. J. Mar. Sci. Technol.*, vol. 18, no. 71, pp. 11–19, 2014.

[6] M. R. Khalilabadi and B. Behrooz, "Simulation of volumetric flow at the Arvandrood estuary using the MIKE21 model," *Hydrophysics*, vol. 5, no. 2, pp. 1–10, 2020.

[7] M. R. Khalilabadi and B. S. H. HASSANTABAR, "Investigation of magnetic field fluctuations due to sea waves in the Strait of Hormuz," 2016.

[8] M. R. Khalilabadi and D. Mansouri, "Effect of super cyclone 'GONU' on sea level variation along Iranian coastlines," 2013.

[9] M. R. Khalilabadi and H. Shahmirzaee, "Marine Magnetic Data Processing and Extracting Magnetic Anomaly," *Hydrophysics*, vol. 3, no. 1, pp. 1–10, 2017.

[10] M. R. Khalilabadi, M. Sadrinassab, V. Chegini, and M. Akbarinassab, "Internal Wave Generation in the Gulf of Oman (Outflow of Persian Gulf)," 2015.

[11] M. Akbarinasab, M. R. Khalilabadi, and M. M. Moghadam, "Impact of relative vorticity on sea level fluctuations on the South coast of Caspian Sea.," *Casp. J. Appl. Sci. Res.*, vol. 5, no. 4, 2016.

[12] A. Ghorbani and M. R. Khalilabadi, "Positioning Using Classification and Regression: Case study of Oman Sea," *Int. J. Coast. Offshore Eng.*, vol. 4, no. 3, pp. 35–41, 2020.

[13] S. H. Hosseini, M. Akbarinasab, and M. R. Khalilabadi, "Numerical simulation of the effect internal tide on the propagation sound in the Oman Sea," 2018.

[14] M. R. Khalilabadi, "2D Modeling of Wave Propagation in Shallow Water by the Method of Characteristics," *Arch. Acoust.*, vol. 47, no. 3, pp. 407–412, 2022.

[15] M. R. Khalilabadi, "An autonomous location prediction model for maritime transport applications: a case study of Persian Gulf," *Ships Offshore Struct.*, pp. 1–8, 2022.

[16] A. Das, A. Kumar, and R. Bahl, "Marine vessel classification based on passive sonar data: the cepstrum-based approach," *IET Radar Sonar Navig.*, vol. 7, no. 1, pp. 87–93, 2013.

[17] D. Santos-Domínguez, S. Torres-Guijarro, A. Cardenal-López, and A. Pena-Gimenez, "ShipsEar: An underwater vessel noise database," *Appl. Acoust.*, vol. 113, pp. 64–69, 2016.

[18] X. Wei, L. I. Gang-Hu, and Z. Q. Wang, "Underwater target recognition based on wavelet packet and principal component analysis," *Comput Simul*, vol. 28, pp. 8–290, 2011.

[19] H. Yang, S. Shen, X. Yao, M. Sheng, and C. Wang, "Competitive deep-belief networks for underwater acoustic target recognition," *Sensors*, vol. 18, no. 4, p. 952, 2018.

[20] L. Zhang, D. Wu, X. Han, and Z. Zhu, "Feature extraction of underwater target signal using mel frequency cepstrum coefficients based on acoustic vector sensor," *J. Sens.*, vol. 2016, 2016.

[21] S. Shen, H. Yang, and J. Li, "Improved auditory inspired convolutional neural networks for ship type classification," in *OCEANS 2019-Marseille*, 2019, pp. 1–4.

[22] X. Cao, X. Zhang, Y. Yu, and L. Niu, "Deep learning-based recognition of underwater target," in *2016 IEEE International Conference on Digital Signal Processing (DSP)*, 2016, pp. 89–93.

[23] F. Yuan, X. Ke, and E. Cheng, "Joint representation and recognition for ship-radiated noise based on multimodal deep learning," *J. Mar. Sci. Eng.*, vol. 7, no. 11, p. 380, 2019.

[24] X. Ke, F. Yuan, and E. Cheng, "Integrated optimization of underwater acoustic ship-radiated noise recognition based on two-dimensional feature fusion," *Appl. Acoust.*, vol. 159, p. 107057, 2020.

[25] K. Lavanya, C. L. Devi, M. D. Sree, and P. N. Shareef, "Predicting the Emotions Based on Emoji's and Speech Using Machine Learning Techniques," 2021.

[26] M. V. Valueva, N. N. Nagornov, P. A. Lyakhov, G. V. Valuev, and N. I. Chervyakov, "Application of the residue number system to reduce hardware costs of the convolutional neural network implementation," *Math. Comput. Simul.* vol. 177, pp. 232–243, 2020.

[27] I. M. Dheir, A. S. A. Mettleq, A. A. Elsharif, and S. S. Abu-Naser, "Classifying nuts types using convolutional neural network," *Int. J. Acad. Inf. Syst. Res. IJAISR*, vol. 3, no. 12, 2020.

[28] H. H. Aghdam and E. J. Heravi, "Guide to convolutional neural networks," *N. Y. NY Springer*, vol. 10, no. 978–973, p. 51, 2017.

[29] D. M. Powers, "Evaluation: from precision, recall and F-measure to ROC, informedness, markedness and correlation," *ArXiv Prepr. ArXiv201016061*, 2020.

INTERNATIONAL JOURNAL OF
COASTAL, OFFSHORE & ENVIRONMENTAL ENGINEERING IJCOE Vol.8/No. 1/winter 2023 (16-25)

Available online at: www. Ijcoe.org

Variation of monthly exploitable wave energy in the Gulf of Chabahar under a high-resolution CMIP6

Mahmoud Pourali [1*], Mohamad Reza Kavianpour[2]

[1] *Faculty of Civil Engineering, K.N. Toosi University of Technology; m.pourali@email.kntu.ac.ir*
[2] *Faculty of Civil Engineering, K.N. Toosi University of Technology; kavianpour@kntu.ac.ir*

ARTICLE INFO

Article History:
Received: 28 Oct. 2022
Accepted: 11 Dec. 2022

Keywords:
Wave energy
Climate change
Weibull-based bias-correction
Gulf of Chabahar
Emission scenario

ABSTRACT

Electric energy consumption is growing almost all over the world. Similarly, using clean resources in coastal such as wave power is also growing. The coasts of Oman Gulf in southeast of Iran is one of the most potential areas for deriving energy from waves. The sea waves are mostly generated by wind and the climate change affect the wind field. Hence evaluating climate change effects on the wave power is essential for energy extraction. In this research, the variation of monthly average in Chabahar bay wave power under the middle scenario of future climate effect has been studied. For this, the CNRM-CM6-SSP2-45 dataset has been downscaled with the Weibull technique, and with a calibrated wave model, wave characteristic has been calculated. Based on the results, the average annual wave power will reach 10.4 kW/m by an increase of 3%. Total wave energy in Chabahar is about 91,000 kWh/m during the year. which will also increase by 3% compared to the same period previous century. In the July and August, the first high energetic months, the wave power increase by 1% on average compared to the previous period. The highest monthly increase occurs in October and with a 277% increase, it reaches 5535 kW/m. The highest monthly decrease of 25% occurs in June and the energy reaches from 13041 to 9513 kW/m.

1. Introduction

As a renewable resource, wave energy represents one of the cleanest sources of energy. There has been an increase in the use of this type of energy in coastal regions over the past two decades. In the regions with higher significant wave heights and longer periods, wave energy can be considered a primary alternative to fossil fuels. In this regard, Chabahar bay, located in the coasts of the Gulf of Oman, has great potential over all the Iranian seas. Several factors in this region, including higher waves, continuity of the long waves, specifically in the summer, and synchronicity of these waves with peak hours of energy consumption in the area, verify the suitability of this area for using the waves as an energy resource. Another crucial factor is the cost of converting fossil fuels to electricity. Generally, in the process of producing electric energy, fossil fuels are transported to a location near the place of use, where they will be transformed into electric energy using fossil power plants. Hence, in areas such as Chabahar in Sistan and Baluchestan province which are far from fossil fuel sources, the final cost of electric energy driven from the fuel is higher than its cost in regions located near fossil energy sources.

Selecting the location of installation for energy exploitation devices, known as Wave Energy Convertor (WEC), is extremely important [1]. The type of device, depth of installation, and amount of achieved energy are related and selected concerning each other. Regions with higher wave heights and periods possess more energy. The wave energy variation due to changing characteristics of the wave components in different seasons is inevitable. Generally, regions with more energy stability are better for energy exploitation [2]. Another crucial factor is the climate change impact on waves energy amount. Therefore, several studies were conducted on wave energy variation due to climate change [3–7].

Global Circulation Models (GCM) are large-scale meteorology models which simulate effective atmospheric variables on the climate in future conditions. These models are based on different scenarios and cannot be used in local-scale models regarding their large scales. Based on the most recent update from Intergovernmental Panel on Climate Change (IPCC) for Coupled Model Intercomparison Project Phase (CMIP6), climate variables under different Shared Socioeconomic Pathways (SSP) have

been presented. Since these results are global and large-scale, they need to be downscaled for use in local models.

Martinez and Iglesias [8,9] investigated the wind resources under different climates and CMIP6 scenarios in Europe and Northern America. While wave variables, such as height, period, etc., are not presented in GCM models directly. Since the waves are created by wind, an intermediate wave model is needed to calculate the wave properties using the wind field. As a result, a numerical model is developed in which the wind velocity components in two axes of x and y (or wind speed and direction), are used as the force that creates waves.

Due to its large scale, GSM data should be downscaled. Wind downscaling previously relied on statistical or dynamic downscaling. Regression models, artificial intelligence, and Weibull distributions are some of the known statistical downscaling techniques, while applying numerical models such as WRF for downscaling is known as a dynamic technique. Weibull's method does not modify the order or sequence of occurrences, which is crucial for wave simulation. The primary Weibull method, which was presented in a summative format, was modified with the knowledge that this equation is naturally multiplicative due to the presence of two form factors [10]. It results in better statistical values compared to those of the common Weibull method. This research utilized the modified Weibull method.

Swell waves from the south of the Indian Ocean reach the Gulf of Oman and the Gulf of Chabahar. The study area in this research is exposed to waves created by the Monsoon winds. As for Chabahar Bay, a safe area was established for landing buoyant, which resulted in resident accumulation and human concentration. According to the listed characteristics, this area has a high potential for energy exploitation. Wave energy in this zone has been studied before in some research [11,12]. These studies were based on the average energy of waves. In [13], a multi-factor procedure has been presented for selecting a combination of WECs and alternative situations in the Caspian Sea, Persian Gulf, and the Gulf of Oman. The noted research considered several factors, including exploitable energy, availability, total obtained energy, and inter-seasonal changes.

One of the main steps for obtaining a reliable result is providing a calibrated numerical model in the study area. Therefore, the wave simulation was conducted using a third-generation DHI MIKE 21 Spectral Wave model [14]. This model calculates wind generated wave characteristics such as height, period, direction, and energy.

In this study, CNRM wind data has been modified with reliable ERA5 wind data. Correction has been based on correction coefficients that has been obtained in past period. For this a modified version of Weibull downscaling has been used. Then, wave simulation was done using the new modified CNRM wind field in past and future periods, and the wave energy was extracted and compared from the results of the wave model.

The data and the selected method are explained in section 2. A summary of the results of this study is presented in Section 3. The conclusion of the study is discussed in section 4.

2. Data and selected method

The general procedure of this research is as follows:

- Selecting the study area
- Collecting data from the considered dataset
- Modifying (downscaling) the wind field
- Investigating the obtained wind field
- Providing the calibrated wave model
- Waves modeling (past and future periods)
- Extracting the wave energy
- Processing and examining the wave power changes

The wave energy is calculated using the MIKE21 SW numerical model. It is based on the third generation of wave equilibrium equations. MIKE21 SW uses a spectral action balance equation considering the growth, decay and transformation of wind-generated waves and swells in offshore and coastal areas. It means that calculates the wind generated wave parameters in each timestep. Therefore, climate change is visible in the studied waves indirectly using downscaled wind field.

2.1. Study area

The study area is the coastal region of the Gulf of Chabahar in the southeast of Iran's coasts in the Gulf of Oman, which has a great potential for wave energy. The measurements in two points near this location were used to calibrate the wave model. The results of the model in these points were investigated to verify their accuracy. Then the wave energy was investigated at a point with 29 meters depth off the coast of Chabahar Bay. Table 1 and Figure 1 show the locations of the points used in modeling and investigating the wave energy.

Table 1. Location of the wave model calibration

Station	Longitude (deg)	Latitude (deg)	Depth (m)	Use
Jask	57.753	25.608	25	Calibration
Chabahar	60.5	25.267	17	Calibration
Energy St.	60.544	25.242	29	Energy Analyze

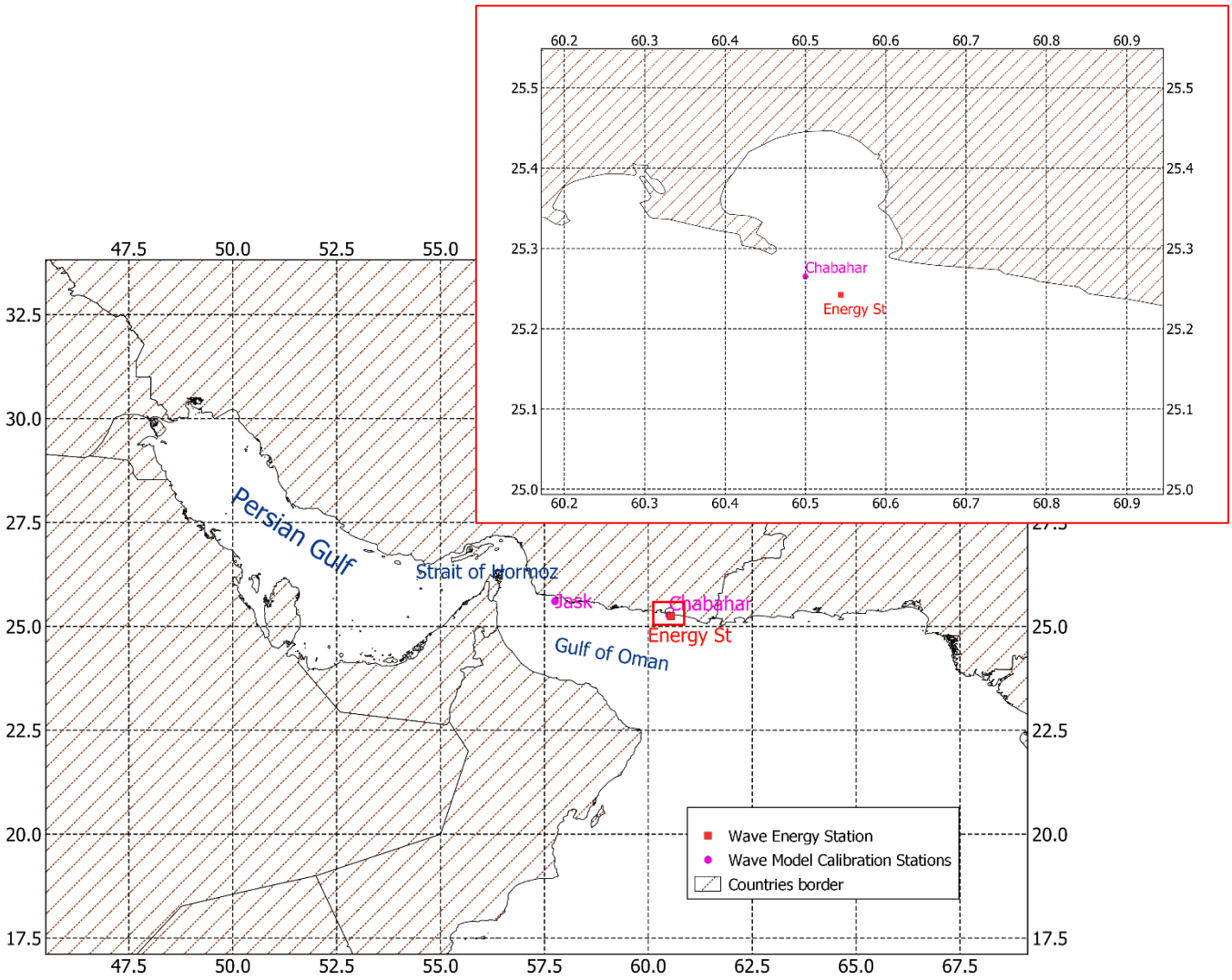

Figure 1. Location of the selected point of the wave model

2.2. The wind data

In this study, data from the CNRM-CM6-SSP2-45 dataset of CMIP6 was used. The dataset is available at https://esgf-data.dkrz.de/search/cmip5-dkrz/. In addition to good congruence with the measured wind data, this dataset has a higher resolution compared to other GCMs. It is related to an intermediate scenario, which means that it calculates metrology parameters in the future with an average amount of Carbon. So, it is not optimistic or pessimistic. As part of the general purpose of this study, which is to investigate long-term variations in energy levels, waves were examined over two 10-year periods with a difference of 100 years in the past and the future. These periods included 1991 to 2000 as the past period and 2091 to 2100 as the future period.

The time resolution of the 3-hour and their spatial resolution of 0.5×0.4993 degree of wind data is available in both the past and the future. Using the improved Weibull method, these data were modified, analyzed, and downscaled. ERA5 data from the reanalysis model were used for this purpose. As a result of previous experience, ERA5 data are in good agreement with measured data. The wind field was therefore modified using this data as the reference. Based on data from 1991 to 2000 years, wind modification was performed.

2.3. Methodology

To improve the asymmetry of data in this study, the improved Weibull method was applied to the wind field. There was a primary version of this technique suggested in [15], and an improved version was proposed in [10]. In general, the Weibull method is as equation 1:

$$f(w) = \frac{k}{A}\left(\frac{W}{A}\right)^{k-1} \exp\left[-\left(\frac{W}{A}\right)^{k}\right] \qquad (1)$$

Where W is the wind speed, and A and k are the coefficients of scale and shape in the Weibull distribution, respectively. Therefore, they are calculated based on the reference data (ERA5) using 2 and 3 equations and are applied using equations 4 and 5 to the CNRM wind data.

$$D_{A(i)} = A^{His}_{ERA5(i)} \Big/ A^{His}_{CNRM\,(i)} \qquad (2)$$

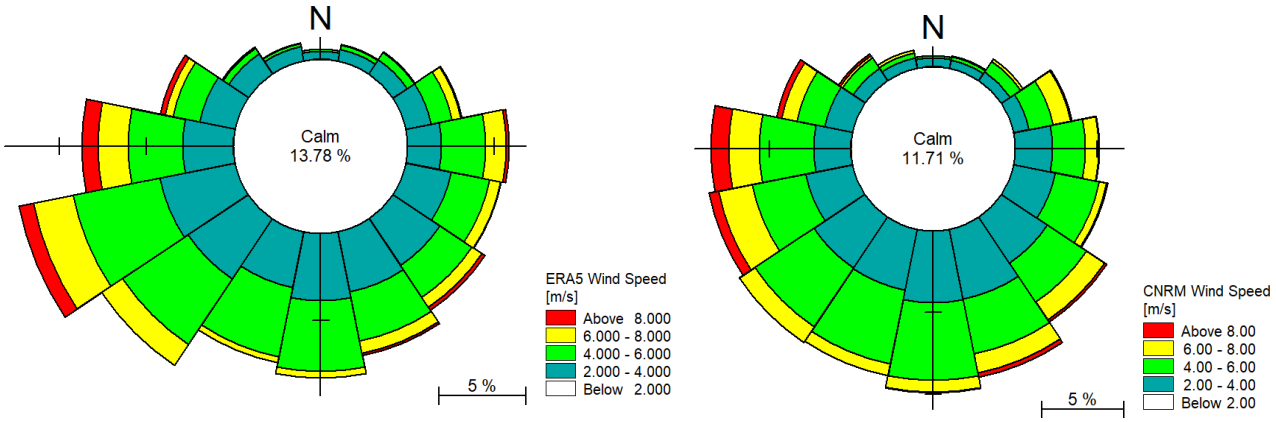

Figure 2. The modified wind rose of CNRM through the modified Weibull method (right), and the reference wind rose of ERA5 (left)

$$D_{k(i)} = k^{His}_{ERA5(i)} \Big/ k^{His}_{CNRM(i)} \quad (3)$$

$$A'^{Future}_{CNRM(i)} = A^{Future}_{CNRM} \times D_{A(i)} \quad (4)$$

$$k'^{Future}_{CNRM(i)} = k^{Future}_{CNRM(i)} \times D_{k(i)} \quad (5)$$

In this research, a preprocess was done on the wind dataset. For this, first of all the values of D_A and D_k has been obtained based on the modified Weibull method. This process has been done on a two-dimensional matrix on wind datasets. These values are based on modified Weibull technique on both ERA5 and CNRM data and compared to each other. In the next step, both past and future datasets of the CNRM collection were modified using the obtained coefficients. It should be mentioned that these datasets have different spatial resolution. for intermediate points, interpolation should also be used. After modifying the wind dataset, the obtained CNRM wind dataset is applied to a calibrated wave model. In the next step, the values the wave power are extracted from the wave model in both past and future period. In the next step, according to the amount of wave power and the duration of these waves, the energy of the wave is calculated and statistical analyzes were performed on the results.
A sample of the modified wind rose is shown in Figure 2. This wind rose is related to the entrance of the Chabahar Bay in the sea.

3. Results

3.1. The wave height

In this research MIKE 21 SW has been used for the wave simulation. MIKE 21 SW, a third-generation Spectral Wave model solves the equations on an irregular triangular mesh and simulates hydrodynamics phenomena, both near shore and offshore. Equation 6 shows the principal equation.

$$\frac{\partial N}{\partial t} + \frac{\partial}{\partial \phi} C_\phi N + \frac{\partial}{\partial \lambda} C_\lambda N + \frac{\partial}{\partial \sigma} C_\sigma N + \frac{\partial}{\partial \theta} C_\theta N = \frac{S}{\sigma} \quad (6)$$

Where N is action density, t is the time, λ and φ are longitude and latitude, respectively, σ is frequency, C is the wave speed, and θ is the wave direction.
To simulate waves, a computational triangular irregular mesh with different elements sizes was provided. Figure 3 illustrates the computational mesh and depths in the simulation domain. The computational domain is within the range of 47.8 to 74 (degrees) longitude and 15 to 30.4 (degrees) latitude.

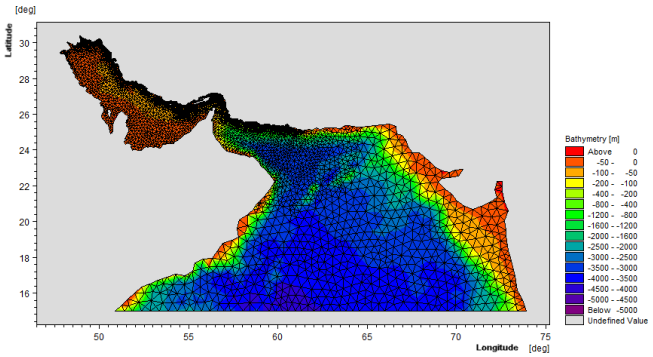

Figure 3. Computational domain and bathymetry the wave simulation

For calibration, the results of the wave model in Jask and Chabahar are compared to the measured values. For this purpose, the simulation has been repeated with different values. Ultimately, values of 2, 0.5, and 0.001 were selected for C_d, delta in the white capping equation, and Nikuradse's bed roughness coefficient respectively. Figure 4 demonstrates the time series of the results in the Jask and Chabahar stations.
For the evaluation of accuracy of the results of the calibrated model, statistical parameters were calculated concerning the measured data. The applied statistical relationships are as equations 7 to 10. Statistical values for the wave model results are presented in Table 2.

$$SI = \frac{\sqrt{\frac{1}{n}\sum (X_p - X_m)^2}}{\overline{X}_m} \quad (7)$$

$$CC = \frac{\sum (X_p - \overline{X}_p)(X_m - \overline{X}_m)}{\sqrt{\sum (X_p - \overline{X}_p)^2 \sum (X_m - \overline{X}_m)^2}} \quad (8)$$

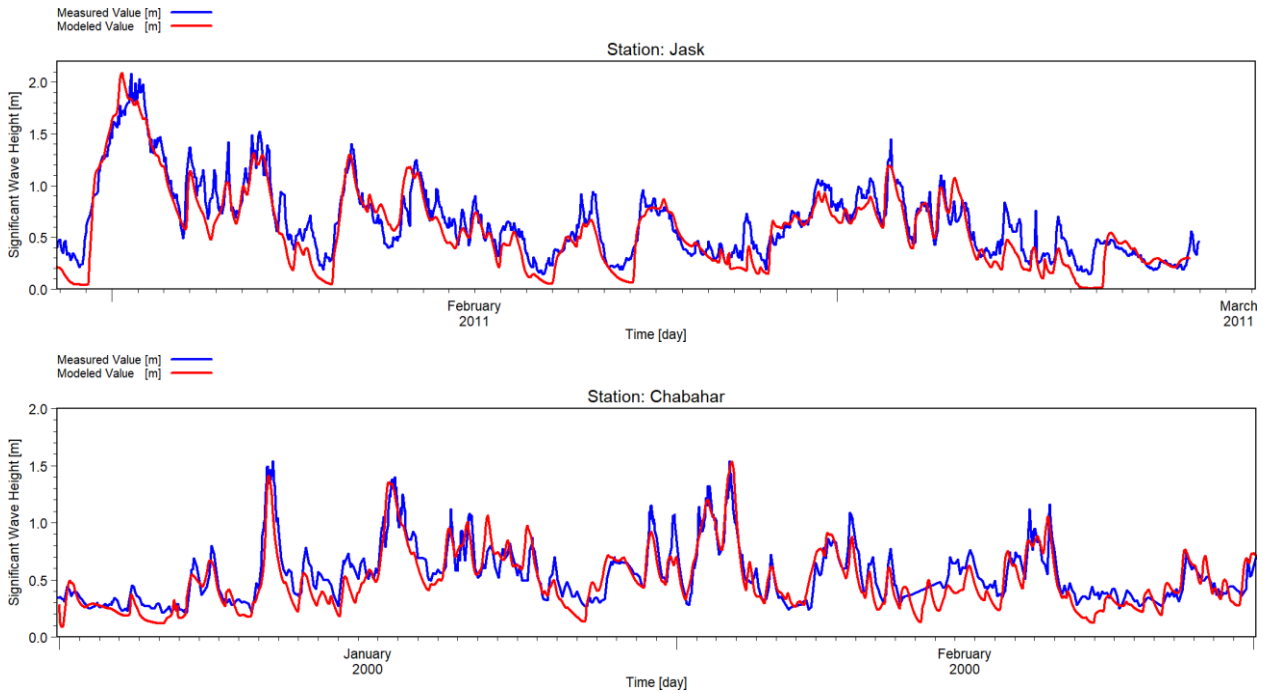

Figure 4. Time series of the simulated and measured wave heights in Jask and Chabahar stations

$$BIAS = \sum \frac{1}{n}(X_p - X_m) \quad (9)$$

$$RMSE = \sqrt{\frac{1}{n}(X_p - X_m)^2} \quad (10)$$

Table 2- Statistical evaluation of simulated waves

Buoy	**Jask**		**Chabahr**	
Period	Feb & Mar 2011		Jan & Feb 2000	
Parameter	Hs (m)	Tp (s)	Hs (m)	Tp (s)
SI	0.33	0.16	0.21	0.1
CC	0.83	0.76	0.91	0.92
BIAS	-0.08	-0.03	-0.04	0.02
RMSE	0.19	0.74	0.14	0.12

Based on the obtained statistical results, the prepared wave model is reliable and its results can be used for further analysis.

Figure 5 shows the average significant wave height in the past and future period. The colored palettes are the same for both periods. Based on the results, the significant wave height value has increased slightly.

3.2. The wave power and energy

The wave power measured in kW/m is based on the values of the significant wave height and the period, as equation 11 [15,16].

$$P \approx 0.49 H_s^2 T_e \quad (11)$$

Where H_s is the significant wave height and t_e is the energy period.

Considering the durations and wave power, the value of Pave can be calculated. Also, with t as the total time per year, the exploitable energy can be calculated.

$$E_t = P_{ave} \times t \quad (12)$$

$$E_e = P_{ave} \times t_e \quad (13)$$

Where t and t_e are the total hours and the hours in which the wave energy is larger than a specific value, according to which the exploitable value through WEC specification. In this research, the value of the threshold is considered 2 kW/m. The ratio between E_e and E_t is defined as exploitability.

$$Exploitability\ (\%) = \frac{E_e}{E_t} \quad (14)$$

Figure 6 shows the average wave power in the past and the future. Based on Figure 6, the difference in the average wave power in these two periods is not remarkable. It was found that the mean annual wave energy increased a little. This increase is estimated to be by around 3% in 100 years. Although the value of the average annual energy in the future did not change significantly, the investigation shows that the monthly wave energy changes are significant, especially in autumn and winter. For evaluating this, at a depth of 29 meters, the energy variations in the study area in Chabahar were extracted, and the values were analyzed. The location of the selected point is shown in Table 1 and Figure 2. Table 3 shows the average value of the wave energy in each month. Table 4 illustrates the exploitable energy percentage. The comparison between energy and exploitable energy in the past and future has been presented in Figure 7.

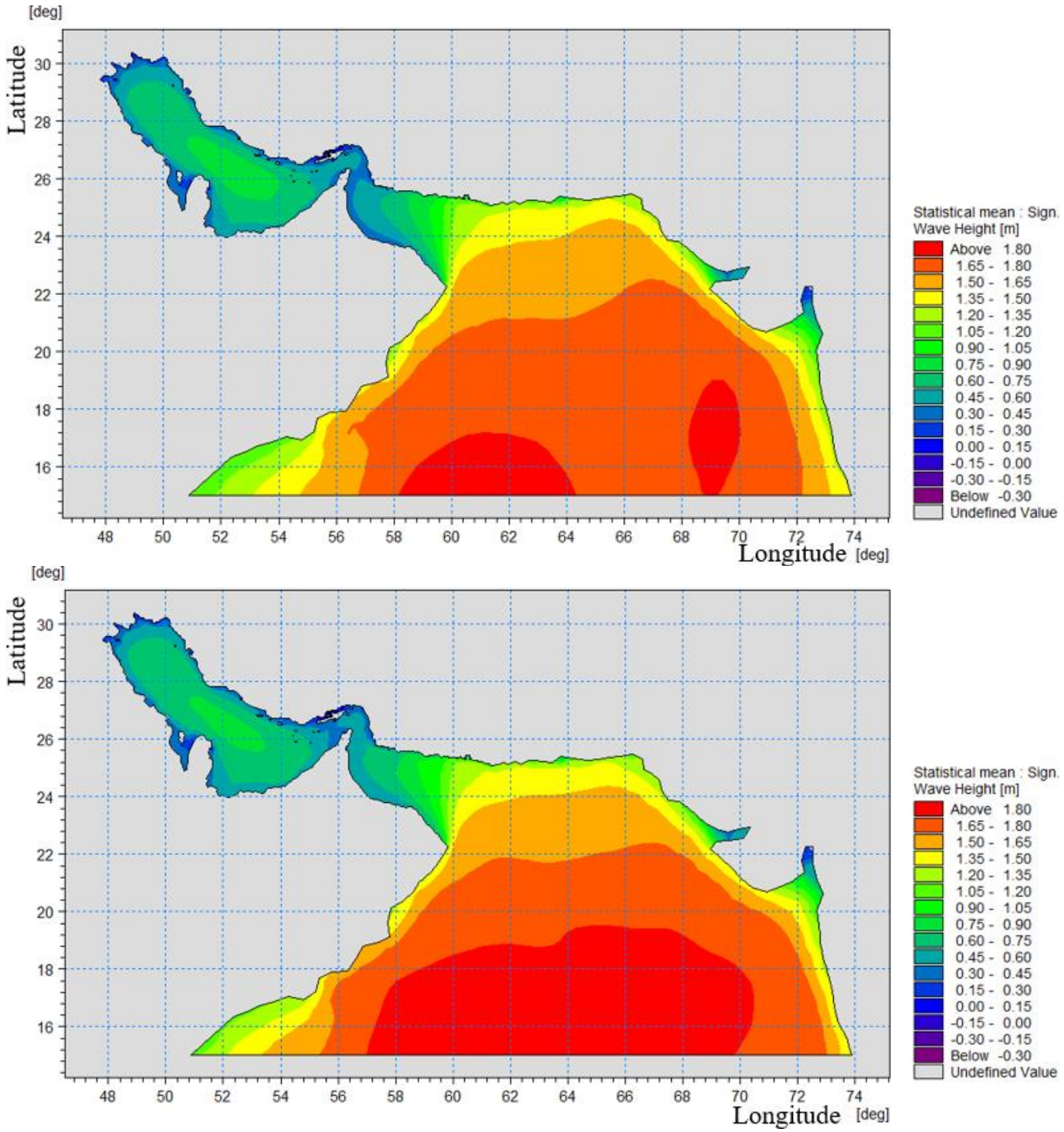

Figure 5. The statistical average of the significant wave height 1991-2000 (up) and 2091-2100 (down)

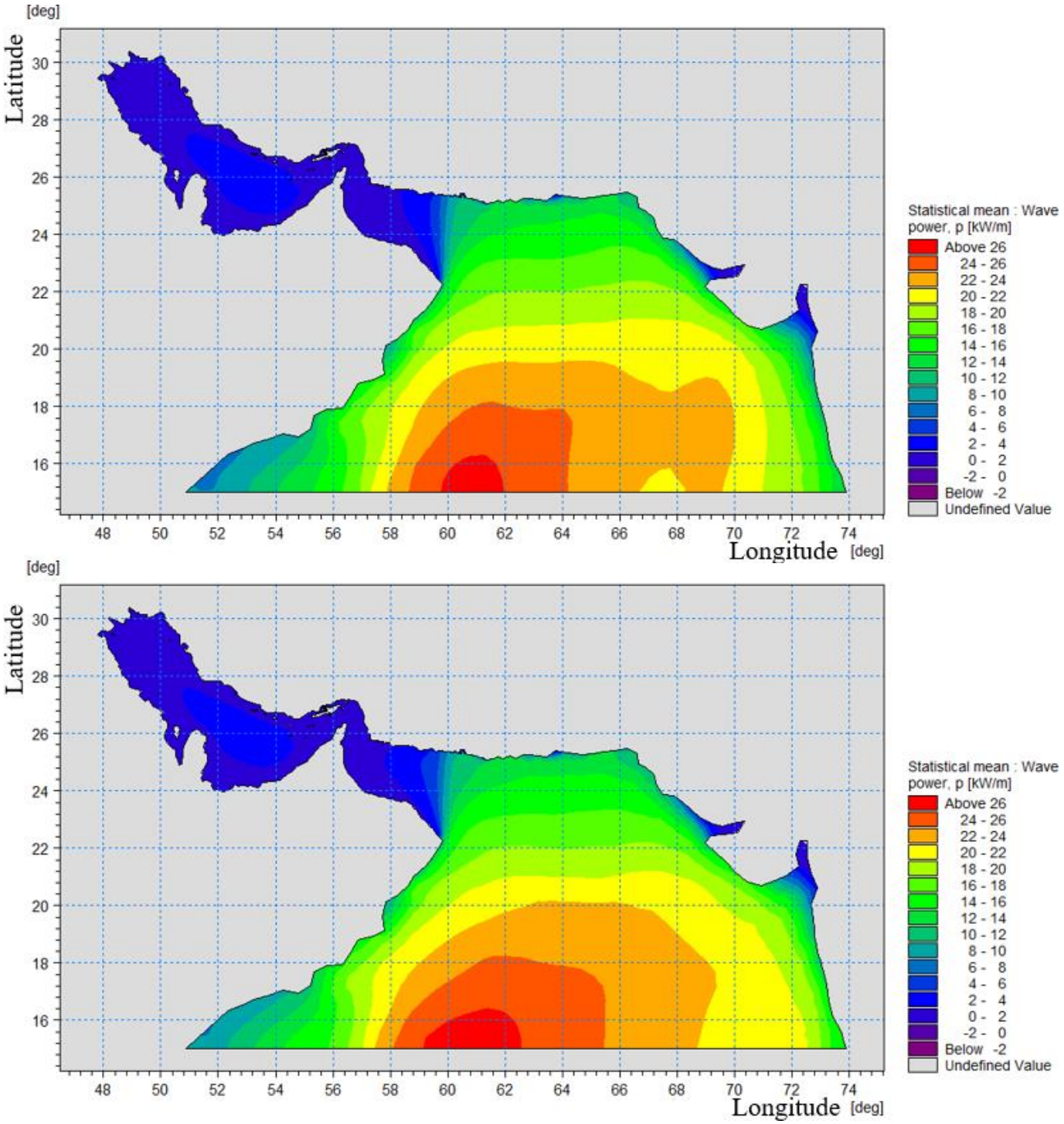

Figure 6. Statistical average of the wave power 1991-2000 (up) and 2091-2100 (down)

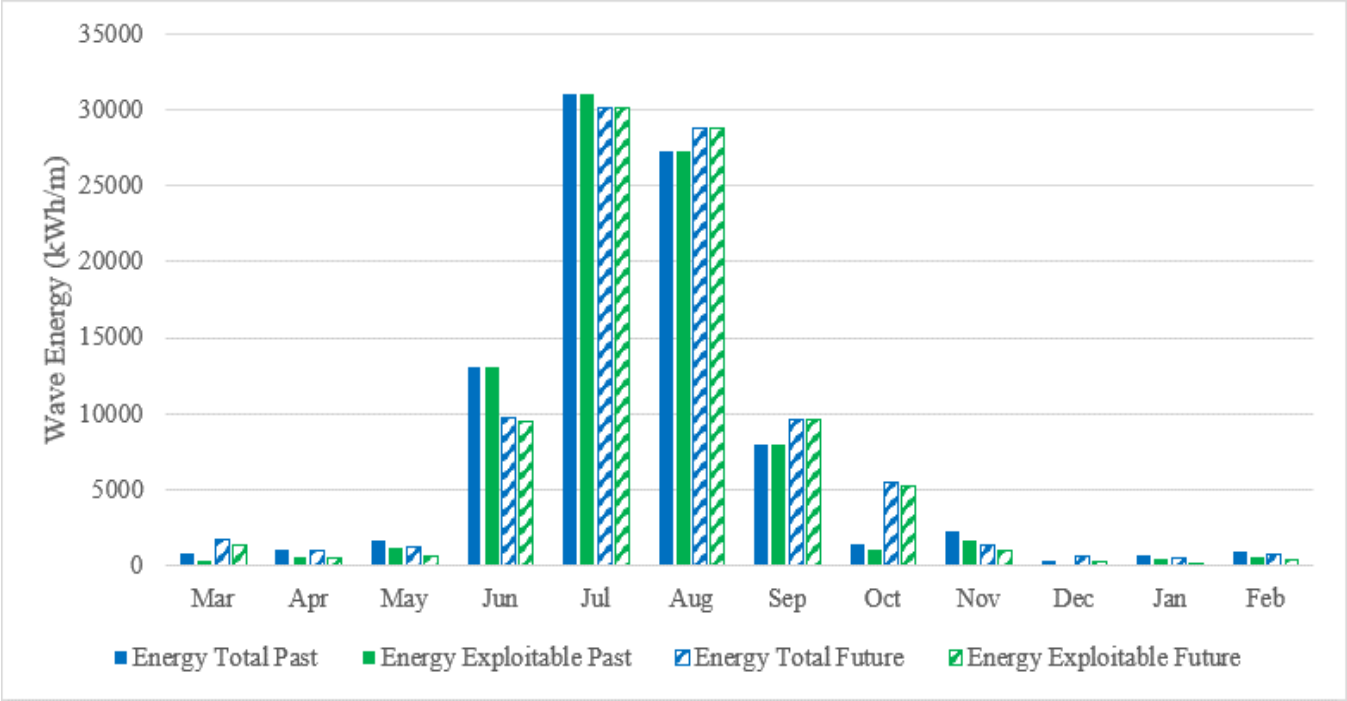

Figure 7. The average value of the wave energy in different months in the future (2091-2100) and past (1991-2000)

Table 3. The average value of the wave energy and power in the past (1991-2000) and future (2091-2100)

		Period	Mar	Apr	May	Jun	Jul	Aug	Sep	Oct	Nov	Dec	Jan	Feb	year
P_{ave} kW/m	Total	Past	1.01	1.52	2.16	18.11	41.69	36.69	11.01	1.97	3.11	0.41	0.92	1.31	10.10
		Future	2.33	1.36	1.65	13.55	40.53	38.71	13.37	7.44	1.84	0.79	0.67	1.14	10.40
	Exploitable	Past	3.38	3.94	3.70	18.11	41.69	36.69	11.01	2.74	10.49	0.00	4.28	6.45	20.10
		Future	7.91	3.59	2.79	16.72	40.53	38.71	13.37	8.97	5.36	0.00	2.71	3.60	20.21
Energy kWh/m	Total	Past	766	1093	1610	13041	31019	27300	7925	1466	2240	305	675	883	88323
		Future	1761	978	1225	9754	30157	28801	9624	5535	1322	584	493	767	91002
	Exploitable	Past	284	630	1214	13041	31019	27300	7925	1065	1699	0	398	600	85174
		Future	1376	485	616	9513	30157	28801	9624	5294	982	252	98	442	87641

Table 4. Exploitability of wave energy

	Period	Mar	Apr	May	Jun	Jul	Aug	Sep	Oct	Nov	Dec	Jan	Feb	year
Explotable time %	Past	11%	22%	44%	100%	100%	100%	100%	52%	23%	0%	13%	14%	48%
	Future	23%	19%	30%	79%	100%	100%	100%	79%	25%	13%	5%	18%	49%
Explotability	Past	37%	58%	75%	100%	100%	100%	100%	73%	76%	0%	59%	68%	96%
	Future	78%	50%	50%	98%	100%	100%	100%	96%	74%	43%	20%	58%	96%

Obviously in the graph, the wave energy is higher in the summer. It is due to the Monsoon wind regime and waves propagated by it. These waves come from the southeast and the Indian Ocean [17]. As can be seen with a glance at the results, the amount of wave energy in the Chabahar area is much higher than other areas of the country's southern coasts, such as the coasts of the Persian Gulf. This is generally due to the presence of monsoon winds and their intensity and the pattern of these winds. The coincidence of this phenomenon with the time of need for energy in southern part of country based on high consumption of electric air-conditions can justify the extraction of energy from waves. Meanwhile, in general, the uniformity of energy throughout the year is not very suitable.

The average wave power and energy will increase by about 3%. The average power is about 10 kW/m. In July, however, the value of power exceeds 40 kW/m. July and August have the most powerful waves. Generally, results from the future wave simulation indicate that the procedure will repeat and this time of year will remain the most powerful month.

The most increase occurs in autumn. In this season, the value is expected to increase by about 2.24 kW/m, which equals 27% of its past period. Wave power is reduced by 2.27 kW/m during winter months. This value is significant regarding that the total wave energy in winter is 5.4 kW/m and shows a 42% reduction. In the two most powerful months (July and August) we have about a 1% increase in the power. July and August are first two powerful months and they also remain the most powerful months in future. In July we will have about 3% decrease in the wave energy while in August wave energy will increase about 5%. Totally we can say there is about 1% increase in wave energy in these two months.

Analyzing the values of the monthly average shows that the monthly energy changes, vary between a 4229 kWh/m increase in October to a 3528 kWh/m reduction in June. Similarly, analyzing the percentage of changes shows that October has also had the largest increase in percentage terms, equal to 277%, and November had the largest reduction, equivalent to 41% or 717 kWh/m.

5. Conclusions

The results of this research are summarized below:

1. In an intermediate climate change scenario, the average annual wave power in the area of Chabahar will increase by about 3 percent and reaches 10.4 kW/m in the decade ending in 2100 compared to a similar period in the previous century.

2. Similar to the past (1991-2000), summer will be the most energetic season in the future (2091-2100). During autumn, wave energy increases the most. The value of power increase is 2.24 kW/m on average in autumn, which shows a 27% increase compared to the past period. due to winter with a reduction of 42%, the average wave power reaches to 3.09 kW/m.

3. In the last decade of the century, October is the month with the greatest increase in energy. In this month the value of energy increasing is 4229 kW/m, which is equivalent to a 277% increase. June and November have the lowest and highest energy reduction percentage, respectively.

8. References

[1] Şan M, Akpınar A, Bingölbali B, Kankal M. Geo-spatial multi-criteria evaluation of wave energy exploitation in a semi-enclosed sea. Energy 2021. https://doi.org/10.1016/j.energy.2020.118997.

[2] Portilla J, Sosa J, Cavaleri L. Wave energy resources: Wave climate and exploitation. Renewable Energy 2013. https://doi.org/10.1016/j.renene.2013.02.032.

[3] Alizadeh MJ, Alinejad-Tabrizi T, Kavianpour MR, Shamshirband S. Projection of spatiotemporal variability of wave power in the Persian Gulf by the end of 21st century: GCM and CORDEX ensemble. Journal of Cleaner Production 2020. https://doi.org/10.1016/j.jclepro.2020.120400.

[4] Sierra JP, Casas-Prat M, Campins E. Impact of climate change on wave energy resource: The case of Menorca (Spain). Renewable Energy 2017. https://doi.org/10.1016/j.renene.2016.08.060.

[5] Rusu L. Evaluation of the near future wave energy resources in the Black Sea under two climate scenarios. Renewable Energy 2019. https://doi.org/10.1016/j.renene.2019.04.092.

[6] Cuttler MVW, Hansen JE, Lowe RJ. Seasonal and interannual variability of the wave climate at a wave energy hotspot off the southwestern coast of Australia. Renewable Energy 2020. https://doi.org/10.1016/j.renene.2019.08.058.

[7] Iribarren D, Martín-Gamboa M, Navas-Anguita Z, García-Gusano D, Dufour J. Influence of climate change externalities on the sustainability-oriented prioritisation of prospective energy scenarios. Energy 2020. https://doi.org/10.1016/j.energy.2020.117179.

[8] Martinez A, Iglesias G. Wind resource evolution in Europe under different scenarios of climate change characterised by the novel Shared Socioeconomic Pathways. Energy Conversion and Management 2021;234:113961. https://doi.org/https://doi.org/10.1016/j.enconman.2021.113961.

[9] Martinez A, Iglesias G. Climate change impacts on wind energy resources in North America based on the CMIP6 projections. Science of The Total Environment 2022;806:150580. https://doi.org/https://doi.org/10.1016/j.scitotenv.2021.150580.

[10] Pourali M, Kavianpour MR, Kamranzad B, Alizadeh MJ. Future variability of wave energy in the Gulf of Oman using a high resolution CMIP6 climate model. Energy 2023;262:125552.

https://doi.org/https://doi.org/10.1016/j.energy.2022.125552.
[11] Saket A, Etemad-Shahidi A. Wave energy potential along the northern coasts of the Gulf of Oman, Iran. Renewable Energy 2012. https://doi.org/10.1016/j.renene.2011.09.024.
[12] Kamranzad B, Chegini V, Etemad-Shahidi A. Temporal-spatial variation of wave energy and nearshore hotspots in the Gulf of Oman based on locally generated wind waves. Renewable Energy 2016. https://doi.org/10.1016/j.renene.2016.03.084.
[13] Kamranzad B, Hadadpour S. A multi-criteria approach for selection of wave energy converter/location. Energy 2020;204:117924. https://doi.org/https://doi.org/10.1016/j.energy.2020.117924.
[14] DHI. MIKE 21 SW - Spectral Wave Model: Scientific Documentation. DHI Water and Environment 2014.
[15] Tucker MJ, Pitt EG. Waves in ocean engineering 2001.
[16] (U.S.) RE and AUP. Technology white paper on wave energy potential on the U.S. Outer Continental Shelf. 2006.
[17] Sanil Kumar V, Singh J, Pednekar P, Gowthaman R. Waves in the nearshore waters of northern Arabian Sea during the summer monsoon. Ocean Engineering 2011. https://doi.org/10.1016/j.oceaneng.2010.11.009.

INTERNATIONAL JOURNAL OF
COASTAL, OFFSHORE & ENVIRONMENTAL ENGINEERING IJCOE Vol.8/No. 1/winter 2023 (26-30)

Available online at: www. Ijcoe.org

A case study diagnosis of cyclogenesis over the Black Sea

Parvin Ghafarian

Faculty member, Iranian national institute for oceanography and atmospheric science; p.ghafarian@inio.ac.ir

ARTICLE INFO

Article History:
Received: 31 Dec. 2022
Accepted: 26 Feb. 2023

Keywords:
Cyclogenesis
Potential vorticity
NCEP/NCAR
Black Sea

ABSTRACT

In this study, cyclogenesis was investigated over the Black Sea from synoptic-dynamic view. While the Black Sea has an important role in precipitation of northwest of Iran, a system that is formed over the Black Sea was selected and it affected Iran on 14th and 15th March 2009 (40 mm precipitation has occurred in some stations). Using archived data of NCEP / NCAR, absolute and thermal vorticity advection in 500hPa level and potential vorticity at 325 degrees Kelvin level were calculated. Within the development process the cutoff low was formed over the Black Sea and the difference between directions of the upper-level cutoff low at 250hPa level and surface low represents a strong baroclinicity which in turn supports cyclogenesis. The results show that the absolute and thermal vorticity advection in mid-level and potential vorticity anomaly has a fundamental role in creating cyclogenesis. In such a way that the absolute vorticity advection gets 15 times larger (about $21 * 10^{-10} s^{-2}$), and cyclogenesis occurs when the mid-level trough axis is altered from northeast-southwest direction to northwest-southeast direction, and the polar jet will be combined with a subtropical jet. Also, a strong dependence of the cyclogenesis in initial stages occurs when a large upper level Potential Vorticity (PV) anomaly advected into a region where there is a meridional potential temperature gradient at low-level.

1. Introduction

The mid-level vorticity, thermal advection and vertical velocity play an important role on atmospheric systems development and decay. Sutcliffe [1] studied cyclones and anticyclones developments. He realized that cyclogenesis is associated with convergence in the low levels, and positive vorticity in the mid-level. Later Peterson [2] using the vorticity and thickness equations found that cyclonic development is dependent on thickness advection, vertical motion and diabatic heating fields. Carlson [3] defined that cyclonic development in the earth surface takes place in regions with baroclinicity and due to starting of thermal and vorticity advection in 500hPa. He also claimed that the cause of mid-level trough development is the positive absolute and thermal vorticity advections, which create a positive vorticity tendency. The seminal article by Hoskins et al [4] introduced a new approach for understanding and diagnosing atmospheric motions using potential vorticity (PV). PV diagnosis can be used to study all aspects of synoptic scale development. Ramalingeswara et al [5] study of cyclogenesis in PV framework shows that at later stages of cyclogenesis, an upper tropospheric PV anomaly development results in the growth of upstream and downstream positive PV anomalies over the cyclone. The large-scale lows and troughs evolving along the polar front jet seem to directly influence the cyclogenesis in the Mediterranean Sea [6-7]. In the presence of a cutoff structure the mass penetration from the middle latitudes has a decisive influence on precipitation [8-9]. The climatological studies [10] reveal the presence of three cyclogenetic regions in western, central and eastern Mediterranean. The eastern Mediterranean is in generally a weaker cyclogenetic region [11] in comparison with the cyclogenetic regions of the western Mediterranean.

Both western and eastern Black Sea coasts seem to be, almost permanently, two major cyclone paths. Sea–land contrast and associated low-level baroclinicity [12] may play an important role in their maintenance on the region. The relative vorticity advection and the potential vorticity anomaly triggered from the highest layers, in the maximum development phase, cause the cyclogenesis process in the Black Sea [13]. The aim of this study is to survey the cyclogenesis, especially from the vorticity viewpoint (relative vorticity, thermal vorticity and potentially vorticity) over the Black Sea and the following results by rainfall systems over northwest of Iran. Also, it can be useful for weather forecaster to diagnose the cyclogenesis in the study area. Thus, a cyclonic event crossing the region and

affecting northwest parts of Iran on 14th and 15th March of 2009 with heavy precipitations or thunderstorms, is selected. Formation, intensification and routing of the system and some synoptical and dynamical quantities are analyzed. The data and methods of diagnosis are described in section 2, and an overview of the case study is provided in section 3. Sections 4 and 5 contain the discussion and conclusions.

2. Data and methods

In this study, reanalysis dataset produced by the US National Center for Environmental Prediction (NCEP) and the US National Centers for Atmospheric Research NCAR) has used [14]. 6-hourly global atmospheric data within a regular grid are used which has a special resolution of $2.5° \times 2.5°$ in latitude and longitude directions at 17 standard pressure levels from 1000hPa up to 10hPa.

Positive absolute and thermal vorticity advections in 500hPa level [15], and Ertel potential vorticity [16] are considered as cyclogenesis indices.

The research domain covers a horizontal regular network in an area between 0-to 80 degrees east in longitude and 10-to 60 degrees north in latitude. The following units are considered respectively for the absolute vorticity advections and the Ertel potential vorticity: $10^{-10}\mathrm{s}^{-2}$ and $10^{-6}\mathrm{m}^2\mathrm{s}^{-1}\mathrm{Kkg}^{-1}$.

3. Case study

In this study, a system which formed over the Black Sea and affected north-west area of Iran on 14th and 15th March of 2009 was considered. Satellite images related to the cyclonic event; show an expanded cloud region from the Black Sea to NW of Iran (Figure 1). 40 mm of accumulated rainfall within 24 hour were recorded in the Urmia synoptic station, a northwest province of Iran on 14th March of 2009, while climatic average recorded precipitation in the region in March is 52 mm. Thus, the system almost provided 77% of the regional long-term rainfall in March. Likewise, the system were accompanied with strong winds which resulted to raising dust particles during its eastward movement in the Ardebil region while losing its moisture content. In figures 2-5, the two stations representing their respective regions are shown with triangle and circle symbols.

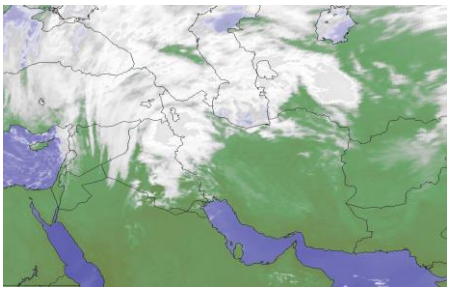

Figure 1. Satellite image of Meteosat-7 for 14th March 2009, 0000 UTC.

4. Results

Figures 2 (a, b, c, d) show the mean sea level pressure and Figure 2 (e, f, g, h) show geopotential height at 500hPa and polar jet for the period 12to 15March 2009. Pressure field at 0000UTC on 12th March 2009, shows a high pressure with 1020hPa iso-lines stretching towards from east of the Black Sea to southwest of Iran (Figure, 2a). Upper-level trough stretching from Europe to south of the Mediterranean Sea has a positive tilt on the same day. Likewise, zonal waves are passing from south of the Black Sea to east of Iran and intrusion of the polar jet is seen across the northern latitudes to the west Mediterranean Sea. A relatively zonal upper-level jet is placed between the Mediterranean region and the Aral Lake and a weak sub-tropical jet is passing from the lower latitudes (Figure, 2e). At 0000 UTC on 13th March 2009, upper-level trough has got entirely a meridional axis and expanded from the northwest of the Black Sea to the south of the Mediterranean Sea. At the same time, intrusion of the polar jet was continued more intensively from higher latitudes and got a cyclonic curvature from mid-Mediterranean to northeast of the Black Sea.

By moving the aforementioned high pressure toward east, the low pressure extends from the southern latitudes to the Black Sea region, Figures (2b and 2c). At 0000UTC on March 14th, the upper-level trough axis acquired a negative tilt and a cutoff low was formed over west of the Black Sea. Investigation of the height field through different levels indicates expansion of the cutoff low from ground to tropopause level (250hPa), which presents a strong baroclinicity in the area, Figure (3). The Jet axis acquires a cyclonic curvature in south of the Black Sea, and also the sub-tropical jet were intensified and combined with the polar jet in south-east of the Black Sea. At this time cyclogenesis is formed meridionally from the north of the Black Sea to the southwest of Iran on the surface, which is beneath the polar jet exit region and it is shown with L sign in the Figures (2c) and (2g). The system had caused 40 mm of rainfall in northwest Iran. At 0000UTC 15th March 2009, the cutoff low continued its activity on the Black Sea and its eastern regions and the center of surface low moving toward east of the Caspian sea and the Aral lake, were deepened and the corresponding central pressure fell to 1000hPa with a 10hPa reduction in the central pressure. It seems that the Caspian Sea thermodynamic effect was the responsible factor for the weakening of the surface pressure. The cyclone moved a remarkable distance during the past 24 hours and the high latitudes polar jet was weakened and the cyclonic curvature was decreasing toward lending to more zonal currents. Due to strong winds (over 7.5 m/s) that were produced by the system passing from northwest Iran, there were some reports of rising dust in the region, Figures (2d) and (2h).

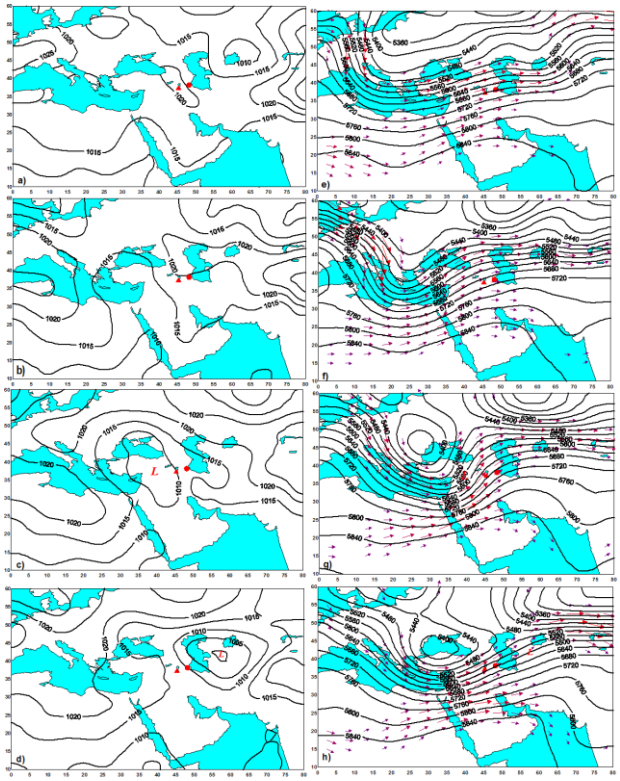

Figure 2. Left panels show sea level pressure (contours intervals is 5 hPa). Right panels show geopotential height at 500hPa (contours intervals is 40 m), and polar jet: (a,e) 12, (b,f) 13, (c,g) 14,(d,h) 15, March 2009, 0000 UTC.

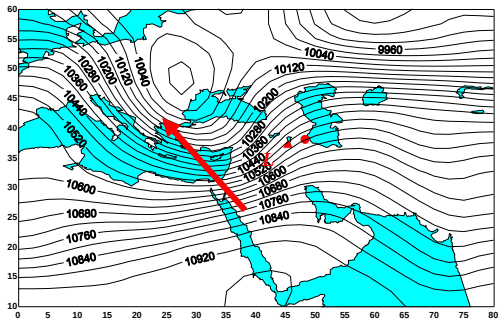

Figure 3. Geopotential height at 250hPa (contours intervals is 40 m), 0000 UTC, 14th March 2009. Red arrow shows the direction of trough axis from surface to the upper tropopause at 250hPa.

Figures 4 (a, b, c, d) show the absolute vorticity advection (shaded), polar jet and geopotential height at 500hPa, (e, f, g, h) show the thermal vorticity advection (shaded), polar jet and geopotential height at 500hPa for the period 12 to 15 March 2009. Consideration of the absolute vorticity advection shows that there are three maximum centers of the quantity with the value of five units over the Black Sea, mid-Mediterranean, and Europe and in front of the trough region, at 0000 UTC on 12th March 2009, Figure (4a). At 0000 UTC, 13th March 2009, with intrusion of the polar jet toward the lower latitudes, absolute vorticity advection moves to the Mediterranean Sea and its isolated maximum centers became combined and placed in east of the trough axis so that its maximum value was placed in the southwest of the Black Sea with a directional expansion from northwest of the Black Sea to south of the Mediterranean (Figure 4b). At 0000 UTC 14th March 2009, the centered of maximum for this quantity with the amount of 21 units, was coincided with the center of cyclone while direction of the polar jet core up to its exit region had a negative tilt with the trough center and its direction is northwest-southeast and expands from the west of the Black Sea to the southwest boundaries of Iran. The same day, cutoff low has formed in the west of the Black Sea (Figure 4c). At 0000 UTC 15th March 2009, along with the zonal Jet, maximum center of this quantity with seven units is observed in the east of Mediterranean Sea (Figure 4d). Study of thermal vorticity advection shows that, at 0000 UTC12th March 2009, the maximum center of this quantity is in the west of the Black Sea and over the North Sea, Figure (4-e). At 0000 UTC 13th March 2009, with intrusion of the polar jet to the lower latitudes, thermal vorticity advection moved toward the lower latitudes. On this day, there are two maximum value centers in the north of Mediterranean Sea and east of trough, Figure (3f). At 0000 UTC 14th March 2009, with the cyclogenesis, thermal vorticity advection flux with northwest-southeast axis flew from northwest of the Black Sea to Saudi Arabia and the maximum center of this quantity got a value of 8 units in the northwest of the cyclone over the Black Sea, Figure (4g). At 0000 UTC 15th March 2009, the maximum center of this quantity with the amount of seven units is placed in the northeast of the Black Sea. Figure (4h).

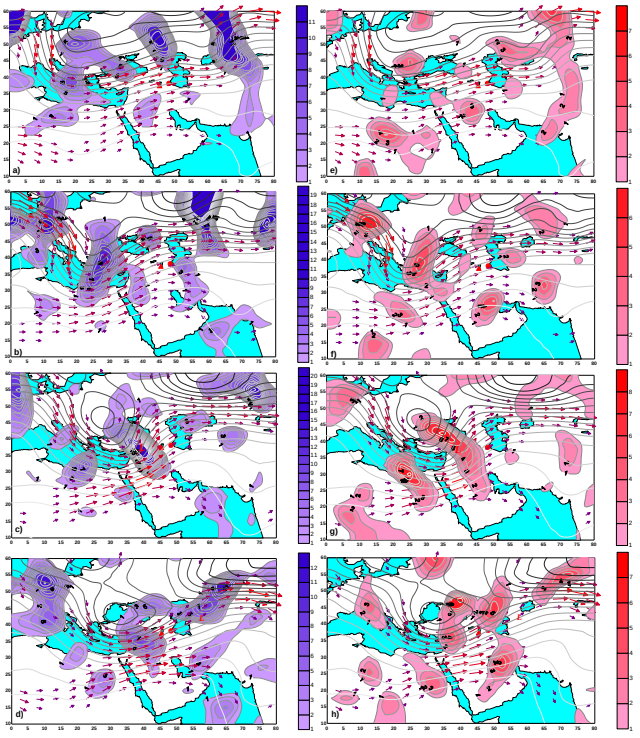

Figure4. Left panels show absolute vorticity advection at 500hPa (shading), geopotential height at 500hPa (contours), and polar jet. Right panels show thermal vorticity advection at 500hPa (shading), geopotential height at 500hPa (contours), and polar jet: (a, e) 12, (b, f) 13, (c, g) 14,(d, h) 15 , 00 UTC, March 2009.

Figure 5 (a, b, c, d) show the evolution of the PV field on the 325 degrees Kelvin isentropic surface, potential temperature at 850hPa and polar jet. The study of potential vorticity on a fixed temperature surface, 325 degrees Kelvin level, shows that the maximum anomaly, PV was observed at 0000 UTC 12th March 2009 in the north of the Mediterranean Sea. Contours of PV are zonal and accompanied the jet flow, Figure (5a). At 0000 UTC 13th March 2009, the maximum PV anomaly in the west of the Black Sea is observed and is meridional. On this day, potential temperature anomaly is seen in 850hPa level, Figure (5b). At 0000 14th March 2009, the maximum PV anomaly in the west of the Black Sea (northwest of cyclone's position) is seen simultaneously with the occurrence of cyclogenesis in the southern of the Black Sea. On this day, the maximum potential temperature anomaly occurs at 850hPa level and warm air and cold air were located in east and west of the cyclone respectively. At 0000 UTC 15th March 2009, the PV anomaly located in the center of the Black Sea, is weakened and direction of contours are altered from meridional to zonal and potential temperature anomaly were reduced, Figure (5c).

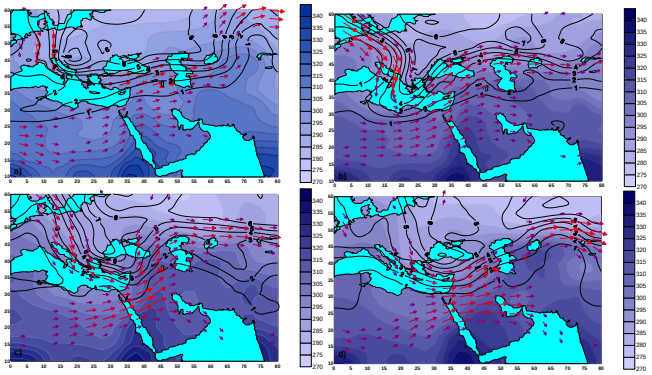

Figure 5. Potential vorticity distribution on the 325 K isentropic surface (PV, bold contours in pvu), potential temperature at 850hPa (shading in K), and polar jet .a: 12, b: 13, c: 14 and d: 15, 0000 UTC, March 2009.

5. Conclusions

cyclogenesis mechanism in the mid-latitude is very different from the cyclone that forms in the subtropical regions [17-18]. In this research the structure of the cyclogenesis over the Black Sea during 12-15 March 2009 was investigated within a synoptic and dynamic framework. Evidence for the importance of effects by developments at 500hPa level, especially in the early stages of rapid cyclogenesis, are manifested by changes in orientation of the trough axis from northeast-southwest (positive) to northwest-southeast (negative). Within the development process the cutoff low was formed over the Black Sea and the difference between directions of the upper-level cutoff low at 250hPa level and surface low represents a strong baroclinicity which in turn supports cyclogenesis. Intrusion of the polar jet from upper latitudes and combination with the subtropical jet along with a cyclonic curvature in the east of the Black Sea produces the cyclogenesis in the exit region of the combined jet stream. Study of quantities of absolute and thermal vorticity advections in, 500hPa level by actual and thermal wind and surface pressure height shows that the maximum values of dynamic parameters is in front of the mid-level trough and that is mainly because of polar jet displacement toward lower latitudes. In the cyclogenesis stage, they are placed on the exit area of the jet current. The difference is that the maximum absolute vorticity advection was in center of the cyclone and the maximum thermal vorticity advection was over the Black Sea and northwest of cyclone. Also at the cyclogenesis stage, absolute vorticity advection has increased 15 units compared to a similar time on the previous day and its value has reached to a large amount, $21 * 10^{-10}s^{-2}$ and the thermal vorticity advection has increased from 5 to 7. Since the development (decay) of the mid-level trough causes strengthening (weakening) pressure systems by convergence (divergence) of the horizontal wind in the lower levels and create an upward (down ward) motion, these two quantities indirectly affect strengthening and development of the Black Sea trough. A strong dependence of the cyclogenesis in initial stages occurs when a large upper level PV anomaly advected into a region where there is a meridional potential temperature gradient at low-level. Maximum PV anomaly in cyclogenesis stage is located in the west of the Black Sea and warm air advection is observed in the east of the cyclone (east of the Black Sea) and cold air advection in the west of it. Finally, for a better understanding of the physical and dynamic process of cyclogenesis over the Black Sea, we need to use the numerical model to evaluate air-sea interaction effects.

6. References

[1] Sutcliffe, R.C., (1938), *On Development in the Field of Barometric Pressure*, Q.J. Roy. Meteorl., Soc., 64, p. 495-509.

[2] Petterssen , S., (1956), *Weather Analysis and Forecasting*, Vol II, Weather and weather system, McGraw Hill, Book Company, New York, p. 266.

[3] Carlson,T.N, (1991) *Mid-Latitude Weather System*.University Press,cambridge.

[4] Hoskins, B.J., Mcintyre, M.E. and Robertson, A. W., (1985) *On the Use Significance of Isentropic Potential-Vorticity Maps*, Q.J., Roy. Meteorol. Soc., 111, p. 877-946.

[5] Ramalingeswara, S., K. Muni Krishna., O. S. R. U. Bhanu Kumar, (2009) *Study of Tropical Cyclone "Fanoos" Using MM5 Model- A Case Study*. Nat. Hazards Earth Syst. Sci., 9, p. 43–51.

[6] Flocas H. A. and Karacostas, T. S. , (1996) *Cyclogenesis over the Aegean Sea: Identifications and synoptic categories*, Meteor. Appl., 3, p. 53–61.

[7] Trigo, I. F., Bigg, G. R., Davies, T. D, (2002) *Climatology of cyclogenesis mechanisms in the Mediterranean*, Mon.Wea. Rev., 130,549–569.

[8] Alpert, P., Reisin, T., (1986) *An early winter polar air mass penetration to the eastern Mediterranean*, Mon. Wea. Rev., 114, p. 1411–1418.

[9] Alpert, P., Neeman, B. U., Shay-El, Y., (1990) *Climatological analysis of Mediterranean cyclones using ECMWF data*, Tellus, 42A,p. 65– 77.

[10] Maheras, P., Flocas, H. A., Patrikas, I., Anagnostopoulou, Chr., (2001) *A 40 year objective climatology of surface cyclones in the Mediterranean region: spatial and temporal istribution*, Int. J. Climatol., 21, p. 109–130.

[11] Radinovic, D. , (1965) *Cyclonic activity in Yugoslavia and surrounding areas*, Arch. Meteorol. Geophys. Bioklim, 14(A), p. 391–408.

[12] Hoskins, B.J. and Valdes, P.J.(1990) *On the existance of Storm-Tracks.* J. of the Atm.Sciences. Vol.47, No.15, p.1854-64.

[13] Georgescu, F., S. Tascu, M. Caian, D. Banciu., (2009) A severe blizzard event in Romania – a case study. Nat. Hazards Earth Syst. Sci., 9, p. 623–634.

[14] Kalnay, E., Kanamitsu, M., Kistler, R., Collins, W., Deaven, D., Gandin, L., Iredell, M., Saha, S., White, G., Woollen, J., Zhu, Y., (1996) The NCEP/NCAR 40-year reanalysis project. Bulletin of the American meteorological Society, 77(3), p.437-472.

[15] Holton, J. R., (1992) *An introduction to dynamic Meteorology*, Academic Press Inc., San Diego, USA.

[16] Nielson-Gammon, J. W., and D.A. Gold, (2008) *Potential Vorticity Diagnosis in the Quasigeostrophic and Nonlinear Balance System*. J. Atmos. Sci., 65, p. 172-188.

[17] Pegahfar, N., Gharaylou, M., (2018) Sensitivity of an Axi-Symmetric Tropical Cyclone Model to Two External Parameters. International Journal of Coastal, Offshore And Environmental Engineering, 3(3), p. 41-51.

[18] Hajivalie, F., Arabzadeh, A., (2017). A 3D Numerical Study of Cyclone Gonu Waves Impact on Ramin Port. International Journal of Coastal, Offshore And Environmental Engineering., 2(1), p. 33-41.

INTERNATIONAL JOURNAL OF
COASTAL, OFFSHORE & ENVIRONMENTAL ENGINEERING IJCOE Vol.8/No. 1/winter 2023 (31-44)

Available online at: www. Ijcoe.org

Export strategy in the context of coronavirus (COVID-19), Identifying drivers and critical success factors, Based on the study of active firms in Iranian ports and maritime industries

Asghar Rashnoodi[1], Aliashraf Ahmadian[*2]

[1] *Department of Business Management, Faculty of Economics andManagement, Khorramshahr University of Marine Science andTechnology,Iran;Asghar.rashnoodi@gmail.com*
[2*] *PhD Business Administration, from the University of Tehran, Iran;Aliashrafahmadian@ut.ac.ir*

ARTICLE INFO

Article History:
Received: 24 Oct. 2020
Accepted: 26 Feb. 2023

Keywords:
Export performance
Export Critical Success Factors
Critical situations
Coronavirus (COVID-19)
Innovativeness

ABSTRACT

The coronavirus (COVID-19) crisis, has put everything in a new and complicated situation. Businesses, especially exporters, have also been affected. The main objective of the present study is to investigate and prioritize the factors effective on the development of export strategy in the context of coronavirus (COVID-19), and to test this Phenomenon in the export firms of Iran through mixed method (qualitative-quantitative) research. To this end, 42 export firms were selected from Iranian ports and maritime industries as the statistical sample of the study and the data were gathered using questionnaire and interview and data analyzed with fuzzy Delphi methods and partial least squares technique. The research findings show that the most important inner firm factors effective on the export performance of Iranian firms in the context of the Corona crisis are: Firm's capabilities and resources; Managerial characteristics; Marketing capacity; Strategic capability and Company human resources. The research findings have led to the identification of vital export incentives and stimuli in critical situations and finally to the introduction of a new typology of factors tailored to critical situations that can be useful for empowering businesses in possible future crises.

1. Introduction

The coronavirus (COVID-19) has affected all aspects of human life, from individual and organizational, economic and social to political and cultural [1, 2]. And this epidemic has turned it into a phenomenon of the century [3, 4].

In business area, the virus has been affected all aspects so hard that it has shut down many companies around the world, forced some firms to decrease their human resources [5, 6, 7].

But in this frustrating situation, innovative companies have not left the scene and are thinking of creating opportunities from the imposed conditions. Using the capacity for innovation, think about creating value for existing customer conditions [6, 8].

On the one hand, There are many complexities and certain ambiguities threatening the exporters if, they decide to enter into foreign markets due to the current unpleasant condition of the world economy. In fact, they have to encounter and cope with certain challenges some of which are the followings: the coronavirus crisis, severe competition in the field of business, the risks existing in some developing markets, limitations of financial resources, providing the raw material, wide changes occurring in the interests of markets, management of costs [9, 1, 10]. As a matter of fact, these are only a small part of the challenges of today's international business world.

The structural change of the world economy since 1980 has had a deserved effect on the competition among corporations, having completely transformed their strategic activity [11].

New global market conditions and widespread environmental changes, coupled with the demands of a new generation of customers, have led business firms to adopt new approaches. Strategic learning concept has led firms to adopt new strategies to overcome environmental uncertainty [9]. Therefore, firms are increasingly forced to try to survive through enhancing their market share in the market of foreign countries. Competition among firms throughout the world will get more and more severe as the World Trade develops. In such a condition, firms are forced to enhance their activity throughout the world or at least in the area beyond their national borders.

On the other hand, to improve export performance is considered by the policy-makers in the field of economy as a main element effective on the national income of each country. In fact, through improvement of export, countries can achieve the following goals: stable growth of economy, reduction of unemployment, and social justice. Moreover, the phenomenon (i.e. improvement of export performance) can play a significant role in equalizing the balance of payments and increase of the countries' resources.

A great deal of research has in the past been done in different countries regarding the factors effective on the development of stable export. In general, two factors have been introduced to be important to this end including inner-firm and outer-firm factors [12, 13].

In critical situations such as the present, many questions arise in the minds of business researchers. In a crisis like the coronavirus, how do business managers view foreign markets?

On what axes is their strategic focus more? What are the critical success factors of firm performance in critical situations?

Although numerous studies have been conducted on the sustainable export performance of firms and the factors affecting it [14, 15, 2, 8], but this issue in the context of critical conditions such as the Covid 19 virus (Corona) requires new and contingent research specific to these conditions.

Firms active in Iran's maritime industry as a value chain, play an important role in developing the country's export performance, currency appreciation in sensitive sanctions conditions and job creation for the young and educated generation.

Examining the status of firms operating in critical situations such as the Covid virus 19 and how to manage the situation and the degree of innovativeness of senior managers in the field of exports can be effective in improving the performance of other firms and also identifying the weaknesses of firms.

Therefore, the present research is aimed to investigate inner-firm factors effective on the development of stable export in critical situations and then to prioritize such factors. Apart from filling some part of the existing gap, the findings can pave the way for policy makers in the area of export inside the country. The results can also be beneficial for subsequent research to be done in this field. In the present study, we will combine the views of successful managers with university professors with a high level of familiarity with the industry, and as a result, we will present innovative findings to introduce successful export strategies in critical situations.

2. Theoretical background of the research

The corona virus has affected the lives of almost all people everywhere in the world and has led to new lifestyles in all areas. In the field of business, the virus has imposed new conditions on businesses and has brought about many changes and developments [16, 17 18, 19].

Accordingly, businesses and their senior executives are thinking of taking advantage of the opportunities at the heart of this crisis to better meet the needs and wants of their customers [20, 21, 22].

One of the main factors and indices which are highly important for the economic growth of each country, especially in today's trembling world is 'stable export'. As a matter of fact, a first step that should be taken toward stable export is to recognize the factors effective on it. The results of the previous studies in this area are all indicative of the existence of two types of factors which are considered highly important and effective on the development of export.

In his classification, Leonidou [12] has divided the factors effective on stable export into two types of factors:

The first type: environmental factors. Such factors are called environmental because they can hardly, or at most restrictively, be controlled by exporters. Among these factors are the ones related to macro economy; social, physical, cultural factors, and political aspects. A simple example for such factors is: the elements related to industry which influences firm's export behavior and performance.The second type: the factors at the level of firm or corporation. They are also referred to as organizational factors and consist of structural and behavioral factors occurring inside the firm which have a potential influence on export performance.

In another classification, other researchers [23] have divided the factors effective on export performance into two types including internal and external factors, for which they have introduced two types of theories including 'resource-based theory' and 'industrial organization theory'. While the industrial organization attitude can be particularly helpful to explain the economic performance of exporters, the effect of internationalization process on internal factors (resource theory) can also be beneficial as the main incentives for such a process. In other words, having access to facilities, knowledge about market, physical distance, management's attitudes and perceptions, and many other capacities are all among the many internal factors effective on the development of export [24].

In a pervasive model, other researchers have also examined the factors effective on the development of export. In his research they have divided these factors into the three following groups [25, 26, 27, 28, 29]:

- Firm's capabilities and resources
- Managerial characteristics
- Attitudes and perceptions of management

Having studied the research done in the area of export and international trade, the factors effective on the

success of exporting firms in world markets can be classified as follows:

Based on the findings of some studies, there are three general factors effective on the development of export performance including: structural factors, managerial factors and export obstacles and incentives [30,31, 19, 32, 33, 34, 35, 36].

Structural factors consist of firm's size, age, managerial system, the state of its technology and structure, the position of research and progress in the firm, innovativeness, etc. [13, 36, 14, 37].

Managerial factors usually refer to the entrepreneurial and managerial characteristics of the supreme management team and those who are responsible for making decisions In a critical situation. Such factors consist of the expected profitability of export performance, attitude towards risk and costs, education level and experience of management team, etc. [38, 32, 39, 40]. And the role of small, creative and flexible enterprises in this situation is undeniable [41, 42, 43].

Another point is that members of a value chain in critical situations move towards more cooperation to use innovative strategies [33, 44, 45, 46, 47]. And all members of the value chain, like members of a family, find greater adaptation to the new wants and needs of customers, especially in foreign markets, by making greater use of the strategy of cooperation and reducing competitive areas within the chain (48, 49, 50, 51).

The obstacles and incentives for export are competition pressure, internal negative trends, accessibility to information, etc. [52, 38, 53, 54, 55].

Cavusgil and Naor (1987), in theor resercah showed that firm size has positive effect on export performance. Hart and Tzokas [56], however, in their study reported that success in export performance is not specifically influenced by firm size. Some studies have also reported that firm size has so little impact on export performance [57, 58].

Capital power is among the most important financial determinants effective on the development of export performance whose positive impact has been shown in most studies in this area [59, 60, 61, 62].

In general, based on the results from numerous studies done in the area of the factors effective on export performance and as far as effectiveness on export performance is concerned, the most important variables in inner-firm spectrum can be classified into three general categories:

Marketing factors: market research, market information, marketing advertisement, marketing strategies, and attendance in international exhibits are among the most important variables effective on export performance.[63, 64,65, 66, 45, 67, 68, 69, 70].

Financial factors: capital power, benefiting from circulating capital and management of financial resources are introduced as the most important financial variables effective on the development of export performance [71, 72, 66, 73].

Managerial power: the attitude of supreme mangers towards risk, organizational learning, organization profitability, supreme managers' education level and their field of study, export commitment of supreme managers' team, technology and IT, the experience and knowledge of supreme managers' team in foreign markets and international trading, creativity and the status of export in the culture dominant over organization are introduced as the most significant variables effective on the development of export performance (74, 80, 79, 66).

In a study investigating the relationship between innovation and firm export behavior, [45] showed that innovation, which was formerly assessed by the research and progress costs, is a key element effective on the growth of export performance.

Other researchera [81] showed that the ratio of research and progress costs to sale has a direct impact on firm's export performance. In their model, export performance had been examined by the ratio of export to total sale.

Lages et al [41] in their model showed that the cost of research and progress is an important factor effective on the export performance of small and medium-sized firms. The variable, however, does not lead so much to competitive advantage in high-tech enterprises. In fact, the effect of the variable "research and progress costs" on export performance is shown in other research models, too. Based on the findings of such models, the cost of research and progress is an important factor increasing the probability of firm's entrance into foreign markets and eventually the increase of export share from the total sale[82,83].

3. Research methodology

The steps for Cavusgils and Zou [19]; collecting and analyzing data, or the process for doing research in general, are shown below. In the first part of the work, a review of the literature was used to identify new business strategies and an initial set of strategies was developed.

Then the interview protocol was designed and after identifying Iranian maritime industry value chain, 42 firms were selected through purposeful sampling for interview. The interviews were semi-structured and the senior managers of the firms were selected for the interviews. The research method used in this study is multiple case study and for data analysis, theme analysis method was used as analysis tool. Fuzzy Delphi technique has also been used after identifying the main themes to objectify them and increase its validity and reliability. In other words, the main themes

extracted from the interviews were distributed through a questionnaire among exporter firms.

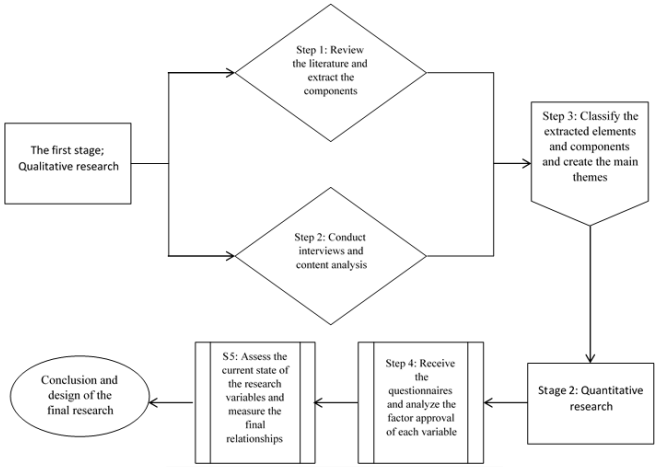

Figure 1. Research method and omplementation steps

The statistical population of the study includes all companies that operated in the value chain of Iran's marine industry in 2019 and 2020 and their service or product has led to the export of this industry to foreign markets. Therefore, the first task in this sector was to identify the value chain in the industry, which eventually led to the figure 2. Value chain identification was performed based on interviews with senior industry executives and related academic professors (consultants and industry researchers).

The statistical sample of the research was selected from the statistical population and in the qualitative part of the research, purposive sampling method was used and 42 aquaculture exporting companies were selected. Theoretical sampling is a type of purposeful sampling that helps the researcher to create or discover a theory or concepts whose theoretical connection with the evolving theory has been proven. In theoretical sampling, events are sampled, not necessarily from individuals, if we go to individuals with the aim of exploring events, events that represent various themes related to the phenomenon under study. In the qualitative part, semi-structured interviews were conducted with the managers of 42 exporting companies and 12 university professors related to the mentioned industry. Also, in the quantitative part, 106 university administrators and professors were examined as a statistical sample

The research has been conducted with multiple methodology in such a way that in the qualitative part of the research, it has been studied using the case study method of aquatic exporting companies. Accordingly, theme analysis has been used to analyze the research data in the qualitative part, and in the quantitative part, three techniques include; Fuzzy Delphi technique, interpretive structural method and partial least squares are used. The reason for using these three techniques is that for screening themes identified in the qualitative section, a suitable technique introduced is the fuzzy Delphi method. On the other hand, in the next stage of the research, in order to determine the level of readiness of firms, as well as the effectiveness and effectiveness of the existing infrastructure of innovation programs, a method is needed that the structural-interpretive technique does well.

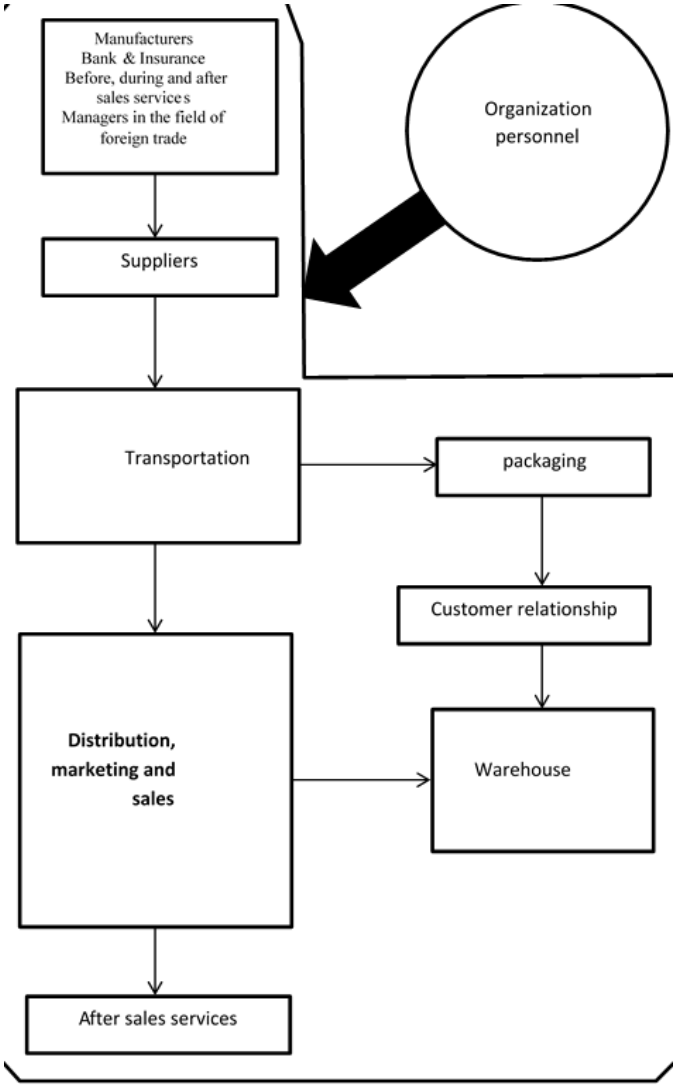

Figure 2. Marine and aquatic industry value

Finally, considering that a general framework of innovative strategies has been presented, a method for confirming the relationships between the introduced indicators or in other words, final approval of the model and validation of the presented indicators and relationships (validity and reliability) is needed. Jizi has done this. Therefore, with the multiple methodology used in the present study, the validity of the final model presented increases the research. The first step of the present study was performed using a qualitative research method. One of the methods of qualitative data analysis or qualitative content analysis is the method of theme analysis. Team analysis is a way to determine, analyze and express the patterns (themes) in the data. This method at least organizes the data and describes it in detail. But it can go beyond this and interpret different aspects of the research topic.

Qualitative data analysis in this study was performed by theme analysis method. Fuzzy Delphi technique will be used to screen early indicators. To fuzzy the view of experts, a spectrum of seven degrees is used according to the table below.

Table 1. Seven fuzzy degrees for evaluating indicators

Completely insignificant	Very insignificant	Insignificant	medium	significant	Very significant	Completely significant
(0.9, 1, 1)	(0.75, 0.9, 1)	(0.5, 0.75, 0.9)	(0.3, 0.5, 0.75)	(0.1, 0.3, 0.5)	(0, 0.1, 0.3)	(0, 0, 0.1)

In the next step, the fuzzy average of people's scores must be calculated. In fact, these aggregation methods are experimental methods that have been proposed by various researchers. For example, a conventional method for aggregating a set of triangular fuzzy numbers is considered to be minimum 1, mean m, and maximum u. In this study, we have used the fuzzy mean method. Fuzzy mean n Triangular fuzzy number will be calculated as follows:

$$\tilde{F}_{AVE} = (\mathrm{L.M.U}) = \frac{\sum l_i^k}{n}.\frac{\sum m_i^k}{n}.\frac{\sum u_k^i}{n} \quad (1)$$

In this equation, the triangular fuzzy number, f̃_i=(l_i^k,m_i^k,u_i^k), Fuzzy equivalent of expert view number k, Around the criteria i. Eventually, fuzzing will take place. The surface center method is used for de-fuzzing as follows:

$$DF_{ij} = \frac{[(u_{ij} - l_{ij}) + (m_{ij} - l_{ij})]}{3} + l_{ij} \quad (2)$$

In this study, the tolerance threshold is considered 0.7. Therefore, the de-fuzzy value greater than 0.7 is acceptable and any index with a score above 0.7 is approved. It should be noted that the steps of using fuzzy technique for the present study are outlined in the figure 3.

Structural-interpretive modeling method can be used to analyze the relationship between multivariate properties defined for a problem (Warfield., 1974; Sage., 1997). Structural-interpretive modeling is a methodology for creating and understanding relationships between elements of a complex system. In other words, interpretive-structural modeling is an interactive process in which a set of different and related elements are structured in a comprehensive systematic model. ISM methodology helps to establish order in complex relationships between elements of a system. Structural-interpretive modeling helps to identify the internal relationships of variables, and a suitable technique for parsing and ISM can be to prioritize and analyze the effect of one variable on other variables. It can also prioritize and level the elements

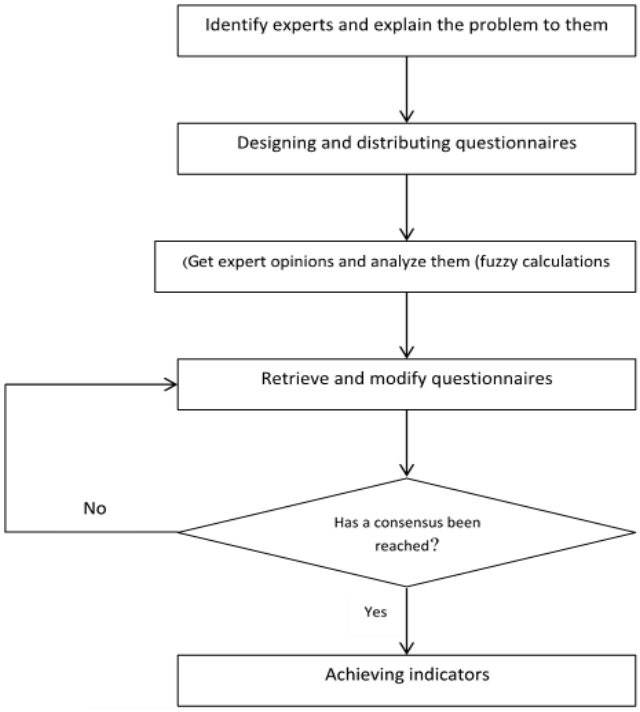

Figue 3. Steps to omplement the fuzzy Delphi method (Hsueh et al., 2013)

of a system, which helps managers to better execute the designed model. Therefore, for the present study, which analyzes the relationships of members of the value chain on the coast and offshore, understanding the set of complexities between the elements of this chain can be made possible and facilitated by this method. In this model, after identifying the dimensions and characteristics of the study, the relationships between the dimensions and the identified indicators are analyzed using the conceptual relationship "leading to". The states and symbols used in this conceptual relationship are presented in Table 2.

Table 2. Signs used in **designing a structural-interpretive model**

O	X	A	V
Lack of relationship	Two-way relationship	The variable j affects i	The variable i affects j

A very important point is that the logic of interpretive structural modeling (ISM) works in accordance with the non-parametric method and is based on mod in frequencies. In this study, the output of the Demetel technique has been used to form the input matrix of the structural-interpretive model. One of the main reasons for the tendency to use the partial least squares technique is that this technique does not rely on the assumption that the statistical population is normal and also the sample size. In the present study, SmartPLS software has been used to solve partial least squares or PLS problems. Finally, the fit of the model is examined. The structural part of the model, unlike the measurement models, does not deal with the questions and observable variables of the model and only pays attention to the hidden variables and the relationships between them. In this research, structural model fitting

is used using coefficient of determination (R2), redundancy and finally GOF statistics.

4. Research Findings

In the qualitative part of the research, the following themes were identified in the critical factors of sustainable export success, key decisions and incentives for Covid 19 virus conditions. Theme analysis was performed based on the 6-step model of Clarke and Braun. (2006), the final findings of which are presented in the tables 3 & 4.

Table 3. Theme analysis of critical factors related to sustainable export success

Row	Basic themes	Comprehensive (main) themes
1	Company financial resources	Firm's capabilities and resources
	The technological capacity of the company	
	The amount of working capital required	
2	Demographic characteristics of management	Managerial characteristics
	The main attitude and approach of management	
	Financial knowledge and marketing management	
	Level of risk management	
3	Company marketing budget	Marketing capacity
	Use of new marketing approaches	
	Customer position in company marketing programs	
4	Intra-firm relationships	Strategic capability
	Inter-firm relations	
	Network and industrial relations	
5	Personnel knowledge	Company human resources
	Staff training	
	International personnel experiences	
	Innovative staff ideas	

After analyzing the theme, the identified themes were left to the experts and for this purpose, fuzzy Delphi technique was used. For the first round of the Delphi technique, managers with a bachelor's degree or higher and university professors related to the industry were selected and a questionnaire related to the items extracted from the theme analysis process was distributed among them. The views of 20 experts on each indicator are shown in the table 5.

Table 4. Key decisions and incentives for Success in Covid 19 virus conditions

Row	Basic themes	Comprehensive (main) themes
1	From the heart of the threats, it creates new opportunities.	opportunities
	In crises, it quickly discovers new market needs and wants.	Discovering
	Flexibility and innovation are two prominent features of the company's core strategy	
2	Always looking to make changes in products and services tailored to the new needs and wants of customers	Innovativeness
	Reward system for presenting new and valuable ideas and suggestions	
3	Use the capacity to collaborate with other members of the value chain For quick response to new requests	Cooperation
	Strengthen the coordination and alignment capacity between different departments within the firm	
	Receive new comments and ideas from the company's loyal customers in critical situations	
4	Receive new comments and ideas from the company's expert staff through the quick suggestion system	Company specialized personnel
	Empowering personnel through the use of the capacity of specialized personnel with a high level of knowledge	
	Strengthen the creative capacity of staff through timely rewards and promotion of their organizational position	
5	Make more use of the capacity of the R&D team in critical situations	Research and development team
	Designing crisis-specific issues and presenting them to the R&D team to find practical solutions	
	Prioritize the reports of the research and development team in critical situations and timely encourage the best solutions	

Table 5. Fuzzy expert panel view for each of the research indicators

Fuzzy	Expert 1	Expert 2	Expert 3	...	Expert 20
Q01	(0.9, 1, 1)	(0.5, 0.75, 0.9)	(0.9, 1, 1)	...	(0.9, 1, 1)
Q02	(0.5, 0.75, 0.9)	(0.9, 1, 1)	(0.3, 0.5, 0.75)	...	(0.9, 1, 1)
Q03	(0.75, 0.9, 1)	(0.5, 0.75, 0.9)	(0.75, 0.9, 1)	...	(0.75, 0.9, 1)

Q04	(0.75, 0.9, 1)	(0.5, 0.75, 0.9)	(0.1, 0.3, 0.5)	..	(0.75, 0.9, 1)
Q05	(0.5, 0.75, 0.9)	(0.1, 0.3, 0.5)	(0.5, 0.75, 0.9)	..	(0.9, 1, 1)
Q06	(0.75, 0.9, 1)	(0.3, 0.5, 0.75)	(0.9, 1, 1)	..	(0.5, 0.75, 0.9)
Q07	(0.75, 0.9, 1)	(0.5, 0.75, 0.9)	(0.9, 1, 1)	..	(0.9, 1, 1)
Q08	(0.75, 0.9, 1)	(0.5, 0.75, 0.9)	(0.75, 0.9, 1)	..	(0.9, 1, 1)
Q09	(0.5, 0.75, 0.9)	(0.3, 0.5, 0.75)	(0.5, 0.75, 0.9)	..	(0, 0, 0.1)
Q10	(0.75, 0.9, 1)	(0.9, 1, 1)	(0.75, 0.9, 1)	..	(0.9, 1, 1)
Q11	(0.1, 0.3, 0.5)	(0.75, 0.9, 1)	(0.9, 1, 1)	..	(0.5, 0.75, 0.9)
Q12	(0.9, 1, 1)	(0.75, 0.9, 1)	(0.9, 1, 1)	..	(0.9, 1, 1)
Q13	(0.5, 0.75, 0.9)	(0.75, 0.9, 1)	(0.3, 0.5, 0.75)	..	(0.9, 1, 1)
Q14	(0, 0, 0.1)	(0.5, 0.75, 0.9)	(0.9, 1, 1)	..	(0.75, 0.9, 1)
Q15	(0.9, 1, 1)	(0.9, 1, 1)	(0.75, 0.9, 1)	..	(0.9, 1, 1)
Q16	(0.9, 1, 1)	(0.9, 1, 1)	(0.5, 0.75, 0.9)	..	(0.75, 0.9, 1)
Q17	(0.75, 0.9, 1)	(0.9, 1, 1)	(0.75, 0.9, 1)	..	(0.5, 0.75, 0.9)
Q18	(0.9, 1, 1)	(0.9, 1, 1)	(0.9, 1, 1)	..	(0.75, 0.9, 1)
Q19	(0.75, 0.9, 1)	(0.1, 0.3, 0.5)	(0, 0.1, 0.3)	..	(0.9, 1, 1)
Q20	(0.9, 1, 1)	(0.9, 1, 1)	(0.9, 1, 1)	..	(0.9, 1, 1)
Q21	(0.75, 0.9, 1)	(0.9, 1, 1)	(0.9, 1, 1)	..	(0.9, 1, 1)
Q22	(0.5, 0.75, 0.9)	(0.3, 0.5, 0.75)	(0.5, 0.75, 0.9)	..	(0, 0, 0.1)
Q23	(0.75, 0.9, 1)	(0.9, 1, 1)	(0.75, 0.9, 1)	..	(0.9, 1, 1)
Q24	(0.1, 0.3, 0.5)	(0.75, 0.9, 1)	(0.9, 1, 1)	..	(0.5, 0.75, 0.9)
Q25	(0.9, 1, 1)	(0.75, 0.9, 1)	(0.9, 1, 1)	..	(0.9, 1, 1)
Q26	(0.5, 0.75, 0.9)	(0.75, 0.9, 1)	(0.3, 0.5, 0.75)	..	(0.9, 1, 1)
Q27	(0.9, 1, 1)	(0.9, 1, 1)	(0.9, 1, 1)	..	(0.9, 1, 1)
Q28	(0.75, 0.9, 1)	(0.3, 0.5, 0.75)	(0.9, 1, 1)	..	(0.5, 0.75, 0.9)
Q29	(0.75, 0.9, 1)	(0.5, 0.75, 0.9)	(0.9, 1, 1)	..	(0.9, 1, 1)
Q30	(0.75, 0.9, 1)	(0.9, 1, 1)	(0.75, 0.9, 1)	..	(0.9, 1, 1)
Q31	(0.75, 0.9, 1)	(0.5, 0.75, 0.9)	(0.75, 0.9, 1)	..	(0.75, 0.9, 1)
Q32	(0.9, 1, 1)	(0.9, 1, 1)	(0.9, 1, 1)	..	(0.75, 0.9, 1)

The next step is to consolidate the views of experts. Various methods have been proposed to aggregate the n respondents' opinions. In fact, these aggregation methods are experimental methods that have been proposed by various researchers. For example, a conventional method for aggregating a set of triangular fuzzy numbers is the minimum l, the geometric mean m, and the maximum u.

$$F_{AGR} = \left(min\{l\}.\prod\{m\}.max\{u\}\right) \quad (3)$$

$$F_{AGR} = \left(min\{l\}.\prod\{m\}.max\{u\}\right) \quad (4)$$

$$F_{AVE} = \left(\left\{\frac{\sum l}{n}\right\}.\left\{\frac{\sum m}{n}\right\}.\left\{\frac{\sum u}{n}\right\}\right) \quad (5)$$

Each triangular fuzzy number resulting from the aggregation of experts' views for the jth index is represented as follows:

$$\begin{aligned} \tau\_j &= (L\_j, M\_j, U\_j) \\ L\_j &= \min(X\_ij) \\ M\_j &= \sqrt{(n\&\prod\_(i=1)\hat{}n X\_ij)} \\ U\_j &= \max(X\_ij) \end{aligned} \quad (6)$$

Index I, refers to an expert. So that;
X_ij: The value of the i-th expert evaluation of the j-th criterion
L_j: The minimum value of evaluations for the criterion j
M_j: The geometric mean of the experts' assessment of the performance of the standard j
U_j: The maximum value of evaluations for the criterion j
In this study, we have used the fuzzy mean method. It is usually possible to sum the sum of triangular and trapezoidal fuzzy numbers by a definite value which is the best corresponding mean. This operation is called de-fuzzing. There are several ways to de-fuzzy. In most cases, the following simple method is used for decapsulation;

$$x\_m\hat{}1 = (L+M+U)/3 \quad (7)$$

In this study, the surface center method is used for de-fuzzing;

$$[\![DF]\!]_{ij}=[(u_{ij}-l_{ij})+(m_{ij}-l_{ij})]/3+l_{ij} \quad (8)$$

The fuzzy mean and the de-fuzzy output are the values for the indices. A de-fuzzy value greater than 7 is acceptable, and any indicator with a score less than 7 is rejected.

Table 6. Results of screening indicators (first round)

Indicators	Bottom line	Probable value	upper bound	Fuzzy average	Definite amount	First round result
Item 1	0.584	0.834	0.937	(0.584,0.834,0.937)	0.785	Accept
Item 2	0.649	0.740	0.911	(0.649,0.740,0.911)	0.766	Accept
….	….	….	….	……	……	…
Item 32	0.599	0.701	0.909	(0.599,0.701,0.909)	0.736	Accept

All items with a score of less than 7 have been removed. After reviewing the accepted indicators (all 32 items), in the second round, the questions related to the mentioned items were again asked by the experts in the second round after the corrections of the higher level (academic) experts. In this round, all items were accepted. So we could finish the Delphi rounds.

Table 7. Results of screening indicators (third round)

Indicators	Round 1result	Round 2 result	Difference	Result
Item 1	0.785	0.798	0.013	Agreed
Item 2	0.766	0.787	0.021	Agreed
….	……	……	…….	……
Item 32	0.736	0.801	0.065	Agreed

The next phase in this research is the use of ISM. Interpretive structural modeling (ISM) was introduced by Sage in 1977. This method classifies the factors and identifies the relationships between the criteria. The steps for performing an interpretive structural model are as follows: Determining effective indicators; SSIM Structural Interactive Matrix Development; Formation of achievement matrix; Segmentation of achievement matrices to different levels; Drawing a diagram of power - dependence and progress. All the above steps were performed and finally classified into three levels as described in the table below. In this section, the key factors and drivers of success along with the required levels of innovation were classified into three main sections and approved by experts.

Table 8. Leveling of identified critical factors and drivers along with levels of innovation

Sub-bases	The main bases	New levels	Access set	Introduction Collection	Level
Managerial characteristics opportunities Discovering	Management factors	Organizational Innovation	**F2-I1**	**I1-F2-F1**	**1**
Strategic capability Research and development team Cooperation	Structural & strategic factors	Personnel innovation	**F4-I5-I3**	**I4-F4-I3**	**2**
Company human resources Company specialized personnel	Personnel factors	Managerial innovation	**F5-I4**	**I4-F5-I2**	**3**
Firm's capabilities and resources Marketing capabilities Innovativeness	Factors related to market conditions	Inter-firm innovation	**F1-F3-I2**	**I2-F3-F1**	**4**

Finally, GOF criterion was used to fit the research model. This criterion is related to the general part of structural equation models. This means that by this criterion, the researcher can control the overall section fit after examining the fit of the measurement part and the structural part of the general research model. The GOF criterion was introduced by Tenenhaus et al (2005).

$$\text{GOF} = \sqrt{Avg(\text{Communalities}) \times \text{R}^2} \quad (9)$$

Communalities is the mean of the common values of each structure and R ^ 2 is the mean value of the explained variance of the model's derivative structures. Three values of 0.1, 0.25, 0.36 have been introduced as weak, medium and strong values for GOF.

$$Avg\ (\text{R}^2) = 0.369$$

$$\text{GOF} = \sqrt{0.713 \times 0.369} = 0.513 \quad (10)$$

Table 9. Structural equation model path analysis

The effect			
Factors	Factors specific to specific conditions	Path coefficient	Statistics . T
Managerial characteristics	Organizational Innovation	0.563	4.625
opportunities Discovering		0.519	4.221
Strategic capability	Personnel innovation	0.580	4.728
Research and development team		0.539	4.311
Cooperation		0.576	4.449
Company human resources	Managerial innovation	0.511	4.09
Company specialized personnel		0.613	4.27
Firm's capabilities and resources	Inter-firm innovation	0.501	5.231
Marketing capabilities		0.629	5.311
Innovativeness		0.678	5.489

As can be seen, all the obtained path coefficients are higher than 0.5 and also the t-statistic related to each path coefficient is greater than 1.96. Therefore, all the assumed relationships (extracted from experts' opinions) between the critical factors, drivers and factors specific to the critical situation in the model are confirmed. In simpler terms, the designed classification of key success factors and the labels for specific conditions, such as the corona virus, have been approved. Another important point is that convergent validity has been calculated for the questionnaire items. Whenever one or more attributes are measured through two or more methods, the correlation between these measurements provides two important indicators of validity. If the correlation between the scores of the tests that measure a single characteristic is high, the questionnaire has convergent validity. The existence of this correlation is critical to ensuring that the test measures what needs to be measured. For convergent validity, the mean of extraction variance (AVE) and composite reliability (CR) were calculated and Cronbach's alpha of all variables was greater than 0.6. Therefore, the reliability of all variables has been confirmed at an acceptable level. Also, the mean value of extracted variance (AVE) for all items of the numerical questionnaire is greater than 0.5. Therefore, convergent validity is also at a moderate to high level. In addition, the value of composite reliability (CR) is also greater than AVE, so the three necessary conditions to confirm the validity and reliability of the questionnaire items have been met and the designed questionnaire has been statistically validated. In other words, the questions designed in the questionnaire have well examined the situation desired by the researcher. The figures related to the above statistics are presented in the table 10.

As can be seen, the known vital factors, incentives as well as specific factors of critical conditions have been approved by experts and the relationship between factors and classification and typology has been confirmed and the validity and reliability of the items of the designed questionnaires have been confirmed. Highly approved.

Table 10. Convergent validity and reliability of research variables

Factors	Cronbach's alpha	AVE	CR
Managerial characteristics	0.823	0.685	0.825
opportunities Discovering	0.876	0.647	0.795
Strategic capability	0.799	0.654	0.811
Research and development team	0.811	0.679	0.748
Cooperation	0.748	0.643	0.783
Company human resources	0.801	0.650	0.739
Company specialized personnel	0.793	0.672	0.823
Firm's capabilities and resources	0.820	0.669	0.758
Marketing capabilities	0.808	0.648	0.844
Innovativeness	0.784	0.653	0.839

5. Discussion and conclusion

The present study dealt with investigating the inner firm factors effective on the development of stable export. The research model was formulated by identifying the critical success factors, incentives, and also by taking into account specific factors of critical conditions such as coronavirus 19 (coronavirus).

According to the research findings, the most important critical factors for the success of companies' export performance are:

- ✓ Firm's capabilities and resources
- ✓ Managerial characteristics
- ✓ Marketing capacity
- ✓ Strategic capability
- ✓ Company human resources

In addition, key incentives for critical situations such as the Covid 19 virus; as follows:

- ✓ Discovering opportunities
- ✓ Innovativeness

- ✓ Cooperation
- ✓ Company specialized personnel
- ✓ Research and development team

Another important finding of the present study, which according to the authors is research innovation; providing a simultaneous combination of critical success factors and specific incentives and innovations is a critical condition for achieving a sustainable export performance. Based on the relationships identified between these factors, four categories of innovation were finally identified and approved by experts at both managerial and academic levels. It placed. Accordingly, the new typology is introduced as follows.

- ❖ Organizational Innovation
- ❖ Personnel innovation
- ❖ Managerial innovation
- ❖ Inter-firm innovation

Therefore, in order to respond promptly and quickly to environmental changes in critical situations such as the Corona virus, it is necessary for businesses to be empowered in these four levels of innovation (organizational, personnel, managerial and inter-firm). Moreover, the findings of the study showed that there is a direct relationship between management's risk-taking behavior (i.e. the amount to which they accept risk) and firms' export performance. In other words, the amount to which managers accept risk and adopt entrepreneurship behavior, is a factor effective on firms' export performance. In fact, the more managers adopt a risk-taking personality and the more creative persons they are, the more they'll decide to seek for generating an environment which leads to the offering of new ideas and attendance in new markets. The most significant of all, the creative personality of manager will in itself be an effective factor that provides the staff with incentives to participate more in the decision makings of the firm, hence leading them to become more satisfied with their jobs. This, in the end, will improve the performance of firm.

With respect to the attitude of management towards export, it is necessary to maintain that managers' knowledge about export is directly related to export performance. As a matter of fact, the more the mangers are aware of export performance (i.e. the more they are familiar with the principles and concepts of export), the more export performance of the firm will improve. Moreover, based on the results, the findings of the Critical Success Factors are consistent with many studies done in this area [12, 19, 84. 85, 20].

And in the section of special incentives for critical situations, the research findings are in line with the research results of Bini et al (2018); [86, 87].

6. Research suggestions

Based on the research findings, the proposed research package and policy of the present study have been designed in two levels;

At the first level, the government and government agencies related to economics and business enterprises and organizations related to crisis management, it is necessary to design new training for managers and other personnel categories on empowering businesses to deal with crisis situations.

At the enterprise level, too, senior managers are needed to empower critical situations at all four levels; Organize organizational, managerial, personnel and inter-enterprise, and include the necessary culture-building in preparation for future crisis situations and discovering opportunities from potential crises as part of the organization's strategies.

An important point, based on the findings of the present study, is the need to focus on innovation to manage crises such as the Corona virus, which requires senior executives to work towards comprehensive empowerment at all four levels.

7. Research Limitations

The main limitation of the present study was its implementation in the corona situation in 2020. Due to social constraints such as maintaining physical distance, researchers were forced to interview the statistical sample through video conferencing with virtual tools such as WhatsApp, etc.

Another point is the combination of the opinions of business managers with university professors that the research team had to select managers with higher university education at this level, which ultimately allows the combination of opinions. In addition, we added a round to the steps of the fuzzy Delphi technique, in which the opinions of both groups and their combinations were returned to the members of the statistical sample (managers and professors) and after their desired corrections were approved.

References

[1] Chakraborty, I., & Maity, P. (2020). COVID-19 outbreak: Migration, effects on society, global environment and prevention. Science of the total environment, 728, 138882.

[2] Bavel, J. J. V., Baicker, K., Boggio, P. S., Capraro, V., Cichocka, A., Cikara, M., ... & Willer, R. (2020). Using social and behavioural science to support COVID-19 pandemic response. Nature human behaviour, 4(5), 460-471.

[3] Harper, C. A., & Rhodes, D. (2020). Ideological responses to the breaking of COVID-19 social distancing recommendations. Group Processes & Intergroup Relations, 13684302221074546.

[4] Seah, I., & Agrawal, R. (2020). Can the coronavirus disease 2019 (COVID-19) affect the eyes? A review of coronaviruses and ocular implications in humans and animals. Ocular immunology and inflammation, 28(3), 391-395.

[5] Nicola, M., Alsafi, Z., Sohrabi, C., Kerwan, A., Al-Jabir, A., Iosifidis, C. & Agha, R. (2020). The socio-economic implications of the coronavirus pandemic (COVID-19): A review. International journal of surgery, 78, 185-193

[6] Chesbrough, H. (2020). To recover faster from Covid-19, open up: Managerial implications from an open innovation perspective. Industrial Marketing Management, 88, 410-413.

[7] Luo, M., Guo, L., Yu, M., Jiang, W., & Wang, H. (2020). The psychological and mental impact of coronavirus disease 2019 (COVID-19) on medical staff and general public–A systematic review and meta-analysis. Psychiatry research, 291, 113190.

[8] Schindehutte, Minet et al (2008). Understanding Market-Driving Behavior: the Role of Entrepreneurship, Journal of Small Business Management, Vol. 46, Issue. 1, pp. 4-26.

[9] Zhao, Q., Meng, M., Kumar, R., Wu, Y., Huang, J., Deng, Y., ... & Yang, L. (2020). Lymphopenia is associated with severe coronavirus disease 2019 (COVID-19) infections: A systemic review and meta-analysis. International journal of infectious diseases, 96, 131-135.

[10] Dhanaraj, C., & Beamish, P. W. (2003). A resource-based approach to the study of export performance. Journal of small business management, 41(3), 242-261.

[11] Porter, M. E. (1981). The contributions of industrial organization to strategic management. Academy of management review, 6(4), 609-620.

[12] Leonidou, L. C. (1998). Factors stimulating export business: an empirical investigation. Journal of Applied Business Research (JABR), 14(2), 43-68.

[13] Leonidou, L. C., Katsikeas, C. S., & Samiee, S. (2002). Marketing strategy determinants of export performance: a meta-analysis. Journal of Business research, 55(1), 51-67.

[14] Racela, O. C., & Thoumrungroje, A. (2019). Enhancing export performance through proactive export market development capabilities and ICT utilization. Journal of Global Marketing, 1–18.

[15] Mittal, R., Aggarwal, V. S., & Rawat, D. (2019). Exploring business networks and its impact on firm performance in an auto-component cluster: A study of gurgaon autocomponent cluster. Research Journal of Humanities and Social Sciences, 10 (2), 449–464.

[16] Huang C, Wang Y, Li X, Ren L, Zhao J, Hu Y, et al (2020), Clinical features of patients infected with 2019 novel coronavirus in Wuhan, China. Lancet 395(10223):497-506.

[17] Guan WJ, Ni ZY, Hu Y, Liang WH, Ou CQ, He JX, (2020), Clinical Characteristics of Coronavirus Disease 2019 in China. N Engl J Med 382(18):1708-1720.

[18] Ziegler CGK, Allon SJ, Nyquist SK, Mbano IM, Miao VN, Tzouanas CN, et al. (2020), SARSCoV-2 receptor ACE2 is an interferon-stimulated gene in human airway epithelial cells and is detected in specific cell subsets across tissues.

[19] Li Q, Guan X, Wu P, Wang X, Zhou L, Tong Y, (2020), Early Transmission Dynamics in Wuhan, China, of Novel Coronavirus-Infected Pneumonia. N Engl J Med 382(13):1199- 1207.

[20] Rodrigues. T (2020), Exploring impacts of COVID-19 from sport business manager's perspective, Master's thesis June 2020, School of Business Degree Programme in Sport Business Management, JAMK.FI.

[21] Kara, Ali et al. (2005). The Effect of a Market Orientation on Business Performance: A Study of Small-Sized Service Retailers Using MARKOR Scale, Journal of Small Business Management, 43 (2), pp. 105-118.

[22] Leonard-Barton, D. (1992). Core Capabilities And Core Rigidities: A Paradox in Managing New Product Development, Strategic Management Journal, 13 (Summer), pp. 111-125.

[23] Zou, S., & Stan, S. (1998). The determinants of export performance: a review of the empirical literature between 1987 and 1997. International marketing review, 15(5), 333-356.

[24] Ling-Yee, L., & Ogunmokun, G. O. (2001). The influence of interfirm relational capabilities on export advantage and performance: an empirical analysis. International Business Review, 10(4), 399-420.

[25] Rhee, Jaehoon et al. (2009). Drivers of innovativeness and performance for innovative SMEs in South Korea: Mediation of learning orientation, Technovation, doi:10.1016/j.technovation.2009.04.008.

[26] Pelham, Alfred M. and Wilson, David T. (1996). A longitudinal study of the impact of market structure, firm structure, strategy, and market orientation culture on dimensions of small-firm performance, Journal of the Academy of Marketing Science, 24 (1), pp. 27–43 .

[27] Sinkula, J.M., Bake, W. and Noordewier, T.G. (1997). A framework for market-based organizational learning: linking values, knowledge

and behavior, Journal of the Academy of Marketing Science, 25 (4), pp. 305–318.

[28] Sinkula, J.M. (1994). Market information progressing and organizational learning, Journal of Marketing, 58, pp. 35–45.

[29] Yasseri, S. (2019). A Systems Engineering Approach to Physical Security of Oil & Gas Installations. International Journal of Coastal and Offshore Engineering, 4(3), 17-31.

[30] Aaby, N. E., & Slater, S. F. (1989). Management influences on export performance: a review of the empirical literature 1978-1988. International marketing review, 6. (4).

[31] Alegre, J. and Chiva, R. (2008). Assessing the impact of organizational learning capability on product innovation performance: an empirical test, Technovation, 28, pp. 315–326.

[32] Morgan, D. P., Rime, B., & Strahan, P. E. (2004). Bank integration and state business cycles. The Quarterly Journal of Economics, 119(4), 1555-1584.

[33] Mira, M., Choong, Y., & Thim, C. (2019). Mediating role of port supply chain integration between involvement of human resource practices and port performance in Kingdom of Saudi Arabia. Uncertain Supply Chain Management, 7 (3), 507–516 .

[34] Manzoor, S. (2016). Furniture industry in Pakistan and its export status. Retrieved from https://www.slideshare.net/jik 1959/1-furniture-industry.

[35] Matsuno, Ken et al. (2002). The Effects of Entrepreneurial Proclivity and Market Orientation on Business Performance, Journal of Marketing, Vol. 66, Issue. 3, pp. 18-32.

[36] Langerak, Fred and Commandeur, Harry R. (1998).The influence of market orientation on competitive superiority and performance of industrial business, 27th EMAC Conference, Stockholm.

[37] Nonaka, I. and Takeuchi, H. (1995). The Knowledge-creating Company: How Japanese Companies Create the Dynamic of Innovation, Oxford University Press, New York, NY.

[38] Shoham, A. (1998). Export performance: A conceptualization and empirical assessment. Journal of international marketing, 6(3), 59-81.

[39] Radzi, M., Junoh, A. S., Hussain, N. S. N., Aziz, Z., & Zawawi, N. (2015). 'the effect of information, communication and technology (ICT) and quality management to export performance of Malaysian's SME in manufacturing sector. Journal of Scientific Research and Development, 2 (14), 146–157.

[40] Nguyen, Tho D., and Barrett, Nigel J. (2006). The Adoption of the Internet by Export Firms in Transitional Markets, Asia Pacific Journal of Marketing and Logistics, 18 (1), pp. 29- 42.

[41] Rekarti, E., Doktoralina, C. M., & Saluy, A. B. (2018). Development model of marketing capabilities and export performance of smes: A proposed study. European Journal of Business and Management, ISSN , 2222–1905.

[42] Mac, L., & Evangelista, F. (2016). The relative impact of market orientation and entrepreneurship on export performance: do we really know enough? Journal of Global Marketing, 29 (5), 266–281.

[43] Liu, S.S., Luo, X. and Shi, Y. (2002). Integrating customer orientation in organizations-in-transition: an empirical study, International Journal of Research in Marketing, 19, pp. 367–382.

[44] Hunt, S. D. and Morgan, R.M. (1996). The Resource Advantages Theory of Competition: Dynamic, Path Dependencies and Evolutionary Dimensions, Journal of Marketing, 60(October), pp. 107-114.

[45] Levitt, Theodore (1980). Marketing Success Through differentiation of Anything, Harvard Business Review, 58 (January/Februrary), pp. 83-91.

[46] Dad, A., & Karim, A. M. (2019). A Literature Review on External Factors Affecting Export Competitiveness of Raw Woven Sector of Pakistan. Malaysian Journal of Social Sciences and Humanities (MJSSH), 4(2), 51-58.

[47] Zhou, X. (2020). Managing Psychological Distress in Children and Adolescents Following the COVID19 Epidemic: A Cooperative Approach. Psychological Trauma: Theory, Research, Practice, and Policy.

[48] Brown, G., & Susskind, D. (2020). International cooperation during the COVID-19 pandemic. Oxford Review of Economic Policy, 36(Supplement_1), S64-S76.

[49] Celec, R., Globocnik, D., & Kruse, P. (2014). Resources, capabilities, export performance and the moderating role of entrepreneurial orientation in the context of smes. European Journal of International Management, 8 (4), 440–464.

[50] Haroon, U., & Mohd Shariff, M. N. (2016). The interplay of innovation, TQM practices and SMEs performance in Pakistan: moderating effects of knowledge inertia and external environment. South East Asia Journal of Contemporary Business, Economics and Law, 9(2), 57-62.

[51] Collins, Jerome H., and Moschler, Joseph (2008). The Life Cycle of Innovations, Defense AR Journal, Vol. 15, Iss. 1, pp. 75-85.

[52] Samiee, S., & Walters, P. G. (1991). Segmenting corporate exporting activities: sporadic versus regular exporters. Journal of the Academy of Marketing Science, 19(2), 93-104.

[53] Liao, S., Fei, W.-C., Liu, C.-T. (2008). Relationships between knowledge inertia, organizational learning and organizational innovation. Technovation 28, 183–195.

[54] Galer, G. and van der Heijden, K. (1992). The Learning Organization: How Planners Create Organizational Learning, Marketing Intelligence & Planning, Vol. 10. No.6, pp. 5-12.

[55] Gatignon, Hubert and Xuereb, Jean-Marc (1997). Strategic Orientation of the Firm and New Product Performance, Journal of Marketing Research, Vol. 34, pp. 77-90 .

[56] Hart, S., & Tzokas, N. (1999). The impact of marketing research activity on SME export performance: evidence from the UK. Journal of small business management, 37(2), 63.

[57] Katsikeas, C. S., Piercy, N. F., & Ioannidis, C. (1996). Determinants of export performance in a European context. European journal of Marketing, 30(6), 6-35.

[58] Calof, J. L. (1994). The relationship between firm size and export behavior revisited. Journal of international business studies, 25, 367-387.

[59] Aulakh, P. S., Kotabe, M., & Teegen, H. (2000). Export strategies and performance of firms from emerging economies: Evidence from Brazil, Chile, and Mexico. Academy of management Journal, 43(3), 342-361.

[60] Lages, L. F., Lages, C., & Lages, C. R. (2006). European managers' perspective on export performance determinants. Journal of Euromarketing, 15(2), 75-92.

[61] Kamalinejad, M., Sheykhbahaee, A., & Mazaheri, S. (2016). Financial feasibility study between purchasing and hiring LNG carrier in Iranian LNG industry. International Journal Of Coastal, Offshore And Environmental Engineering, 1(1), 25-31.

[62] Mehra, E., Fathi, Z., & Minouei, M. (2023). Identify Environmental Risks Affecting Financial Performance of Ports and Maritime Organization in Iran. International Journal Of Coastal, Offshore And Environmental Engineering.

[63] Voerman, J.A. , M.Wodel and P.S. Zwart, (2000), "Export Market Information Behaviour of SMEs: the Influence of firm Characteristics" SOM theme B: Marketing and Network.

[64] Norman R. (1985). Developing capabilities for organizational learning. In: Pennings JM, editor. Organizational strategy and change. San Francisco (CA): Jossey-Bass.

[65] Cavusgil, S. T., & Zou, S. (1994). Marketing strategy-performance relationship: an investigation of the empirical link in export market ventures. Journal of marketing, 58(1), 1-21.

[66] Lages, B. G., Fleury, B. G., Hovell, A. M., Rezende, C. M., Pinto, A. C., & Creed, J. C. (2012). Proximity to competitors changes secondary metabolites of non-indigenous cup corals, Tubastraea spp., in the southwest Atlantic. Marine Biology, 159, 1551-1559.

[67] Boubakri, N., Mansi, S. A., & Saffar, W. (2013). Political institutions, connectedness, and corporate risk-taking. Journal of International Business Studies, 44, 195-215.

[68] Avlonitis, George J. and Gounaris, Spiros P. (1999). Marketing orientation and its determinants: An empirical analysis, European Journal of Marketing, 33 (1999) (11/12), pp. 1003–1037.

[69] Baker, W.E., Sinkula, J.M. (1999). The synergistic effect of market orientation on organizational performance, Journal of the Academy of Marketing Science, 27, pp. 411–427.

[70] Cooper, R.G. (2000). New product performance: what distinguishes the star products, Australian Journal of Management, 25 (1), pp. 17–45.

[71] Chetty, S. K., & Hamilton, R. T. (1993). Firm-level determinants of export performance: a meta-analysis. International Marketing Review, 10.(3).

[72] Francis, J., & Collins-Dodd, C. (2000). The impact of firms' export orientation on the export performance of high-tech small and medium-sized enterprises. Journal of international Marketing, 8(3), 84-103.

[73] Goes, J.B. and Park, S.H. (1997). Interorganizational links and innovation: the case of hospital services, Academic Management Journal, 40(3), pp.673–96.

[74] Calantone, R.J., Cavusgil, S.T., Zhao, Y. (2002). Learning orientation, firm innovation capability, and firm performance, Industrial Marketing Management, 31, pp. 515–524.

[75] O'Cass, A., & Julian, C. (2003). Examining firm and environmental influences on export marketing mix strategy and export performance of Australian exporters. European journal of marketing, 37(3/4), 366-384.

[76] Brockman, Beverly K. and Morgan, Robert M. (2003). The Role of Existing Knowledge in New Product Innovativness and Performance, Decision Sciences, 34 (2), pp. 385-419.

[77] Cooper R.G., and Kleinschmidt, E.J. (1987). New products: what separates winners from losers?, Journal of Product Innovation Management,4, pp.169–84.

[78] Abeykoon, M., & De Alwis, C. (2015). The impact of total quality management practices on export performance of apparel exporters in Sri Lanka. Kelaniya Journal of Human Resource Management, 10 (1).

[79] Boso, N., Adeola, O., Danso, A., & Assadinia, S. (2017). The effect of export marketing capabilities on export performance: Moderating role of dysfunctional competition. Industrial Marketing Management.

[80] Craven, M., Mysore, M., Singhal, S. & Wilson, M. (2020). Covid-19: Business Implications. McKinsey & Company's website. Accessed on 29 April 2020.

[81] Johanson, J., & Vahlne, J.-E. (2011). Markets as networks: implications for strategymaking. Journal of the Academy of Marketing Science, 39 (4), 484–491.

INTERNATIONAL JOURNAL OF
COASTAL, OFFSHORE & ENVIRONMENTAL ENGINEERING IJCOE Vol.8/No. 1/winter 2023 (45-60)

Available online at: www. Ijcoe.org

Experimental and Numerical Investigation of Degree of Freedom Effects on Hydrodynamic Performance of Floating Breakwaters Under Regular Waves

Naser Abasi [1], Cyrus Ershadi [2*], Mohamad Ali Lotfollahi Yaghin [3], Alireza Mojtahedi [4]

[1] *PhD. in marine engineering, University of Hormozgan; N.Abasi.Phd@hormozgan.ac.ir*
[2*] *Assistant professor, University of Hormozgan; Cyrusershadi1@yahoo.co.uk*
[3] *Professors, University of Tabriz; Lotfollahi@tabrizu.ac.ir*
[4] *Associate professor, University of Tabriz; A.Mojtahed@tabrizu.ac.ir*

ARTICLE INFO

Article History:
Received: 05 Sep. 2022
Accepted: 28. Jan 2023

Keywords:
Floating Breakwater
Degree of Freedom
Stiffness of Anchorage System
Hydrodynamic Performance
Transmission Coefficient

ABSTRACT

In designing of any system that deals with forces and displacements some of the effective parameters on hydrodynamic behavior that needs to be investigated are the degree of freedom, and the stiffness of the support systems. In the present study, the effects of degree of freedom on hydrodynamic performance of a box type floating breakwaters (FB) is investigated experimentally and numerically. The experiments were conducted in the 2D wave flume of the (SCWMRI). Regular waves were generated by a piston type wave paddle controlled by 'DHI wave generating' software. The effect of incident waves characteristics on efficiency of FB is examined in four configurations. In this paper, a new dimensionless parameter (DB/L^2, i.e., draft times width divided by wavelength squared) is identified as an essential parameter for comparison between theories and the experimental data. Generally, the most efficient configuration is the fixed breakwater, but considering the tidal phenomenon, providing the required draft of FB will increase the cost of project. For short wavelengths, it is seen that the efficiency of pile-restrained FB is good same as the fixed type in mild conditions. Regarding the cost-effectiveness, the configuration of the FB with the pile should be considered the most efficient for design purposes in mild conditions.

1. Introduction

With the increasing importance of port construction economics, one of the most useful possible options can be floating breakwaters. Moreover, they have less damage to coastal ecosystem. The safety of these structures under wave action is of utmost importance to avoid significant economic losses, and negative environmental and social impacts. A conventional solution for protecting marine structures and fragile shorelines is to use bottom-founded breakwaters which can be constructed by using quarried rocks or concrete caissons resting on a foundation on the seabed. While the bottom-founded breakwater solution is effective in blocking ocean waves, it may not be economical for water depths larger than 6m or for soft seabed due to the enormous foundation costs [1]. The importance of this issue is doubled when the mild wave conditions become dominant in the port location. Nowadays, the use of floating breakwaters is increasing, so more research is needed to expand human knowledge about their hydrodynamic behaviors. Floating breakwaters have many benefits, including low running costs, no dependence on seabed soil characteristics, and rapid installation and operation but the main problem with them is their low efficiency against long waves. Floating breakwaters (FBs), compared with the traditional fixed-bottom breakwaters, are less dependent on the bottom topography and seabed conditions, they are more economical, and they can be easily installed, assembled, and removed. Furthermore, floating breakwaters are eco-friendly. Therefore, this type of breakwaters has been considered by researchers and a lot of studies have been done on them in recent decades (Abul-Azm and Gersha; Carr; Duan et al.; Weng and Chou).

Dai et al, classified FBs into seven categories according to their shapes: (1) box-type, (2) pontoon-type, (3) frame-type, (4) mat-type, (5) tethered float type, (6) horizontal plate type, and (7) other types. Since the shape of the structure affects the mechanism of wave energy dissipation, it is an important parameter for its efficiency. In addition to the shape of the structure, the

type of structural restraint system also affects the hydrodynamic performance of the structure. FBs have been investigated in three modes namely, fixed breakwaters (no degree of freedom), FBs restrained by pile (1 degree of freedom) and FBs restrained by mooring lines (6 degree of freedom). Moored FBs can have different hydrodynamic performance depending on the length, stiffness, and angle of mooring lines.

Carr developed an equation for the transmission coefficient of a rectangular cross-section assuming linear damping. The solution was introduced for shallow water waves; hence the pressure distribution was hydrostatic [26].

1.1. Experimental studies

Koutandos et al. studied a fixed and pile-restrained box-type FB experimentally and explored the effect of attaching a plate to the structure. They concluded that the heave motion FB operated in a dissipative manner, with much lower reflection than that of the single fixed breakwater. Also, a numerical and experimental investigation was conducted by Koutandos and Prinos, [4].

In the mentioned study, the wave interaction with a fixed, partially immersed breakwater of box type with a plate attached (impermeable–permeable) to the front part of the structure was investigated. Based on the hydrodynamic characteristics, it was inferred that the breakwater with an impermeable plate attached to its bottom is more efficient. The comparison of horizontal and vertical forces acting on the breakwater for all cases examined reveals that the plate porosity influences slightly the vertical force and severely the horizontal force acting on the structure, reducing maximum values in both cases.

Tolba investigated experimentally the effect of the draft and width of the fixed box-type breakwater. The results illustrated that, with increasing the draft and width of the structure, the transmission coefficient decreased. Also, Tolba and Isaacson and Bhat studied experimentally the influence of the heave motion on the efficiency of the pile-restrained FBs and. Ruol et al. studied the effect of mooring stiffness on the behavior of π-type FB experimentally and numerically. They compared FB anchored by pile, tethered with elastic lines and loose chain. The results concluded that the most effective restraining system depended on the range of periods and the ratio between draft and depth. The performance of the FBs moored with tethered lines was better than that of the FBs moored with loose chains. For periods shorter than the natural period of FB, pile supported FBs performed better than tethered supported ones. Also, for periods close to the natural period of FB, chain moored FBs behaved better than pile supported FBs.

Ruol et al. developed a modification factor for the formula of Macagno to approximate the wave transmission coefficients of floating breakwaters anchored by chains or cables. This modification factor is based on a dataset of experimental data, and it is a function of the relative period χ which is defined as the wave peak period over the natural heave period (T_p/T_h). Based on examination of the applicability of this formula, it is concluded that this formula is valid for ordinary pontoon type and π-type floating breakwaters anchored by chains. Furthermore, the formula is valid for a relative draft (D/d) range between 0.20 and 0.60 and for relative period range ($T_p/T_h = \chi$) between 0.50 and 1.50. The dimensionless parameter χ is determined as follows [5]:

$$\chi = {T_p}/{T_h} = \frac{T_p}{2\pi}\sqrt{\frac{g}{D+0.35B}} \quad (1)$$

where g is acceleration due to gravity, D is the draft, d denoted the water depth and B is the FB's width. Ruol considered the peak period T_p (irregular waves), but Macagno assumes mean period T_m in his theory (only regular waves), hence, to apply Macagno in combination with χ, the wave period T_m for the calculation of χ should be increased by 10%.

Peña et al. investigated wave transmission coefficient experimentally, mooring lines with four different configurations of FBs. A comparison of elastomeric mooring versus chains was made. Results revealed that with the elastic mooring lines, the static loads were greater, but the dynamic ones were lower. Also, the mooring lines configuration had no influence on the wave transmission [9].

Yamamoto investigated a rectangular cross-section and a hydrodynamically shaped 'three-cycle cylinder' breakwater. The results showed that the dynamic mooring force in the sea-side line was considerably larger than that in the leeside [28].

Ning et al. examined and introduced a pile-restrained WEC-type floating breakwater. Vertical piles prevent horizontal movement and permit only the heave motion. However, the pile restrained FB is relatively expensive. In addition, it has some disadvantages such as strong abrasion between structure and pile, withstanding large wave loads and not being suitable for deep water and poor foundation [1].

Ozeren et al. setup a laboratory investigation of the hydrodynamic interaction of cylindrical breakwaters with monochromatic waves in deep and transmissional water depths. Results showed that, when the breakwater models were fixed, the reflection was higher than the partially restrained models, and the efficiency was strongly dependent on draft ratio (z_d/d, where z_d is the draft and d represent the height of the structure).

For the measured range of waves, z_d/d=0.7 was the best value of the tested draft ratios for the pile-restrained model and horizontal restraint was found to be more important than vertical restraint in terms of improving the breakwater efficiency.

Veldee showed that in any ratio of wavelength to breakwater length, with increasing wave height, the mooring force also increased. Ji et al. setup a 2D experiment to study four models; including a traditional box-type FB, namely the traditional cylindrical FB, the cylindrical FB with cage and the cylindrical FB with cage and suspended balls. They concluded that mooring forces increased with the wave period for all four models. Forces acting on the windward mooring lines of the cylindrical model with cage and suspended balls were at least 50% larger than the other two cylindrical models [21]. An experimental study of a porous floating breakwater was carried out by Wang and Sun. They considered two mooring modes; directional mooring, and bidirectional mooring. They concluded that the transmission coefficient of the bidirectional mooring declined 20% by comparing it with the directional mooring. Loukogeorgaki et al. set up an experimental investigation by a 3D physical model focusing on the structural response (connector and mooring line loads) for assessing the wave attenuation effectiveness of a FB, consisting of an array of multiple floating box-type modules, under the action of perpendicular and oblique regular and irregular waves. They concluded that the FB's structural response depends strongly upon the wave period, while the wave height and the angle affect this response mainly in the low frequency range. The increase of the wave obliqueness may lead to a more efficient FB in terms of both functional and structural integrity issues.

1.2. Numerical studies

Zhang et al. used the CFD method to simulate the hydrodynamic properties and the vorticity characteristics of a fixed rectangular, inverted π-type and L-type breakwater. The numerical accuracy of the viscous model is confirmed by comparison of the wave transmission and reflection coefficients between the viscous flow, potential flow, and experimental results. Furthermore, the vorticity field on these two types of FBs are discussed and compared respectively. Further, the characteristics like the vortex evolution, the flow pattern, and the vorticity magnitude around the inverted π-type fixed breakwater is analyzed in detail. They proposed the L type breakwater and showed that this model had a better performance than the other two models.

Using a theoretical and numerical study, Drimer et al. investigated a box-type FB with various mooring stiffness. The implementation of simplifying assumptions concerning the flow beneath a pontoon-type floating breakwater leads to an analytical solution of the two-dimensional linearized hydrodynamic problem. They suggested a flexible mooring system, which reacted to the drift force only, was a more practical solution for large structures [1]. Gesraha investigated the reflection and transmission of incident irregular waves interacting with a π-type floating breakwater using an eigenfunction expansion method [15].

Chen et al. studied theoretically the hydrodynamic behaviors of a floating breakwater consisting of a rectangular pontoon and horizontal plates. They concluded that the mooring force of the floating breakwater with plate was less than that of the single pontoon floating breakwater.

Ouyang et al. investigated Bragg reflection from a train of fixed breakwaters. A numerical model of boundary discretization type was developed to calculate the wave field. The results showed that the Bragg reflection exhibited significant dependence on the relative spacing between the breakwaters. Since fixed breakwaters in areas with tides require a lot of materials and as a result have no economic justification, it is preferred to use pile-restrained FBs rather than fixed ones in these areas. The performance of a floating breakwater with cage aquaculture was investigated by Tang et al. using numerical wave tank. They studied the influences of net depth and net width on the dynamic response. The results revealed that the mooring force decreased as the net depth increased, especially in the vicinity of the resonant frequency.

It is obvious that most of the research on floating breakwaters is investigated by two-dimensional models. Furthermore, a comparative review of 3D basin experiment against 2D wave flume experiment can make this fact clear that 3D experiments can obtain more affecting parameters on FB's dynamic characteristics and wave dissipation mechanism. However, prior to finding a remarkable solution in 3D environment, it is necessary to have a better understanding of hydrodynamic behavior in 2D experiments and recognizing most effectual parameters in this regard. The aim of this study is to present a comprehensive study of box-type floating breakwater anchorage systems. For this purpose, a box-type FB is investigated experimentally and numerically in four modes of restrains, which are fixed, pile-restrained, moored by loose chains and tethered by cables. The experiments are conducted under regular waves with different wave heights and wave periods.

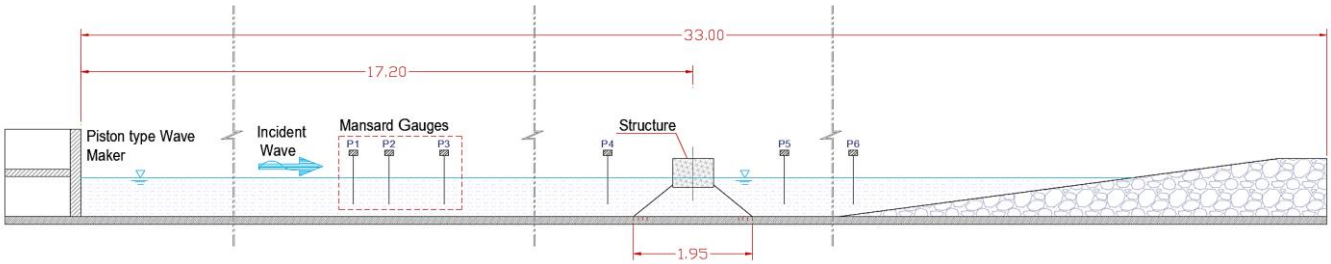

Figure 1. Side view of wave flume and wave gauges position

2. Experimental and numerical procedures

2.1. Experimental setup and test conditions

The experiments were conducted in a 2D wave flume of the research institute (SCWMRI), located in Tehran, Iran. The length, depth and width of the flume were 33*m*, 1*m* and 1*m* respectively. A piston-type wavemaker (made by DHI) was installed at the end of the flume (Figure 3.d) and a wave absorbing beach was located at the other side to prevent the reflection of transmitted waves. The floating breakwater was located 17*m* away from the wavemaker. Figure 1 shows a general layout of the wave flume.

A rectangular box was chosen as the floating breakwater because a lot of research have been done with the mentioned shape. the main geometric parameters of the physical model are presented in Figure 2. where *B* is width of the model, *d* represents water depth and *D* is the draft. Three different drafts of the floating breakwater are implemented in the present study (*D/d*=0.20, *D/d*=0.25, and *D/d*=0.40). To summarize the results, all the results are shown for the relative draft of *D/d*=0.2.

Mansard wave gauges were used to separate the incident and reflected waves. The water depth was 0.67m and the bed was completely flat through the flume length. An absorbing beach in the rear side was used to dissipate the transmitted energy. Several regular waves were generated with different periods and different wave steepness. Resistance type wave gauges (made by DHI) were used for gathering data with sampling frequency of 10*Hz* (Figure 3.a). To calculate the displacement of the floating breakwater, ship movement gages made by DHI Company were used (Figure 3.c). The movement in these experiments were in three directions, heave, sway, and roll. Also,

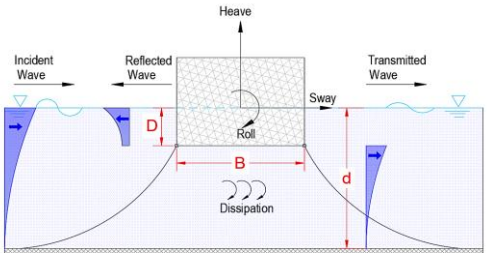

Figure 2. Main geometric parameters of the physical model

the loads on the mooring system were measured by four strain gauges with sampling frequency of 100*Hz*. A pressure sensor was attached on the submerged part of the breakwater in front of the generated waves.

Figure 3. Measurement equipments of the present investigation; (a): Wave gauges, (b): Data logger, (c): Movement gauge, (d): Wavemaker paddel

Numerous wave heights and periods were generated during the experiments to cover the range of intermediate waters. Table 1 shows the experimental test conditions. In the table, *L* is the wavelength and *H* denotes the wave height.

In this research, the Zero-up crossing method is used to analyze the data recorded by the sensors. The MATLAB software is used to code the mentioned method. An example of regular wave analysis output generated in the laboratory is shown in Figure 4. The WAFO module of MATLAB software also is used to control the distribution of the generated waves. The normal probability distribution as well as the up-crossing intensity diagram for the waves are plotted in

Table 1. Experimental test conditions

CONFIGURATION	H(*m*)	T(*s*)	L(*m*)	D(*m*)	D/d	B(*m*)	B/L	T_H
Fixed	0.07-0.1	0.70-4.20	0.77-10.5	0.13-0.27	0.20-0.40	0.67	0.064-0.87	1.22-1.35
Pile-restrained	0.07-0.1	0.70-4.20	0.77-10.5	0.13-0.27	0.20-0.40	0.67	0.064-0.87	1.22-1.35
Anchored by chain	0.07-0.1	1.00-4.20	1.55-10.5	0.13-0.27	0.20-0.40	0.67	0.43-0.87	1.22-1.35
Tethered by cable	0.07-0.1	1.00-4.20	1.55-10.5	0.13-0.27	0.20-0.40	0.67	0.43-0.87	1.22-1.35

Figure 5 to examine the generated waves degree of similarity with the Gaussian Sea waves (in this figure the number of up-crossings of wave data is plotted and compared with an estimation based on the assumption that the data is a realization of a Gaussian Sea).

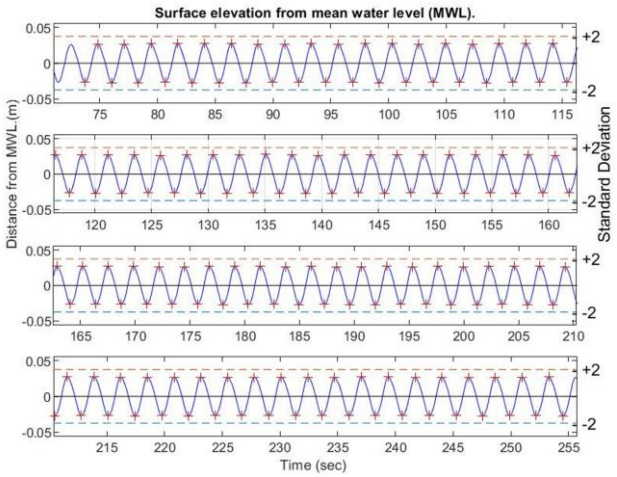

Figure 4. A sample of regular wave analysis output generated in the laboratory

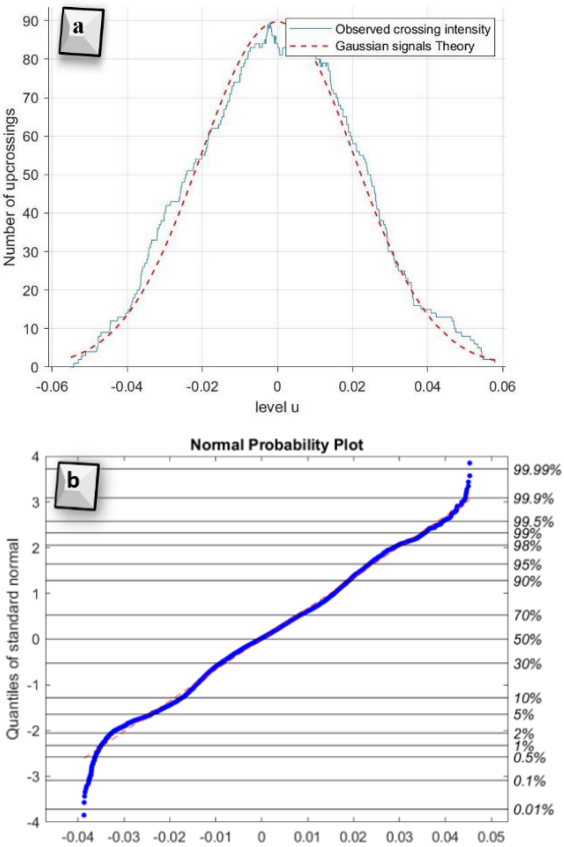

Figure 5. (a): Up-crossing intensity diagram, (b): Normal probability distribution

In the case of the pile-restrained model, the desired drafts were provided by attaching extra weights to the physical model. These extra weights were distributed uniformly on the model's mass point level. To provide feasible movement of the structure in the heave direction, two iron rails were attached to the flume walls (Figure 6). The mentioned rails restrained horizontal and rotational motions and the model was only allowed to have motion in the heave direction with minimum friction. All of the movement gauges were calibrated before use.

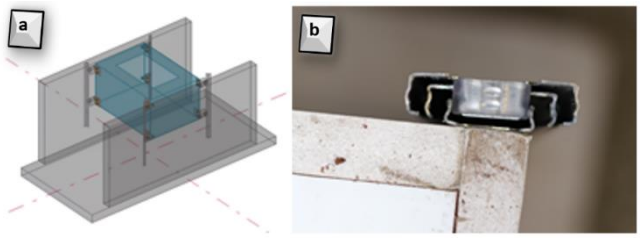

Figure 6. Provided supports for the fixed and pile-restrained FB; (a): Fixed Breakwater 3D model, (b): Iron rails cross section

In the case of the model with mooring lines, four cables (or chains) were connected to the submerged part of the model and on the other side, they were hooked to the bed of the flume with the angle of 45 degrees (Figure 7). The length of the cables were adjusted so that the desired drafts were achieved, and the cables were always in a state of tension simultaneously. Chains were in loose condition and had submerged weight of 259 *g/m* and the length was 3.35*m*, i.e., five times the water depth. The initial mooring stiffness was low, and no shocks were observed during the experimental tests.

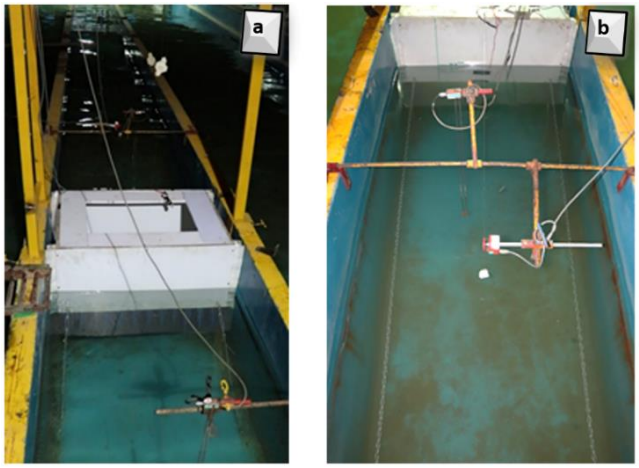

Figure 7. Provided mooring lines for the physical model; (a): Model with tethered cable, (b): Model with loose chain

Figure 8. The installed physical model in the wave flume;
(a): Anchored by cable, (b): Fixed Breakwater, (c): Anchored by chain.

The model was 0.67m in width and 0.50m in height. The length of the model was approximately equal to the flume width. To avoid unnecessary friction or collisions between the walls and the physical model, a gap was provided between the model and the walls. Also, for restricting wave transmission through the mentioned gap, some flexible polystyrene sheets were attached to the floating breakwater. The installed model is shown in Figure 8.

2.2. Data acquisition and analysis

Wave reflection and transmission were estimated for every case. A three-point method, proposed by Mansard and Funke, was employed to separate incident waves from reflected waves [3]. Six resistance wave gages made by DHI Denmark were used along the wave flume surrounding the structure to record the wave profile. Four of them were placed in the seaside of the model and two gauges were placed in the leeside. The transmission and reflection coefficients are calculated according to equations (2) and (3), respectively [20].

$$C_t = \frac{H_t}{H_i} \tag{2}$$

$$C_r = \frac{H_r}{H_i} \tag{3}$$

where H_t is the transmitted wave height, H_r represents the reflected wave height and H_i denotes the incident wave height. The transmission coefficient (C_t), the reflection coefficient (C_r), and the dissipation coefficient (C_d) satisfy equation (4). Using the following equation energy dissipation was studied in floating breakwater's region [4].

$$C_r^2 + C_t^2 + C_d^2 = 1 \tag{4}$$

The motion responses of the floating breakwater were measured by ship movement gages which were made by DHI Company. The movement in these experiments were in three directions, heave, surge, and pitch. The heave, surge, and pitch RAOs (Response amplitude operators) were calculated using equations (5)-(7) (He et al. 2013). The data extracted from the gages were analyzed by Wavepack software. Figure 3 shows the gages and the data recording systems.

$$RAO_{surge} = \frac{A_{surge}}{A_i} \tag{5}$$

$$RAO_{heave} = \frac{A_{heave}}{A_i} \tag{6}$$

$$RAO_{pitch} = \frac{A_{pitch}}{A_i} \tag{7}$$

In which, A_{surge}, A_{heave} and A_{pitch} are the amplitude of the surge, heave, and pitch respectively, and Ai is the amplitude of the incident wave.

2.3 The basic FB structures for the numerical analysis

In the present study, a finite-volume software, is applied based on the RANS (Reynolds Averaged Navier-Stokes) equations. RANS coupled with the continuity equation for incompressible flows in Cartesian coordinates are considered as the governing equations as follows [29]:

$$\frac{\partial \rho \overline{u_i}}{\partial x_i} = 0 \tag{8}$$

$$\frac{\partial}{\partial t}(\rho \overline{u_i}) + \frac{\partial}{\partial x_i}\left(\rho \overline{u_i u_j}\right) = -\frac{\partial P}{\partial x_i} + \frac{\partial}{\partial x_i}\left[\mu\left(\left(\frac{\partial \overline{u_i}}{\partial x_j} + \frac{\partial \overline{u_j}}{\partial x_i}\right)\right) - \frac{2}{3}\mu \frac{\partial \overline{u_i}}{\partial x_i}\delta_{ij}\right] + \frac{\partial}{\partial x_j}\left(-\rho \overline{u_i' u_j'}\right) + \rho f_j \tag{9}$$

where $\overline{u_i}$ $\overline{u_j}$ is the time average velocity component, for this 2D simulation, i,j =1,2, represent the horizontal direction of x and the vertical direction of y respectively, P is the pressure intensity, ρ represents the fluid density, f is the unit body force and μ denoted the dynamic viscosity.

Based on the Airy's linear wave theory, the regular wave equation for the free surface elevation $\eta(x,t)$, the velocity potential $\varphi(x,z,t)$, and velocity components in x and z directions $u(x,z,t)$ and $w(x,z,t)$ are written as:

$$\eta = A\cos(kx - \omega t + \phi) \tag{10}$$

$$\varphi(x,z,t) = xU + \frac{A\omega \cosh[K(z+h)]\sin(kx-\omega t+\phi)}{k \sinh kh} \tag{11}$$

$$u(z,x,t) = U + \frac{A\omega \cosh[k(z+h)]\cos(kx-\omega t+\phi)}{\sinh kh} \tag{12}$$

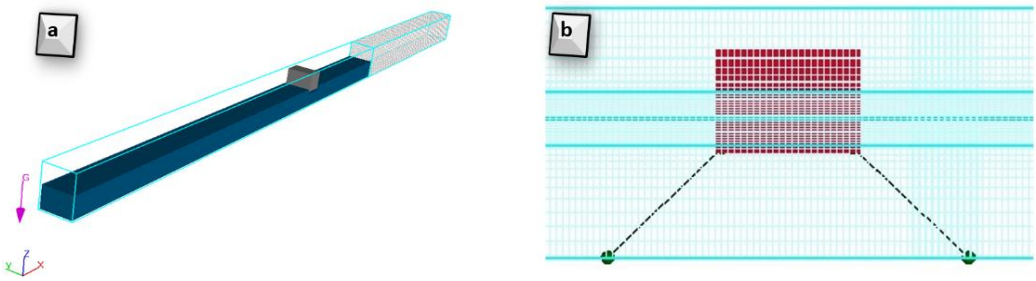

Figure 9. Numerical model computational domain
(a): 3D view of numerical model, (b): Created mesh for simulation

$$w(x,z,t) = \frac{A\omega \sinh[k(z+h)]\sin(kx-\omega t+\phi)}{\sinh kh} \quad (13)$$

in which ω is the angular frequency, k represents the wave number, ϕ is the phase shift angle, h is the water depth and A denotes the wave amplitude. The dispersion equation in terms of wave speed $c = \frac{\omega}{k}$, is given by:

$$(c-U)^2 = \frac{g}{k}\tanh kh \quad (14)$$

In the present study, in order to numerically investigate the effect of the mentioned effective parameters on the hydrodynamic behavior of the floating breakwater, all models of floating breakwaters have been simulated with the application of a finite element software.

The results have been validated with the laboratory data. For numerical modelling, the Cartesian mesh is used in the computational domain. The grid is distributed in the whole computational domain evenly. At the vicinity of the water surface, the mesh densities are increased. The selection of a proper computational mesh is vital in numerical simulations for the solution accuracy and efficiency. Thus, a set of initial numerical simulations were conducted to evaluate the sensitivity of the numerical solutions to the mesh size and an optimum mesh size was obtained. The numerical domain was created in the software. At the left boundary of the computational domain, a numerical wavemaker was established by prescribing the velocities and the free surface elevation according to the linear monochromatic wave. This boundary condition is readily available in the software. The numerical domain is shown in Figure 9. No-slip condition was applied at the bottom and wall boundaries. All numerical wave tanks need to have a dissipation zone to prevent wave reflection and its subsequent problems [30]. A wave absorbing component is installed before an outflow boundary to absorb wave motion, which reduces the wave reflection from the boundary.

The mesh size is one of the important aspects which influences the calculation results. The mesh size relates to the maximum wave frequency which can be calculated by the model. A small mesh size allows high wave frequencies to be calculated. To investigate the effect of the mesh size, several models with the same wave input were made where the mesh size increases from a coarse mesh to a fine mesh. Totally ten calculations were performed to evaluate that whether the results were dependent on the mesh resolution. When the calculation results (C_t) do not change by size decreasing, it can be concluded that convergence has occurred.

2.4. Model calibration and validation

The data of the two-dimensional experiments performed by Koutandos et al. is used to compare for model calibration and validation [4].

In the mesh-independence study, the transmission coefficient at different cell numbers is simulated. The selected wave height is 0.10 m, and the wavelength is 3.35m. The results of the mesh-independence study are shown in Table 2. It is seen that the results are converged to a specific coefficient as the total cells are increased.

Table 2. Mesh-independence test

case	cell number	transmission coefficient
1	1300000	0.635
2	1700000	0.621
3	2000000	0.6113
4	2400000	0.6105
5	2700000	0.6102

3. Results and Discussion

In this section, the results of this investigation are discussed, with emphasis on the effect of the incident wave characteristics, the anchorage systems and draft of the model. In order to compare how well the experimental and numerical results are, the Root Mean Square Error (RMSE) parameter is used:

$$RMSE = \sqrt{\frac{\sum_{i=1}^{N}(Ct_{theory}-Ct_{exp})^2}{N}} \quad (15)$$

where N is the number of data points. RMSE is the standard deviation of the residuals (prediction errors). Residuals are a measure of how far from the regression line data points are; RMSE is a measure of how spread out these residuals are. The difference of the wave transmission coefficient between theories and experimental data is shown in a bar plot to identify

where the largest differences occur. The Root Mean Square Error (RMSE, given in Eq.15) is determined for each theory to see how well the theories behave compared to with the experimental and numerical data. The RMSE applied in this case is a measure of the spread of the experimental data (measured transmission coefficients) and the predicted transmission coefficients (wave transmission theories). The RMSE presents the same units which are used to calculate RMSE, i.e., when the RMSE is calculated with transmission coefficients defined as percentages, the RMSE will indicate the spread of the experimental data around the theories in percentages as well. The plots for each experimental dataset and the RMSE values are given in the following sub-section. Also, the conclusion of each comparison is discussed.

3.1. Anchorage system

The effect of incident waves characteristics, such as wave period and wave heigth, on efficiency is examined in through four different FB configurations: (1) fixed breakwater, (2) pile-restrained (heave motion FB), (3) anchored by chains, and (4) tethered by elastic cable.

3.1.1. Fixed breakwater

Results related to transmission, reflection and dissipation coefficients of the incident waves on the model compared with the other research are presented in Figure 10(a,b,c). Also, a comparative diagram among the experimental dataset, theories and the measured data points are plotted in figure 10-d.

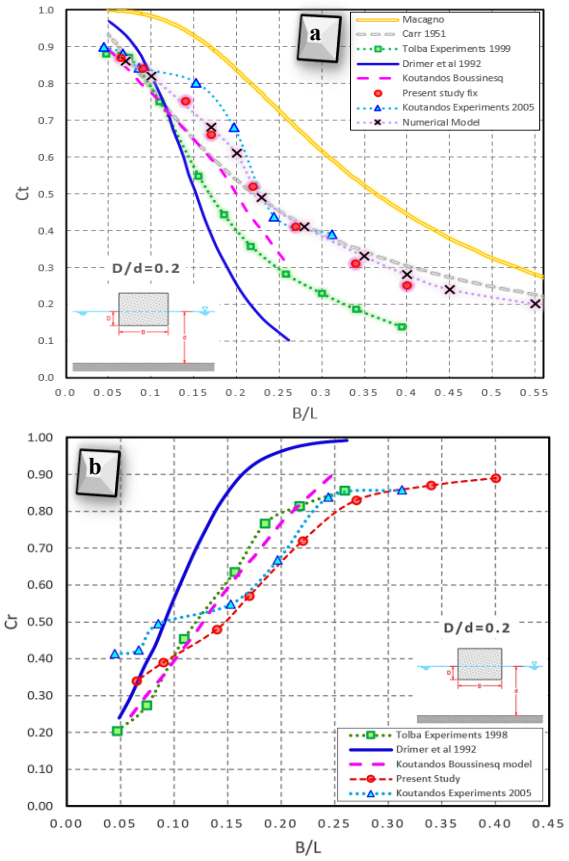

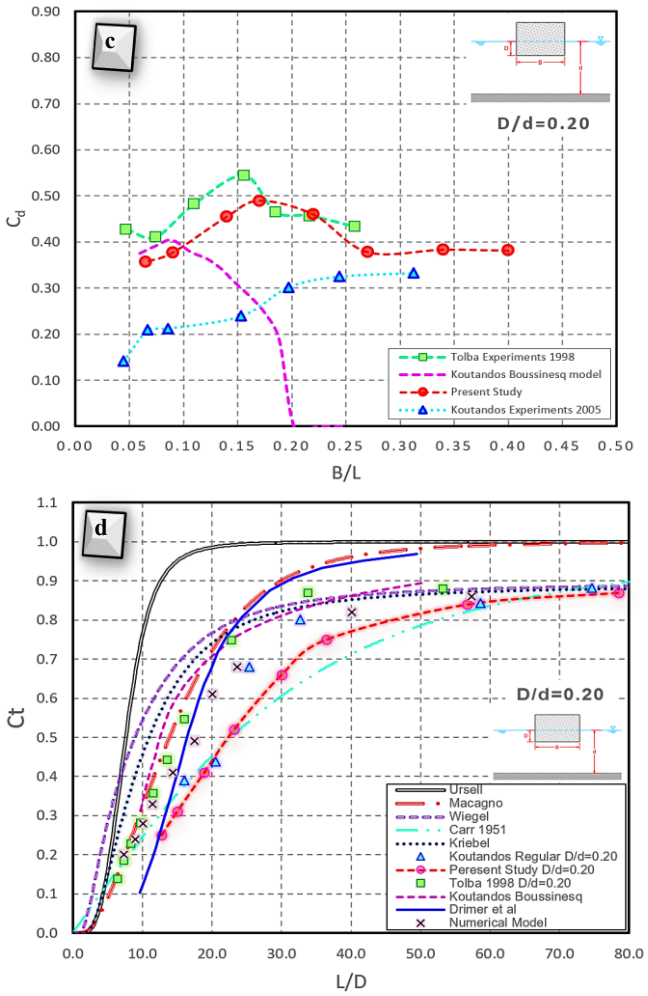

Figure 10. Comparison between theories and the experimental data – For the fixed breakwater;
(a): Variation of transmission coefficient (C_t) against *B/L*
(b): Variation of reflection coefficient (C_r) against *B/L*
(c): Variation of dissipation coefficient (C_d) against *B/L*
(d): Variation of transmission coefficient (C_t) against *L/D*

The difference between theories and the experimental data is shown in Figure 11-b. Also, the Root Mean Square Error (RMSE) for each theory for this dataset is shown in Figure 11-a.

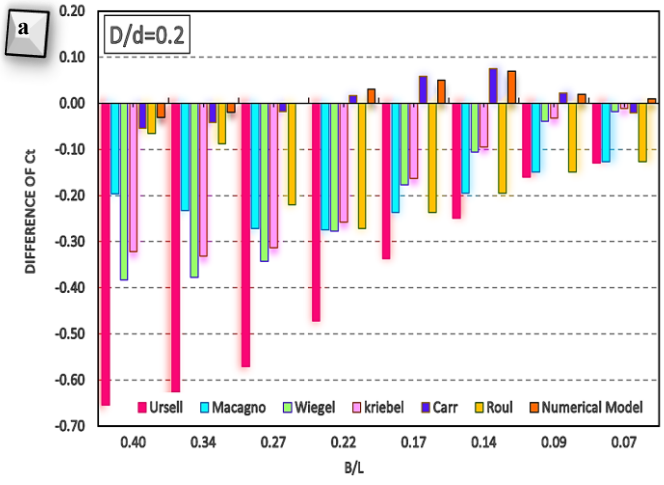

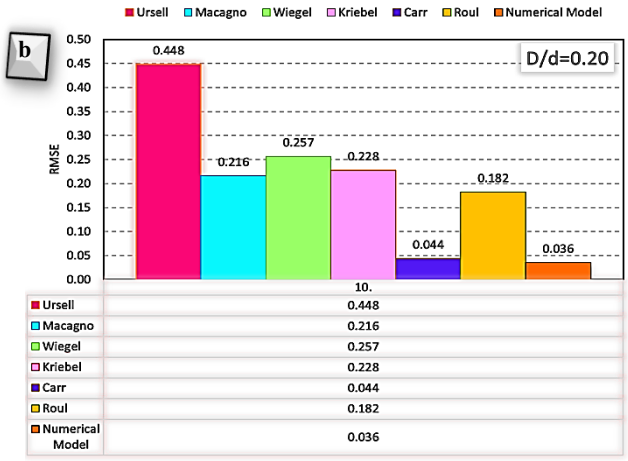

Figure 11. (a): Differences of the C_t between theories and the experimental data,
(b): RMSE between theories and the experimental data in case of the fixed Breakwater

Based on the experimental data obtained from different researchers, several conclusions can be drawn for fixed breakwaters. In general, it can be concluded that the RMSE is large (more than %10) and there is a poor agreement between most of the theories and the experimental data, see Figure 11. The dataset of the present study is overestimated by all of the theories, but Carr formulation has a good agreement with the present data. From this figure and related table, it turns out that the theory of Carr has the smallest RMSE, and this theory might be the most appropriate one to apply for this dataset.

This overestimation becomes larger when the B/L-values increase, hence shorter waves occur. With attention to the large RSME, when the above theories are applied, the wave transmission will be overestimated in general, but for a preliminary design the theories will give a good estimation regarding the effectiveness of the fixed structure. According to the RMSE, a good agreement can be seen between numerical results and experiments of the present study. The RMSE applied regarding numerical model is a measure of the experimental transmission coefficients spread compared with the modelled transmission coefficients by numerical software. On the other hand, results of this study have a good agreement with Koutandos experiments [4].

Based on the present investigation, and with considering the dispersion of laboratory and numerical data obtained from the research on the transmission coefficient, a new non-dimensional parameter (DB/L^2, i.e., draft times width divided by wavelength squared) is identified as an essential parameter to compare all of recent studies. Therefore, it is recommended to use the dimensionless parameter DB/L^2 to compare the transmission coefficient of floating breakwaters. As it can be seen in Figure 12-a (compared with Figure 10-a), the data of different research have a large dispersion, and this is due to the fact that the wavelength parameter (L) has much greater effect than the width of the model (B).

Therefore, in order to have a parameter that can take this effect into account, it is better to use the dimensionless parameter DB/L^2. This parameter brings the existing data to a good consistency and with the convergence that it creates between the data, it helps a lot to understand the results obtained from research with different conditions. An example of this data uniformity for a fixed breakwater under regular waves and D/d=0.2 is shown in Figure 12. In this Figure, data is distributed in a narrow band and there is no much disparity.

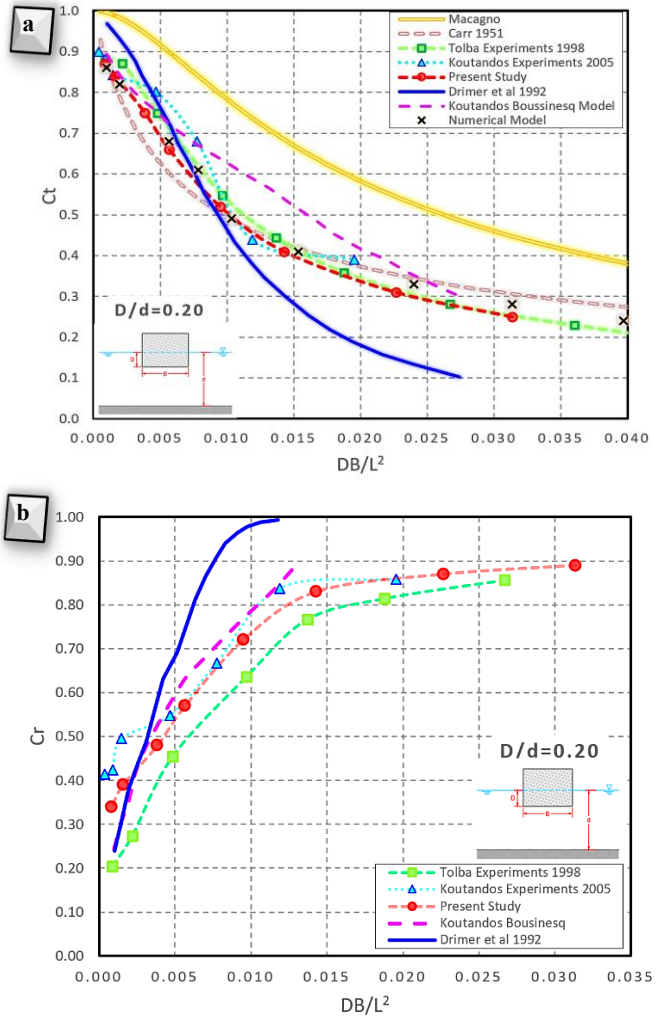

Figure 12: (a): Transmission coefficient (C_t) variation against DB/L^2 parameter, (b): Reflection coefficient (C_r) variation against DB/L^2 parameter – The fixed Breakwater

3.1.2. Pile-restrained floating breakwater

For the FB anchored by pile, the model is free to move just in the heave direction, so it has one degree of freedom. Ruol et al. investigated the natural heave period for pi-type floating breakwaters and compared the analytical calculations with the experimental measurements. Based on this investigation, the dimensionless parameter χ which has been mentioned earlier, is defined in Eq. 1. Therefore, this parameter will be used to set on the x-axis for floating breakwaters

anchored by piles (without fixed vertical screen), because all of the parameters which influence the transmission coefficient are included there [5].

Results related to transmission, reflection, and dissipation coefficients of the incident waves on the model compared with the other research are presented in Figure 13. In this figure, $C_{t,measured}$ represent derived C_t from Macagno formula.

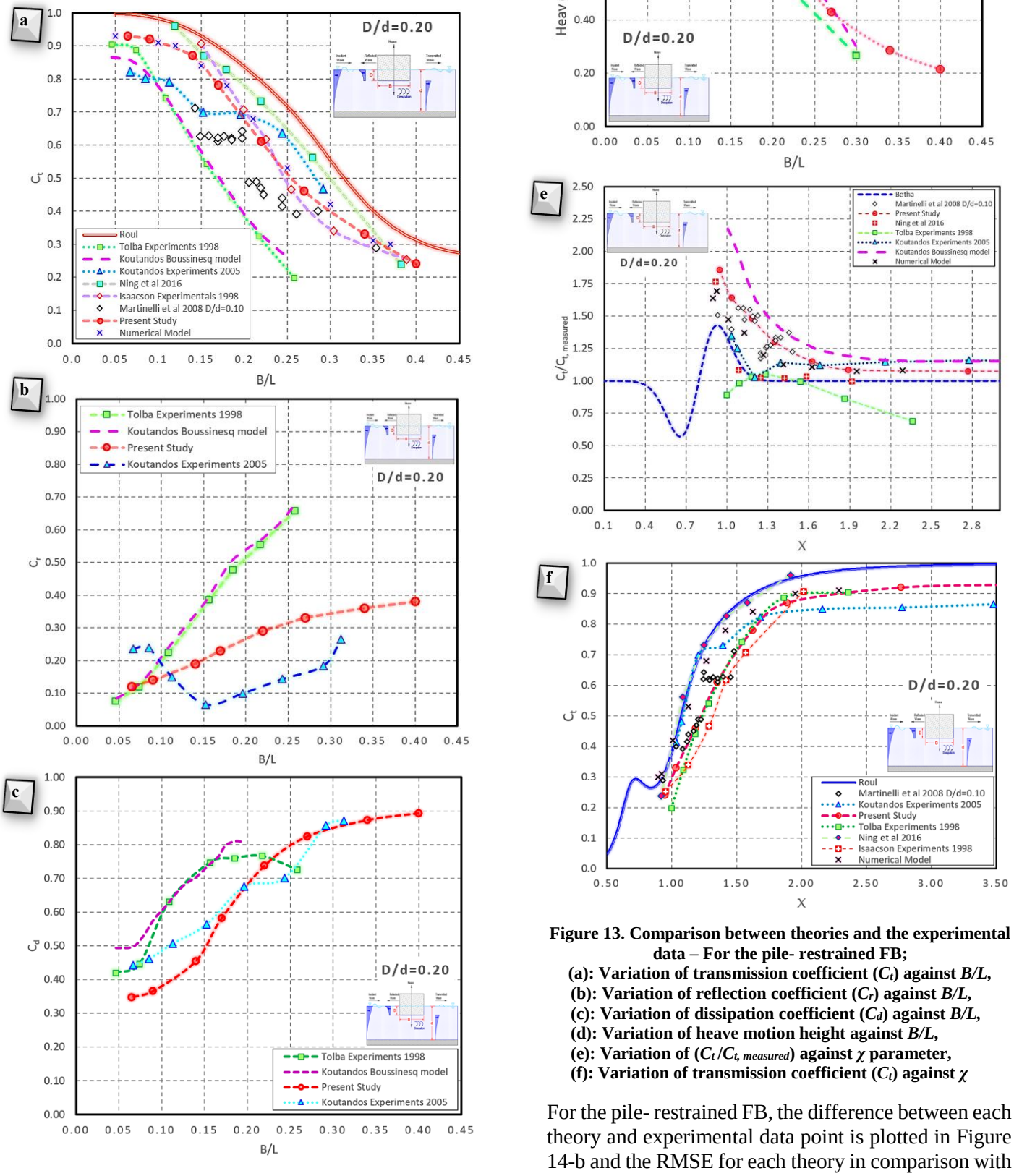

Figure 13. Comparison between theories and the experimental data – For the pile- restrained FB;
(a): Variation of transmission coefficient (C_t) against B/L,
(b): Variation of reflection coefficient (C_r) against B/L,
(c): Variation of dissipation coefficient (C_d) against B/L,
(d): Variation of heave motion height against B/L,
(e): Variation of ($C_t/C_{t,\,measured}$) against χ parameter,
(f): Variation of transmission coefficient (C_t) against χ

For the pile- restrained FB, the difference between each theory and experimental data point is plotted in Figure 14-b and the RMSE for each theory in comparison with this dataset is shown in Figure 14-a. From this figure and related table, the theory of Roul and Carr has the

smallest RMSE, and these theories might be the most appropriate ones to apply for this dataset.

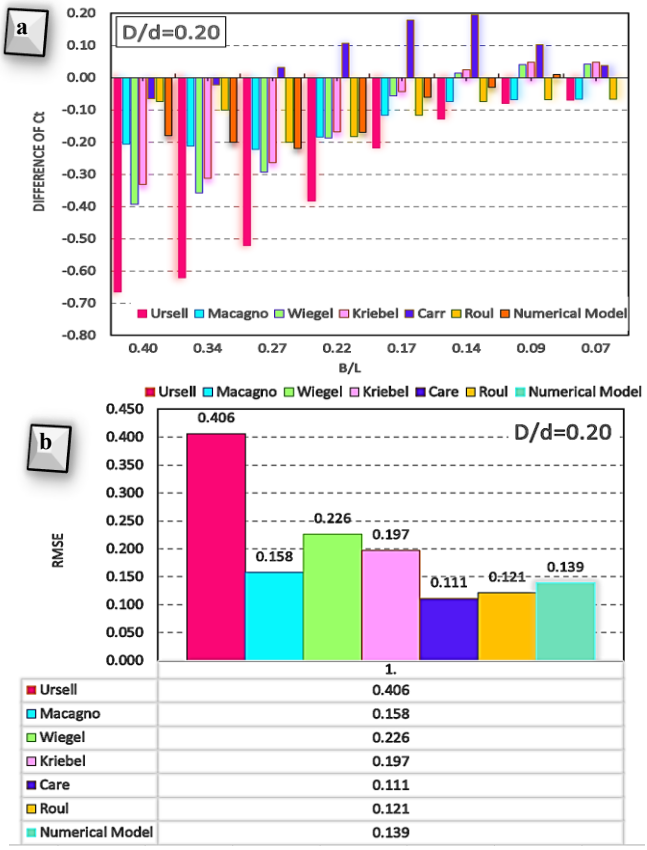

Figure 14: (a): Differences of the C_t between theories and the experimental data, (b): RMSE between theories and the experimental data in case of pile- restrained FB

Also, for the FB anchored by pile it is recommended to use the dimensionless parameter DB/L^2 to compare the transmission coefficient of floating breakwaters. The data for this type of FB under regular waves and D/d=0.2 is shown in the Figure 15. it is obvious that data for this type of breakwater distributed in a narrow band and there is no significant disparity.

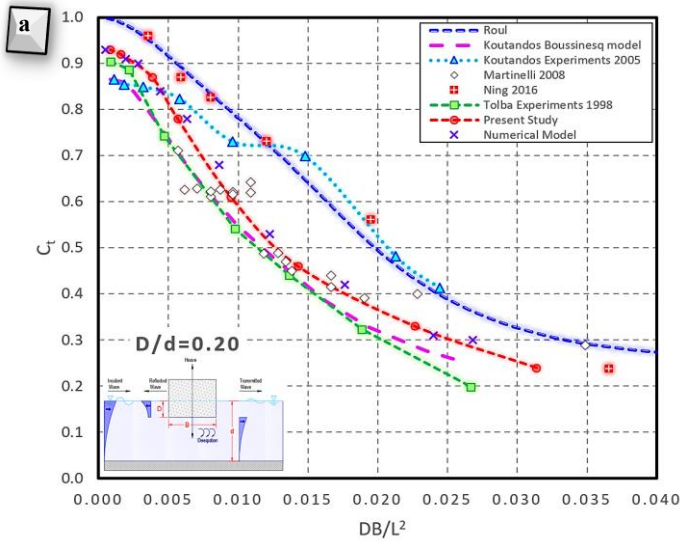

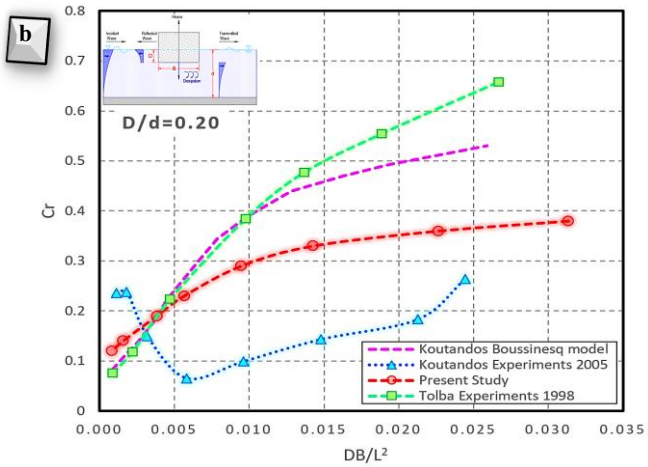

Figure 15: a: Transmission coefficient (C_t) variation against DB/L^2 parameter, b: Reflection coefficient (C_r) variation against DB/L^2 parameter – Pile-restrained FB

All the theories used for the comparisons with experimental data are derived for fixed structures, and a poor agreement is found for floating breakwaters with one degree of freedom. As it can be seen from Figure 13 and Figure 15, the relative period χ and dimensionless parameter DB/L^2 are two appropriate values to set on the x-axis for efficiency comparison of floating breakwaters anchored by pile. These two mentioned ratios contain all the parameters which influence the wave transmission coefficient.

3.1.3. Floating breakwater anchored by chain

For the FB anchored by chain, there are six degrees of freedom. Since all tests are conducted in the two-dimensional flume, there are three degrees of freedom, which are heave, sway, and roll. Chains were in loose condition and had submerged weight of 259 *g/m*. Their length was 3.35*m*, i.e., five times the water depth.

Ruol et al. [2013b] investigated the ranges of χ and D/d in which their formula would be applicable. They concluded that for χ-values between 0.5 and 1.5 and for D/d-values between 0.20 and 0.60, their formula is suitable to apply for both π-type and pontoon-type floating breakwaters. When the data of Brebner and Ofuya was compared with the formula of Ruol et al. a good agreement was found between the experimental data and the predicted values [12].

Martinelli et al. performed experiments in a flume (two-dimensional) and performed experiments in a basin (three-dimensional). Both experiments were performed with a D/d ratio equal to 0.13. For the two-dimensional dataset, a good agreement was found for the theory of Macagno. For the three-dimensional dataset, a good agreement was found for the theory of Ruol et al. and the wave transmission coefficients for this dataset are smaller than for the two-dimensional dataset. In this section only two-dimensional datasets are considered and therefore the three-dimensional dataset is neglected here [6].

Results related to the transmission coefficients of the incident waves on the model compared with the other research are presented in Figure 16.

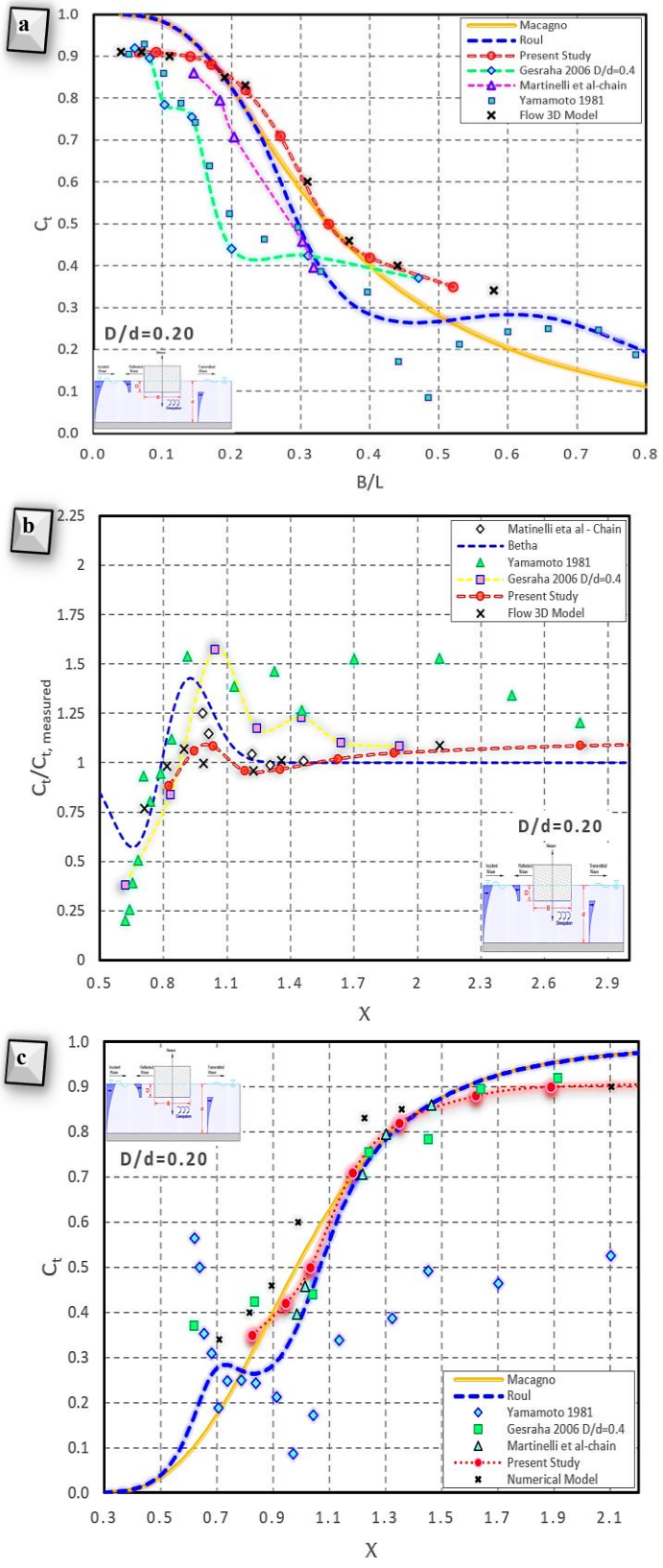

Figure 16: Comparison between theories and the experimental data – For the FB anchored by chain;
(a): Variation of transmission coefficient (C_t) against *B/L*,
(b): Variation of ($Ct/C_{t,\ measured}$) against χ parameter,
(c): Variation of transmission coefficient (C_t) against χ

For the FB anchored by chain, the difference between each theory and experimental data point is plotted in Figure 17-b. The RMSE for each theory in comparison with this dataset is shown in Figure 17-a. From this figure and related table, the theory of Roul and Macagno has the smallest RMSE, and this theory might be the most appropriate one to apply for this dataset.

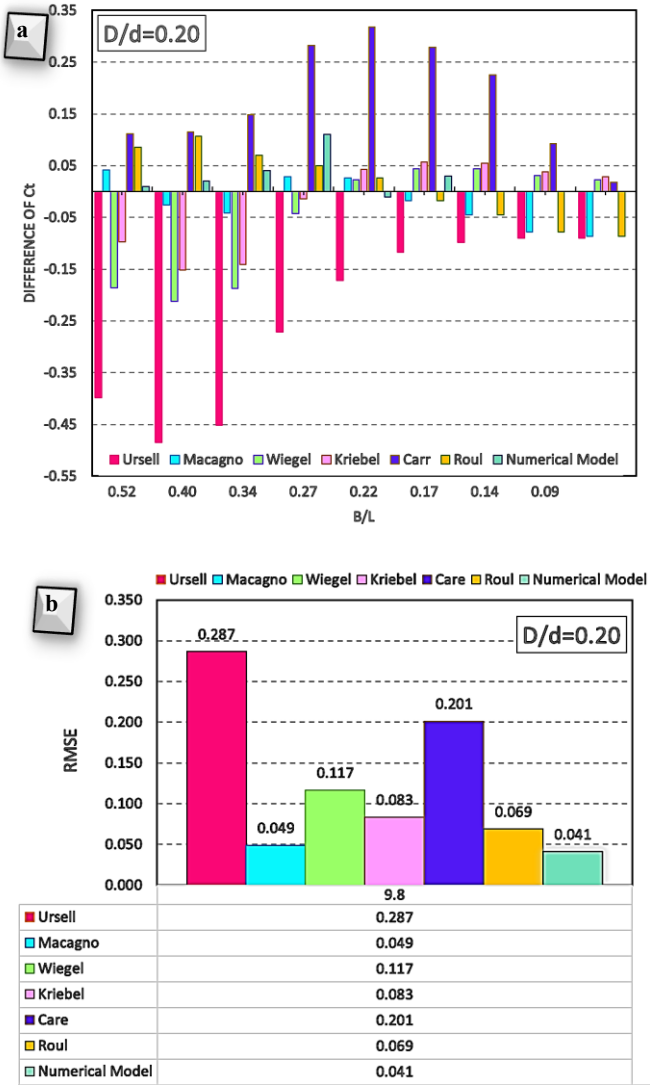

Ursell	0.287
Macagno	0.049
Wiegel	0.117
Kriebel	0.083
Care	0.201
Roul	0.069
Numerical Model	0.041

Figure 17: (a): Differences of the C_t between theories and the experimental data,
(b): RMSE between theories and the experimental data – The FB anchored by chain

In Figure 18, transmission coefficient (C_t) variation against DB/L^2 parameter is plotted for the FB anchored by chain under regular waves and D/d=0.2. As it is seen, the dimensionless parameter DB/L^2 is an appropriate value to set on the x-axis for floating breakwaters anchored by chain. This dimensionless parameter could gather all the datasets in a meaningful narrow band and decrease the disparity of data very well.

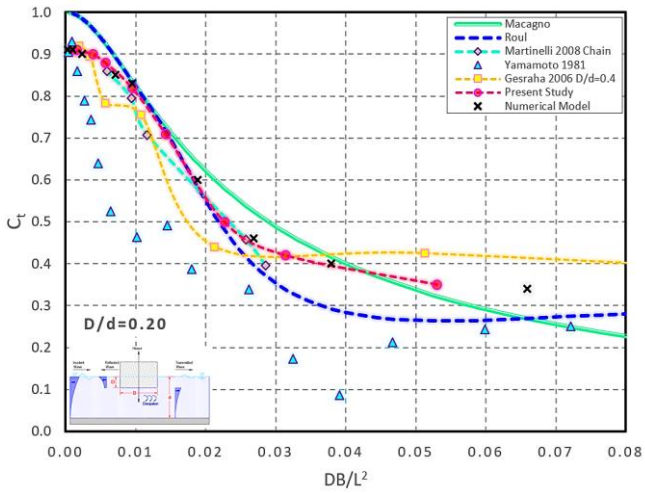

Figure 18: Transmission coefficient (C_t) variation against DB/L^2 parameter - FB anchored by chain

3.1.4. Floating breakwater anchored by tethered cable

As it has been mentioned above, there are also six degrees of freedom for the FB anchored by cable. In this case, the pretension cables were used as mooring lines. These mooring lines control the structure's movement to a considerable extent. Results related to the transmission coefficients of the incident waves on the model compared with the other research are presented in Figure 19.

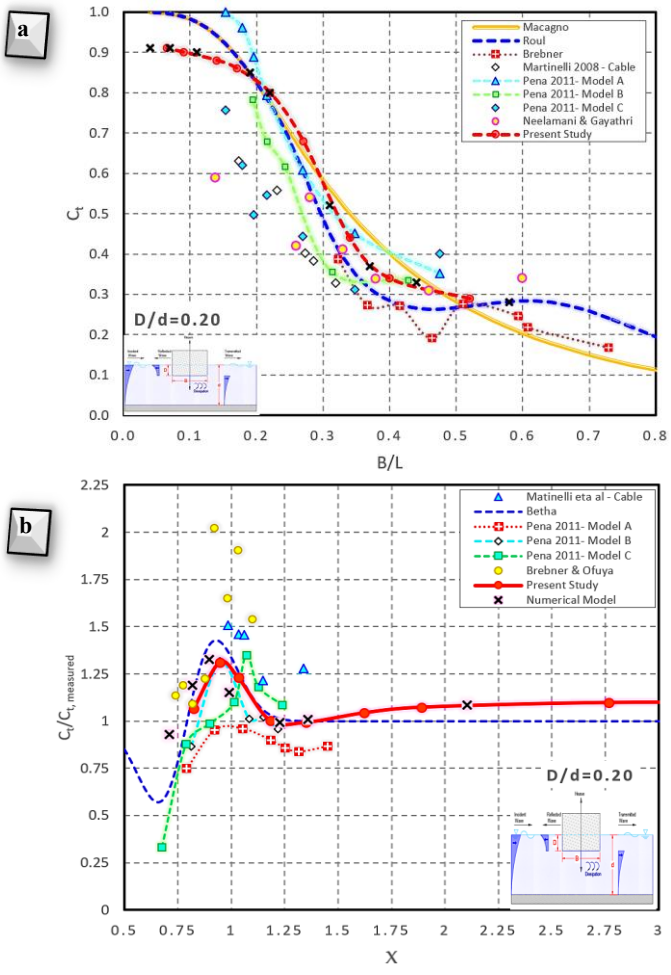

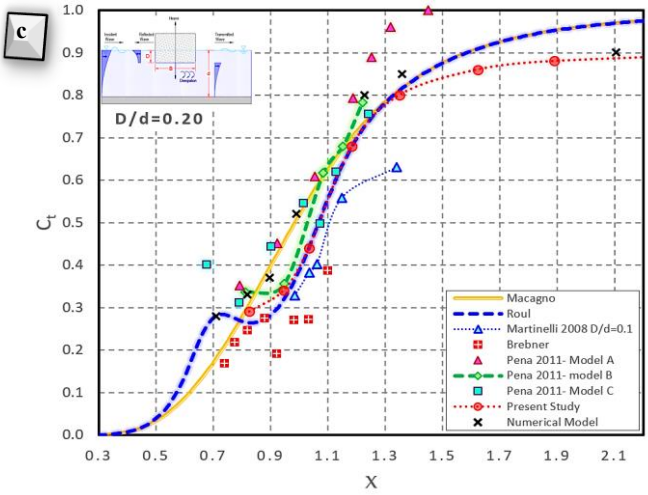

Figure 19: Comparison between theories and the experimental data -The FB anchored by tethered cable; (a): Variation of transmission coefficient (C_t) against B/L, (b): Variation of ($Ct\ /C_{t,\ measured}$) against χ parameter, (c): Variation of transmission coefficient (C_t) against χ

Figure 20-b shows the difference between each theory and experimental data point. The RMSE for each theory in comparison with this dataset is shown in Figure 20-a. From this figure, the theory of Roul and Macagno has the smallest RMSE, and this theory might be the most appropriate ones to apply for this dataset.

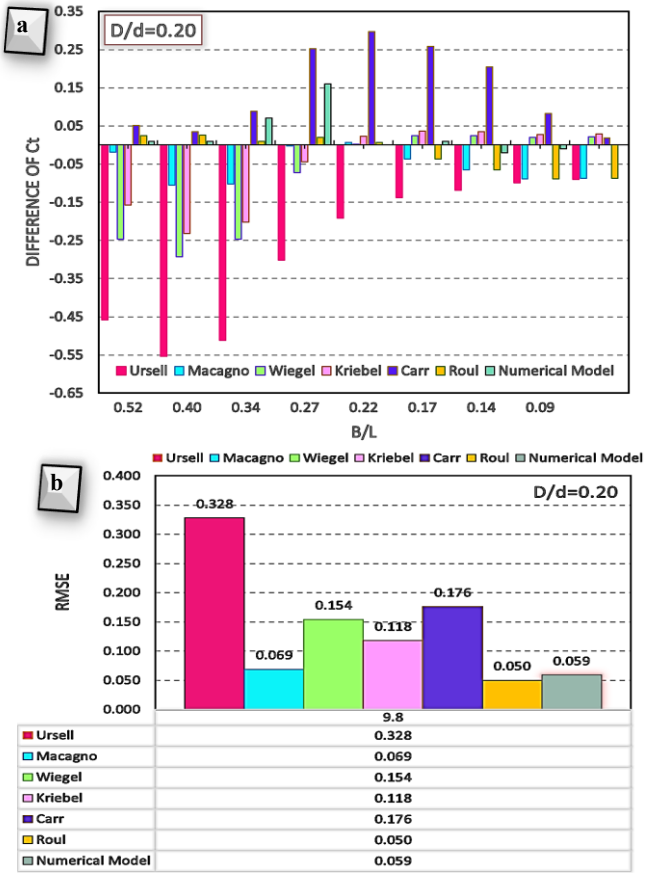

Figure 20: (a): Differences of the C_t between theories and the experimental data, (b): RMSE between theories and the experimental data -FB anchored by tethered cable

In Figure 21, the transmission coefficient (C_t) variation against DB/L^2 parameter is plotted for FB anchored by tethered cable under regular waves and D/d=0.2. As it is seen in this figure, the dimensionless parameter DB/L^2 is an appropriate value to be set on the x-axis for the floating breakwaters anchored by cable as well.

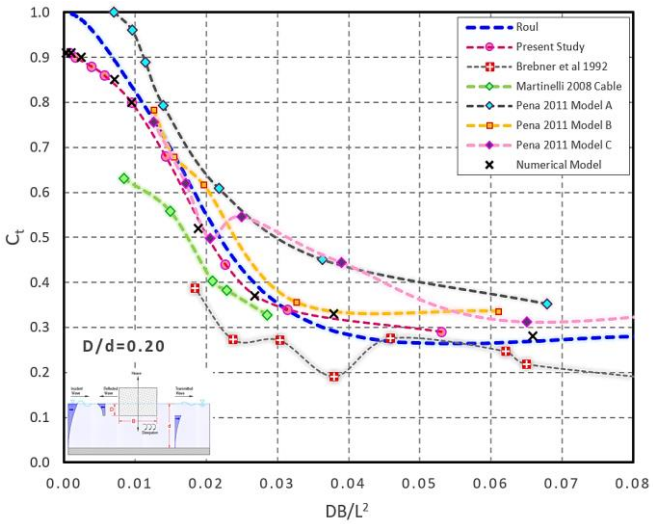

Figure 21: Transmission coefficient (C_t) variation against DB/L^2 parameter – The FB anchored by tethered cable

3.1.5. General comparative discussion

After a general review of each anchorage system and comparison of each one with previous research, the effect of the anchorage system on the transmission coefficient was compared with each other. Figure 22 shows the laboratory results obtained from the present study.

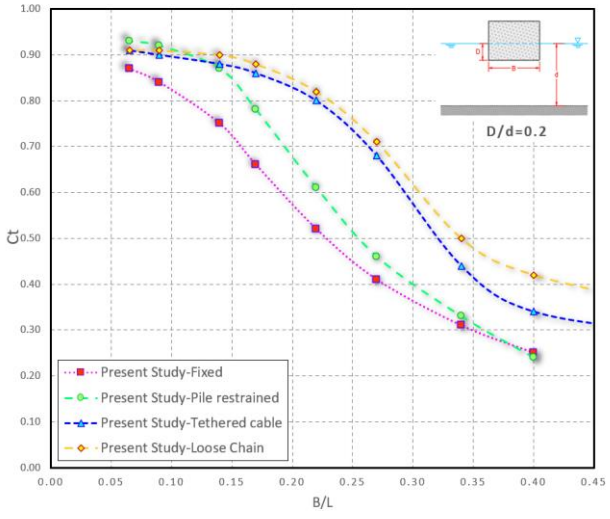

Figure 22: Comparison of the effect of anchorage system on wave transmission coefficient (C_t)

4. Conclusions

In this paper, a rectangular box floating breakwater was studied experimentally in four different FB configurations: (1) fixed breakwater, (2) pile-restrained (heave motion FB), (3) anchored by chain, and (4) tethered by elastic cable. In addition, the CFD method was used to study the mentioned configurations numerically. On the other hand, the effect of the draft of models were investigated. Based on deducted results, all the configurations were in acceptable range and had good agreements with previous investigation. According to Figure 22, the general results of the research are as follows:

1. For almost all wavelengths, the hydrodynamic behavior of the fixed breakwater was better than the other configuration.
2. Comparison of fixed breakwater with pile-restrained FB shows: In waves with short periods, the hydrodynamic behavior of breakwater with one-degree of freedom is almost very close to the fixed breakwater. For short wavelength, pile-restrained FB can have the same hydrodynamic behavior as the fixed one, even slightly better than it. This is due to the fact that when the breakwater located in the trough of the waves, Because of the heave degree of freedom the standing level of the breakwater is lower than the fixed type. When trough of waves is getting to turn to crest, because of wavelength shortness, there is not enough time that breakwater can match its standing level with the wave oscillations. Therefore, the breakwater has more draft in front of the waves and shows better performance than the fixed breakwater.
3. In high period waves (long waves), the hydrodynamic behavior of the pile-restrained FB is weaker than other configurations. This is due to the freeness of heave motion. In this configuration in the direction of heave, there is no movement restriction for the breakwater, so practically the breakwater mounts on the waves and shows the lowest efficiency.
4. Comparison of the breakwater anchored by cable with the breakwater anchored by chain shows: the effect of anchorage system's stiffness is more noticeable in waves with lower period, and since the chain has less restriction for displacement and the breakwater has more motion amplitude, its hydrodynamic performance is poor, so the wave transmission coefficient is higher. On the other hand, in waves with high period, the effect of stiffness of the anchorage system on the transmission coefficient is reduced.
5. Generally, the most efficient configuration was the fixed breakwater. However, regarding cost-effectiveness, the configuration of the FB with pile should be considered the most efficient for design purposes in mild conditions.

5. References

[1] McCartney, B.L., (1985), *Floating Breakwater Design*, Journal of Waterway, Port, Coastal, and Ocean Engineering, Vol.111(2), p.304-318.
[2] Biesheuvel A.C, (2013), *Effectiveness of floating breakwaters*, Msc Dissertation, Delf University of Technology.

[3] Mansard, E., and Funke, E., (1980), *The measurement of the incident and reflected spectra using the least squares method*, In: Proceedings of the 17th Coastal Engineering Conference ASCE, Sydney, p.154-172.

[4] Koutandos, E.V., Prinos, P., and Gironella, X., (2005), *Floating breakwaters under regular and irregular wave forcing: reflection and transmission characteristics*, Journal of Hydraulic Research, Vol.43(2), p.174-188.

[5] Ruol, P., Martinelli, L., and Pezzutto, P., (2013a), *Formula to predict transmission for π-type floating breakwaters*, Journal of Waterway, Port, Coastal, and Ocean Engineering, Vol.139(1), p.1-8.

[6] Ruol, P., Martinelli, L., and Pezzutto, P., (2013b), *Limits of the new transmission formula for π-type floating breakwaters*, Coastal Engineering Proceedings, Vol.1(33), p.47.

[7] Ursell, F., (1974), *The effect of a fixed vertical barrier on surface waves in deep water*, In Proc. Cambridge Philos. Soc, Vol.43, p.374-382.

[8] Macagno, E., (1954), *Wave action in a flume containing a submerged culvert*, La Houille Blanche.

[9] Pena, E., Ferreras, J., Sanchez-Tembleque, F., (2011), *Experimental study on wave transmission coefficient, mooring lines and module connector forces with different designs of floating breakwaters*, Journal of Ocean Engineering, Vol.38, p.1150-1160.

[10] Abul-Azm, A.G., Gesraha, M.R., (2000), *Approximation to the hydrodynamics of floating pontoons under oblique waves*, Journal of Ocean Engineering, Vol.27, p.365-384.

[11] Bettess, P., Liang, S.C., and Bettess, J.A., (1984), *Diffraction of waves by semi-infinite breakwater using finite and infinite elements*, International Journal for Numerical Methods in Fluids, Vol.4(9), p.813-832.

[12] Brebner, and Ofuya, A.O., (1968), *Floating breakwaters*, In Proceedings of 11th Conference on Coastal Engineering, p.1055-1094.

[13] Cox, R., Coghlan I., and Kerry, C., (2007), *Floating breakwater performance in irregular waves with particular emphasis on wave transmission and reflection, energy dissipation, motions and restraining forces*, Coastal Structures Conference, Venice.

[14] Kriebel, D.L., and Bollmann, C.A., (1996), *Wave transmission past vertical wave barriers*, In Coastal Engineering Conference, Vol.2, p.2470-2483.

[15] Gesraha, M.R., (2006), *Analysis of π-shaped floating breakwater in oblique waves: I. Impervious rigid wave boards*, Journal of Applied Ocean Research, Vol.28, p.327-338.

[16] Drieman, R., (2011), *Feasibility study on the use of a floating breakwater to protect a new artificial beach in Balchik, Bulgaria*, Msc thesis, Delft University of Technology.

[17] Fousert, M.W., (2006), *Floating breakwaters*, Msc thesis, Delft University of Technology.

[18] Hales, L.Z., (1981), *Floating breakwaters: State of the art literature review*, Technical report, DTIC Document.

[19] Dong, G.H., Zheng, Y.N., Li, Y.C., Teng, B., Guan, C.T., and Lin, D.F., (2008), *Experiments on wave transmission coefficients of floating breakwaters*, Journal of Ocean Engineering, Vol.35, p.931–938.

[20] He, F., Huang, Zh., and Wing-Keung Law, A., (2013), *An experimental study of a floating breakwater with asymmetric pneumatic chambers for wave energy extraction*, Journal of Applied Energy, Vol.106, p.222-231.

[21] Ji, Ch., Cheng, Y., Cui J., Yuan, Zh., and Gaidai, O., (2018), *Hydrodynamic performance of floating breakwaters in long wave regime: An experimental study*, Journal of Ocean Engineering, Vol.152, p.154-166.

[22] Liu, Zh., Wang, Y., Wang, W., and Hua, X., (2019), *Numerical modeling and optimization of a winged box-type floating breakwater by Smoothed Particle Hydrodynamics*, Journal of Ocean Engineering, Vol.188, p.106246.

[23] Williams, A.N., Lee, H.S., and Huang, Z., (2000), *Floating pontoon breakwaters*, Journal of Ocean Engineering, Vol.27, p.221-240.

[24] Harms, V.W., (1979), *Data and procedures for the design of floating tire breakwaters*, Water Resources and Environmental Engineering Rep, No.79-1, Dept of Civil Eng., State University of New York at Buffalo.

[25] Harms, V.W., Westerink, J.J., Sorensen, R.M. and McTamany, J.E., (1982), *Wave transmission and mooring force characteristics of pipe-tire floating breakwaters*, Technical Paper No. 82-4, US. Army, CERC.

[26] Carr, J.H., (1951), *Mobile Breakwaters*, Proceeding of the Second Conference on Coastal Engineering, Vol.28(1), p.281-295.

[27] Yamamoto, T., (1982), *Moored floating breakwater response to regular and irregular waves*, Journal of Applied Ocean Research, Vol.3, p.114-123.

[28] Yamamoto, T., Yoshida, A., and Ijima, T., (1980), *Dynamics of elastically moored floating objects*, Journal of Applied Ocean Research, Vol.2, p.85-92.

[29] Mohammd-Beigi.K, M., Kazeminezhad, M.H., Yeganeh-Bakhtiary, A., (2018), *Numerical Study on Hydrodynamic Force and Wave Induced Vortex Dynamics around Cylindrical Pile*, IJCOE, Vol.3, No.4, p.1-11.

[30] Zabihi, M.K.Kh., Mazaheri, S., Rezaee Mazyak, A., (2017), *Wave Generation in a Numerical Wave Tank*, IJCOE, Vol.2, No.4, p.33-43.